

SINGLE MOLECULE FORCE SPECTROSCOPY OF SINGLE STRANDED DNA BINDING
PROTEIN AND REP HELICASE

BY

RUSTEM KHAFIZOV

DISSERTATION

Submitted in partial fulfillment of the requirements
for the degree of Doctor of Philosophy in Physics
in the Graduate College of the
University of Illinois at Urbana-Champaign, 2012

Urbana, Illinois

Doctoral Committee:

Professor Taekjip Ha, Chair
Assistant Professor Yann R. Chemla, Director of Research
Professor Yoshitsugu Oono
Professor John D. Stack

Abstract

Single-stranded DNA binding (SSB) proteins are essential accessory proteins that protect single-stranded DNA (ssDNA) during genome maintenance. *Escherichia coli* SSB is a prototypical homo-tetrameric SSB protein that can wrap up to 65 nucleotides of ssDNA in one of its binding modes. Here we present mechanical studies of *E. coli* SSB bound to ssDNA using high-resolution optical tweezers. This method allows us to probe the interaction of individual SSBs to ssDNA in real time, with nanometer resolution. By detecting directly the wrapping of ssDNA by a single protein, we are able to characterize the thermodynamics and kinetics of nucleoprotein complex formation. Mechanical pulling of ssDNA in the presence of SSB reveals that the protein condenses ssDNA in the force range 0-10pN and that tension can be used to modulate the ssDNA wrapping state of SSB. Measurements of SSB kinetics indicate that SSB-ssDNA complex formation occurs in a two-step process consisting of a diffusion-limited binding step in which the protein associates weakly with its substrate, followed by a fast wrapping step in which ssDNA is condensed. We also quantify how tension modulates the ssDNA wrapping state of SSB, revealing features of the energy landscape for SSB-ssDNA interactions. Lastly, we carried out measurements of SSB interaction with long ssDNA binding substrate as a function of mechanical force. The data indicate that SSBs bound to longer stretches of ssDNA bound much tighter, probably due to nucleoprotein filament formation. And we have evidence that SSB can bind to ssDNA in intermediate wrapping states and are transiently wrapping and unwrapping from their substrates.

In addition we present for the first time study on the conformational control of Rep helicase using an optical trap. We found that crosslinking-mediated conformational arrest of a dynamic subdomain in so-called “closed” orientation converted the Superfamily I (SFI) helicase, Rep, from a very poor DNA helicase into a powerful motor protein with a highly processive DNA unwinding activity. In contrast, the wild type Rep helicase cannot efficiently unwind DNA over 18 bp *in vitro*. A single Rep-X (cross-linked Rep) molecule can processively unwind DNA up to 4 kbp and generate forces in excess of 40 pN, making it the most powerful helicase known. The same modification on the related PcrA helicase produced the same activity increase characteristics strengthening the possibility of widespread application of this conformational control technique. Thus our results directly answer the question of the role of different

conformations observed in SF-I helicase crystal structures and offer a mechanism for how partner proteins *in vivo* may regulate helicase function via conformational control.

Dedicated to my parents and brother

Acknowledgements

Graduate studies would have not been possible without the help and support of many of my friends, family members and mentors. I thank them from the bottom of my heart in helping me achieve success and reaching my goals.

Thanks to my advisor Dr. Yann Chemla, who was a guiding light for me; he sacrificed his time for me to help in switching from fundamental physics into biophysics. Weekly discussion provided me with the sense of deepness and a direction of science I would like to explore further.

I would also thank our collaborators from Washington University in St. Louis, Timothy Lohman and his post doctorate Alex Kozlov for providing us with an exciting project, the opportunity to work on single stranded DNA binding protein, and stimulating discussions about the results.

I thank our lab neighbors Dr. Taekjip Ha and his graduate student Sinan Arslan for introducing me to the world of helicases. It was a pleasure to work with them and the joy of obtaining awesome results is still in my heart.

Special thanks to my lab mates: Taejin Min, Zhi Qi, Patrick Mears, Sukrit Suksombat, Markita Landry, Kiran Girdhar, Kevin Whitley and Matt Comstock. They were always supportive and I will remember exciting discussions we had.

I would also extent my appreciation to former and current graduate students and post doctorates from Dr. Paul Selvin's and Dr. Taekjip Ha's labs: Melikhan Tanyeri, Erdal Toprak, Comert Kural, Hasan Yardimci, Burak Okumus, Murat Baday and Hamza Balci for giving me advice and mentoring me. I am thankful for the football games we used to play together every week.

I must also express my gratitude to my parents for their encouragement and support all along this journey to graduation. While words cannot describe their contribution, my parents and brother inspired me to become what I am today.

Contents

List of Figures	x
List of Abbreviations	xii
Introduction.....	1
Chapter 1. Introduction to single molecule optical trap	6
1.1 Optical Trapping	6
1.1.1 Introduction	6
1.1.2 Basic trap principles	7
1.1.3 Detection in optical traps	10
1.1.4 Optical Trap Calibration.....	11
1.1.5 Trapping geometries	12
1.2 High resolution optical trapping.....	13
1.2.1 Introduction	13
1.2.2 Dual Trap Setup.....	14
1.2.3 Differential detection improves spatial resolution.....	16
1.2.4 Application of high resolution optical traps	18
1.3 References	18
Chapter 2. Introduction to <i>E. coli</i> SSB protein.....	23
2.1 Historical perspective.....	23
2.2 <i>E. coli</i> SSB and its Binding Modes	23
2.3 Interaction with Other Proteins	26
2.4 Influence of DNA Binding Modes on SSB Function.....	26
2.5 Previous studies.....	27
2.6 References	28
Chapter 3. Observing binding of <i>E. coli</i> SSB using optical trap	34

3.1 Experimental Design	34
3.1.1 DNA construct design	34
3.1.2 Flow chamber	36
3.1.3 Single-stranded DNA protein purification	37
3.1.4 Buffer conditions	37
3.1.5 Tether formation	37
3.2 Gradual unwrapping of SSB as a function of force	38
3.3 Tension and its effect on SSB-ssDNA conformation.....	40
3.4 Discussion	44
3.5 Summary	46
3.6 References	46
Chapter 4. Binding Dynamics of (SSB) ₆₅ Binding Mode	48
4.1 Introduction	48
4.2 Experimental results.....	48
4.2.1 Diffusion limited binding process	49
4.2.2 Force spectroscopy of binding rates	50
4.3 Discussion	53
4.4 Summary	55
4.5 References	55
Chapter 5. Interaction of <i>E.coli</i> SSB with long ssDNA	57
5.1 Introduction	57
5.2 Experimental procedures.....	57
5.2.1 Medium length ssDNA construct	57
5.2.2 Long construct	58
5.3 Protein clustering on 175nt poly-dT.....	59

5.4 Binding dynamics of SSB to Kbps of random sequence DNA.....	60
5.5 Discussion	61
5.6 Summary	61
5.7 References	62
Chapter 6. Enhancing Rep helicase activity	63
6.1 Introduction	63
6.1.1 SF-I helicases.....	64
6.1.2 Oligomeric nature of most helicases.	64
6.1.3 <i>E. coli</i> Rep DNA helicase.....	65
6.1.4 Structure of <i>E. coli</i> Rep	67
6.2 Cross-linking 2B domain activates unwinding ability of Rep helicase	69
6.3 Observing DNA unwinding by Rep-X using optical trap	71
6.3.1 Experimental design	71
6.3.2 Processive unwinding of Rep helicase	72
6.3.3 Heterogeneity of unwinding rates.....	75
6.3.4 Mutation in 1B-2B domain interaction surface enhance unwinding activity	76
6.3.5 A powerful super helicase	77
6.4 Extending conformational control to another SF1 helicase, PcrA	80
6.5 Summary	81
6.6 References	81
Appendix A.....	86
Appendix B.....	87
Protocols	88
DNA constructs	88
3.2 kbp dsDNA + short ssDNA construct	88

3.4 kbp dsDNA	90
dsDNA (~3kbp) + long ssDNA (~1700nt)	91
6 kbp dsDNA+3'-overhang	94
Bead preparation	95
Anti Digoxigenin coated beads.....	95
Streptavidin beads.....	95

List of Figures

Figure 1-1. Ray optics description of the gradient force.	8
Figure 1-2. Back focal interferometry.	10
Figure 1-3. Power spectrum of a trapped bead.	11
Figure 1-4. Typical examples of OT experimental layouts..	12
Figure 1-5. A generic optical tweezer diagram.....	14
Figure 1-6. Dual trap instrument layout.....	15
Figure 1-7. Demonstrations of antisymmetric and symmetric modes of fluctuations.....	17
Figure 1-8. Demonstration of 1-basepair resolution with DNA-tethered beads.....	17
Figure 2-1. <i>E. coli</i> SSB. Structural model and schematic representation of SSB.....	24
Figure 3-1. DNA Construct.....	35
Figure 3-2. Laminar flow cell.....	36
Figure 3-3. Schematic of optical trap experiment.	38
Figure 3-4. Representative force-extension behavior of bare DNA molecule (red) and SSB-bound molecule (blue)	39
Figure 3-5. Conformation of SSB-DNA complex under mechanical tension	41
Figure 3-6. Schematic representation of Δx	42
Figure 3-7. Δs vs. N_w based on a “toy” model and based on the crystal structure of the protein in (SSB) ₆₅ wrapping mode	43
Figure 3-8. Proposed energy landscape for SSB-ssDNA interactions.....	45
Figure 4-1. Kinetics of SSB binding and unbinding under mechanical tension.....	49
Figure 4-2. SSB binding kinetics	50
Figure 4-3. Binding rate force spectroscopy.....	51
Figure 4-4. Average binding and unbinding rates vs. tension	52
Figure 5-1. SSB binding constructs.....	58
Figure 5-2. Binding of multiple SSB. F-x behavior for “dT-175” ssDNA construct with and without protein.....	59
Figure 5-3. Binding of multiple SSB. F-x behavior for “dN1700” constructs with and without protein.....	60
Figure 6-1. The domain structure of <i>E. coli</i> Rep monomer.....	66
Figure 6-2. Crystal structures: “open” and “closed” forms of Rep helicase.....	67

Figure 6-3. Amino acids within the Rep monomer that appear to contact the ss-DNA.	68
Figure 6-4. Rep-X smFRET study assay.	70
Figure 6-5. Rep-X DNA construct.	71
Figure 6-6. Schematic of optical trap experiment.	72
Figure 6-7. Schematic representation of the two merging streams with different solution conditions and schematics of buffer exchange by moving chamber relative to dual trap positions.	73
Figure 6-8. Duplex DNA unwinding example traces at force feedback of 10 pN.....	74
Figure 6-9. Example traces of DNA length change versus time at 10 pN force and 1 mM ATP. 75	
Figure 6-10. Rep-X unwinding speed distribution	76
Figure 6-11. Example traces with no helicase activity and unwinding activity.	77
Figure 6-12. Dissociation and slip force measurement experiment traces.	78
Figure 6-13. Normalized rates versus force plots from individual traces of dissociation force measurement from Figure 6-12 with the same color coding.	79
Figure 6-14. Dissociation (blue) and slippage (red) force histograms.....	79
Figure 6-15. Duplex DNA unwinding traces by PcrA-X at force feedback of 10pN.....	81

List of Abbreviations

ATP	Adenosine-5'-triphosphate
bp	Base pair
BS	Binding Site
BSA	Bovine Serum Albumin
CM	Camera
DM	Dichroic Mirror
DNA	Deoxyribonucleic Acid
<i>E.Coli</i>	<i>Escherichia coli</i>
<i>Eco</i>	<i>Escherichia coli</i>
EM	Electron Microscope
FRET	Fluorescence resonance energy transfer
HSA	Human Serum Albumin
kbp	1000 base pairs
L	Lens
LH	Left Handle
NA	Numerical Aperture
NDP	Nucleoside-diphosphate
nt	nucleotide
O	Objective
OB	Oligonucleotide/Oligosaccharide Binding
OD	Outer Diameter
OT	Optical Trap
Pi	Phosphate
Pol III HE	Polymerase III Holoenzyme
RF	Replication Form
RH	Right Handle
RNA	Ribonucleic Acid
RNAP	RNA polymerase
SF	Superfamily
sm	single molecule

SM	Steerable Mirror
SNR	Signal-To-Noise Ratio
SSB	Single Stranded DNA Binding protein
T	Telescope
WP	Wave Plate
XP	Xeroderma Pigmentosum

Introduction

Protein-nucleic acid interactions lie at the heart of many fundamental processes in the living cell. They are involved in all facets of nucleic acid metabolism, ranging from regulation of transcription (ex: transcription factors), replication (ex: single-stranded DNA binding proteins), and recombination (ex: RecA and homologs), to compaction and packaging of the genome (ex: chromatin), to name just a few examples. Loosely speaking, Nature has explored two themes in nucleic-acid binding proteins. On one hand, sequence-specific proteins such as endonucleases and transcriptional repressors and activators must localize and bind to target sites in the DNA. Typically, these bind tightly to the genome in low numbers at a handful of highly specific base sequences. There, they either act directly on their substrates (ex: cleave the DNA) or regulate the activity of other proteins (ex: repress gene expression). At the other extreme, non-sequence-specific proteins bind non-specifically to the genome but may target particular nucleic acid structures. These include, for instance, architectural proteins like histones, single-stranded DNA binding proteins, and RecA-like proteins. In contrast to sequence-specific proteins, they generally act in larger numbers, oligomerizing to form nucleoprotein filaments (ex: RecA-DNA), or complex and highly organized superstructures (ex: chromatin). Often, these nucleic acid-protein complexes themselves act as substrates to recruit various other cellular proteins involved in maintenance of the genome.

While the main subject of enquiry in sequence-specific proteins is how they find their target on DNA, the central question in the other class is how they associate with each other and interact with other proteins, modulating their activity. In this study we aim to study protein-nucleic acid interactions using single-stranded DNA binding proteins (SSB) as a model system. To achieve this aim, we use techniques from traditional biochemistry and molecular biology, in combination with single-molecule biophysics. In particular, the use of high-resolution optical traps [1-3] enables us to study dynamics at the single-protein level in unprecedented detail.

Protein-nucleic acid interactions have long been studied by traditional methods such as crystallography and ensemble kinetics. Though structural methods provide an atom-scale description of protein-DNA interactions, the pictures are static. Ensemble biochemical techniques on the other hand can measure the kinetics of protein-DNA associations, but must rely on synchronizing populations of molecules to detect conformational dynamics. Often this is

difficult due to heterogeneity in the ensemble. Single-molecule techniques provide a powerful alternative to study these dynamics. Unlike traditional bulk methods, these techniques do not rely on temporal and population averaging, instead collecting statistics from individual molecules. In single-molecule studies, conformational dynamics are detected directly, providing a clear advantage over ensemble methods. Techniques such as single-molecule fluorescence, optical traps, and magnetic tweezers [4-12] have been instrumental in deciphering the mechanism of a wide range of molecular machines involved in nucleic acid metabolism, protein-DNA interactions, and the mechanical properties and dynamics of nucleic acid secondary and tertiary structures, to name just a few examples.

Optical traps (OT) or “tweezers” utilize the momentum carried by light to exert forces on micrometer-size dielectric objects. By tightly focusing a laser beam, a dielectric object such as a micrometer-size polystyrene bead can be stably trapped in all three dimensions near the focus of light [13]. Coupled with the ability to manipulate microscopic objects, OTs are sensitive quantitative tools. Because the trap behaves as a linear, “Hookean” spring near its center, it can be used—once properly calibrated—to detect displacements of the bead and measure the forces exerted on it.

Protein-DNA interactions have been studied extensively with single-molecule techniques in the last decade. OT-based assays have been used to characterize various DNA-binding proteins: chromatins [14-18], RecA and homologs [19-23], SSBs [24-26], and others [27]. However, many of these OT assays have suffered limitations. With some notable exceptions (ex: [17, 18]), many have lacked the resolution to detect dynamics at the single-protein level and thus have been limited to: (1) studying global properties of nucleoprotein interactions and how they are affected by substrate tension [19, 24-26], or (2) using OTs for manipulation purposes only, and employing another readout (fluorescence) for detecting the protein [20-22]. Single-molecule fluorescence methods pose a powerful alternative to OT assays, and have been used to detect protein interactions with DNA at the single-protein level [22, 28, 29]. However, fluorescence readouts are also limited in quantitative information content; they can relay the presence or absence of a protein [22], or uncalibrated, relative (and not absolute) changes in distances [28, 29]. An ideal measurement technique would allow one to distinguish not only the presence of a protein but also measure the conformational state of the nucleoprotein complex. Proteins that bind to DNA must interact with their substrates on length scales on the order of several basepairs

(1 bp = 3.4Å in duplex DNA). As a result, direct observation of these protein-nucleic acid interactions requires sensitivity to motions on the nanometer and even sub-nanometer scale.

The main goal of this thesis is to detect nucleic-acid binding protein dynamics at high spatial and temporal resolution. To achieve this aim, we use high-resolution optical traps that allow us to detect binding of SSBs to DNA at the individual-protein level. In Chapter 1 we give a brief introduction to optical trapping and discuss the nature of optical forces acting on a small, dielectric sphere in an aqueous medium. An overview of two popular theoretical models for optical trapping—the ray optics model and the electromagnetic field model—is provided. We describe the layouts of a generic single optical trap set-up and more sophisticated set-ups used for different applications in physics and biophysics. Example applications of optical traps in biophysics are given from the work of well-known labs. Recently, the resolution of optical tweezers has been improved by introducing a second trap. This technical development is discussed, and the theoretical model explaining the achievement of high resolution by differential detection is presented.

In Chapter 2 we give an introduction to single-stranded DNA binding proteins (SSB). We discuss historical perspective, biological importance of SSB in nucleic-acid metabolism, and the physical nature of SSB-DNA interactions. The detailed description of the force spectroscopic study of individual SSB using optical traps is given in Chapter 3. We describe the use of a DNA substrate where only a single SSB can bind, and discuss how applied tension on DNA affects the conformation of SSB-DNA complex. We also present a theoretical model for the SSB-DNA complex conformation that agrees with our experimental observations.

In Chapter 4 we extend our high-resolution optical trap studies of SSB-DNA interaction to the SSB binding dynamics. In Chapter 5 we discuss whether having multiple binding sites for SSB on the DNA substrate affects the interaction of SSB with DNA.

In Chapter 6 we move from the binding interaction of single-stranded DNA with SSBs to the enzymatic interaction of double-stranded DNA with a motor protein Rep helicase. We explore how the protein conformation of helicases can modulate the way they interact with DNA: change in helicase conformation results in enhanced unwinding activity and increased processivity. These results suggest that accessory proteins may regulate helicase activity by conformation control *in vivo*.

References

1. Abbondanzieri, E.A., et al., *Direct observation of base-pair stepping by RNA polymerase*. Nature, 2005. 438(7067): p. 460-465.
2. Carter, A.R., Y. Seol, and T.T. Perkins, *Precision surface-coupled optical-trapping assay with one-basepair resolution*. Biophys J, 2009. 96(7): p. 2926-34.
3. Moffitt, J.R., et al., *Differential detection of dual traps improves the spatial resolution of optical tweezers*. Proc Natl Acad Sci U S A, 2006. 103(24): p. 9006-11.
4. Mehta, A.D., et al., *Single-molecule biomechanics with optical methods*. Science, 1999. 283(5408): p. 1689-95.
5. Bustamante, C., Z. Bryant, and S.B. Smith, *Ten years of tension: single-molecule DNA mechanics*. Nature, 2003. 421(6921): p. 423-7.
6. Peterman, E.J., H. Sosa, and W.E. Moerner, *Single-molecule fluorescence spectroscopy and microscopy of biomolecular motors*. Annu Rev Phys Chem, 2004. 55: p. 79-96.
7. Myong, S., B.C. Stevens, and T. Ha, *Bridging conformational dynamics and function using single-molecule spectroscopy*. Structure, 2006. 14(4): p. 633-43.
8. Greenleaf, W.J., M.T. Woodside, and S.M. Block, *High-resolution, single-molecule measurements of biomolecular motion*. Annu Rev Biophys Biomol Struct, 2007. 36: p. 171-90.
9. van Mameren, J., E.J. Peterman, and G.J. Wuite, *See me, feel me: methods to concurrently visualize and manipulate single DNA molecules and associated proteins*. Nucleic Acids Res, 2008. 36(13): p. 4381-9.
10. Allemand, J.F., D. Bensimon, and V. Croquette, *Stretching DNA and RNA to probe their interactions with proteins*. Curr Opin Struct Biol, 2003. 13(3): p. 266-74.
11. Ha, T., *Single-molecule fluorescence methods for the study of nucleic acids*. Curr Opin Struct Biol, 2001. 11(3): p. 287-92.
12. Bockelmann, U., *Single-molecule manipulation of nucleic acids*. Curr Opin Struct Biol, 2004. 14(3): p. 368-73.
13. Ashkin, A., *Observation of a single-beam gradient force optical trap for dielectric particles*. Opt Lett, 1986. 11(5): p. 288-290.
14. Brower-Toland, B. and M.D. Wang, *Use of optical trapping techniques to study single-nucleosome dynamics*. Methods Enzymol, 2004. 376: p. 62-72.
15. Mihardja, S., et al., *Effect of force on mononucleosomal dynamics*. Proc Natl Acad Sci U S A, 2006. 103(43): p. 15871-6.
16. Bennink, M.L., et al., *Unfolding individual nucleosomes by stretching single chromatin fibers with optical tweezers*. Nat Struct Biol, 2001. 8(7): p. 606-10.
17. Dame, R.T., M.C. Noom, and G.J. Wuite, *Bacterial chromatin organization by H-NS protein unravelled using dual DNA manipulation*. Nature, 2006. 444(7117): p. 387-90.
18. Brower-Toland, B.D., et al., *Mechanical disruption of individual nucleosomes reveals a reversible multistage release of DNA*. Proc Natl Acad Sci U S A, 2002. 99(4): p. 1960-5.
19. Hegner, M., S.B. Smith, and C. Bustamante, *Polymerization and mechanical properties of single RecA-DNA filaments*. Proc Natl Acad Sci U S A, 1999. 96(18): p. 10109-14.
20. Galletto, R., et al., *Direct observation of individual RecA filaments assembling on single DNA molecules*. Nature, 2006. 443(7113): p. 875-8.

21. Mameren, J., et al., *Dissecting elastic heterogeneity along DNA molecules coated partly with Rad51 using concurrent fluorescence microscopy and optical tweezers*. Biophys J, 2006. 91(8): p. L78-80.
22. van Mameren, J., et al., *Counting RAD51 proteins disassembling from nucleoprotein filaments under tension*. Nature, 2009. 457(7230): p. 745-8.
23. Shivashankar, G.V., et al., *RecA polymerization on double-stranded DNA by using single-molecule manipulation: the role of ATP hydrolysis*. Proc Natl Acad Sci U S A, 1999. 96(14): p. 7916-21.
24. Hatch, K., et al., *Measurement of the salt-dependent stabilization of partially open DNA by Escherichia coli SSB protein*. Nucleic Acids Res, 2008. 36(1): p. 294-9.
25. Pant, K., et al., *Mechanical measurement of single-molecule binding rates: kinetics of DNA helix-destabilization by T4 gene 32 protein*. J Mol Biol, 2004. 336(4): p. 851-70.
26. Shokri, L., et al., *Kinetics and thermodynamics of salt-dependent T7 gene 2.5 protein binding to single- and double-stranded DNA*. Nucleic Acids Res, 2008. 36(17): p. 5668-77.
27. Ali, B.M., et al., *Compaction of single DNA molecules induced by binding of integration host factor (IHF)*. Proc Natl Acad Sci U S A, 2001. 98(19): p. 10658-63.
28. Roy, R., et al., *Dynamic structural rearrangements between DNA binding modes of E. coli SSB protein*. J Mol Biol, 2007. 369(5): p. 1244-57.
29. Joo, C., et al., *Real-time observation of RecA filament dynamics with single monomer resolution*. Cell, 2006. 126(3): p. 515-27.

Chapter 1. Introduction to single molecule optical trap

1.1 Optical Trapping

1.1.1 Introduction

In the last few decades novel laser trapping and manipulation techniques have been developed. Their application ranges from trapping of neutral atoms to manipulation of live bacteria and viruses [2, 3]. The particle types that can be studied are as diverse as atoms, molecules, submicron particles, and macroscopic dielectric particles hundreds of micrometers in size [4, 5]. Even living biological cells and organelles within cells can be trapped and manipulated free of optical damage [2, 6, 7]. The unique capabilities of these techniques have had a great impact in various sub-fields of science. To name a few examples, in the field of light scattering, particularly in studies of Mie scattering, high resolution observations of the resonant behavior of macroscopic spherical particles have been observed for the first time [4, 5]. The results have led to applications of these resonant frequencies in linear and nonlinear optics and lasers [10]. In atomic physics, for the first time individual atoms have been laser trapped and cooled down to the lowest man-made temperatures [11, 12]. These techniques have led to the study of a new state of matter: the Bose–Einstein condensate [13]. Practical advances in the biological sciences and chemistry have also been made. Use of laser techniques has had a revolutionary impact on the study of single molecule biophysics: trapping and manipulation of single living cells [3, 14], organelles within cells, single biological molecules [15, 16], and the measurement of physical properties of biopolymers [17, 18].

It was not known previously that one could use radiation pressure forces to make a stable 3-dimensional optical trap. In the early 1970s Arthur Ashkin and co-workers pioneered the field of laser-based optical trapping. In a series of fundamental papers they demonstrated that micron-sized dielectric particles could be manipulated using optical forces in both water and air [19] and they came up with a stable, three-dimensional trap based on counter propagating laser beams [20]. In 1986 came the development of the single-beam gradient force optical trap [21] which is known today as “optical tweezers” [22]. Ashkin and co-workers showed that one could use forces from focused laser beams to significantly affect the dynamics of small transparent micrometer-sized neutral particles. Two basic light pressure forces were identified: a *scattering*

force in the direction of the incident light beam, and a *gradient* force in the direction of the intensity gradient of the beam. It was shown experimentally that, using just these forces, one could accelerate, decelerate, and even stably trap small micron sized neutral particles using mildly focused laser beams. Ashkin and co-workers employed the unique capabilities of optical trapping technology to a wide range of applications ranging from the cooling and trapping of neutral atoms [23] to manipulating live bacteria and viruses [2, 24]. Today, optical traps continue to find applications in both physics and biology.

Technology developments to optical traps have allowed researchers to apply piconewton-level forces to micron-sized particles and simultaneously measure displacement with nanometer-level precision and with high temporal resolution. Optical tweezers are now routinely applied to the study of molecular motors at the single-molecule level [15, 25-34] the physics of colloids and mesoscopic systems [35-42] and the mechanical properties of polymers and biopolymers [18, 25, 39, 43-55]. While optical traps are applied in different sciences, theoretical and experimental work on fundamental aspects of optical trapping is still ongoing [22, 39, 56-60]. Many excellent reviews of optical trapping [15, 61-63] and specialized applications of optical traps as well as several comprehensive guides for building optical traps are now available [64-67].

1.1.2 Basic trap principles

For a dielectric particle trapped with optical tweezers, the main optical forces can be divided into two categories: absorption and scattering forces on one end, and conservative gradient forces on the other. Absorption forces can be minimized by choosing a trapping particle that is off-resonance. Hence, only the scattering force and the gradient force are considered significant for optical tweezers [64]. As its name suggests, the scattering force arises due to the direct scattering of photons. The scattering force acts in the same direction as incident light and is proportional to the intensity of incident light. The gradient force arises from the time-averaged interaction of the induced dipole with the inhomogeneous field. Gradient forces occur whenever a transparent material with a refractive index greater than its surrounding medium is placed within a light gradient. The gradient force acts in the direction of increasing light intensity and is proportional to the gradient of light intensity. If a dielectric particle is placed within the narrow waist of a sharply focused beam of light, the scattering force will have a tendency to push the particle away, while the gradient force will have a tendency to hold the particle within the waist. Stable trapping occurs when the gradient force is strong enough to overcome the scattering force.

A strong gradient force can be achieved by using a high numerical aperture (NA) lens to focus a laser beam tightly.

Although the physics behind optical tweezers is not trivial, its behavior can be explained using two different theoretical models. For a trapped particle with diameter d much larger than the wavelength λ of the trapping laser ($d \gg \lambda$), a ray optics model shows good agreement with measured results, whereas for a particle with diameter much smaller than the trapping wavelength ($d \ll \lambda$), an electromagnetic field model provides best agreement [68]. In the intermediate size regime ($d \sim \lambda$), electromagnetic theory has yielded better results than ray optics, but neither model has been satisfactory [68, 69]. In the absence of an accurate model for the intermediate regime, the behavior of trapped particles in this regime is determined empirically.

The ray optics model is valid for particles in the Mie regime in which particles are much larger than the laser wavelength (in practice, $d > 10\lambda$). According to this model, the basic operation of optical tweezers can be explained by the momentum transfer associated with the redirection of light at a dielectric interface. Light that has an intensity gradient increasing from left to right impinges on the bead (**Figure 1-1a**). Two rays of light of different intensities are

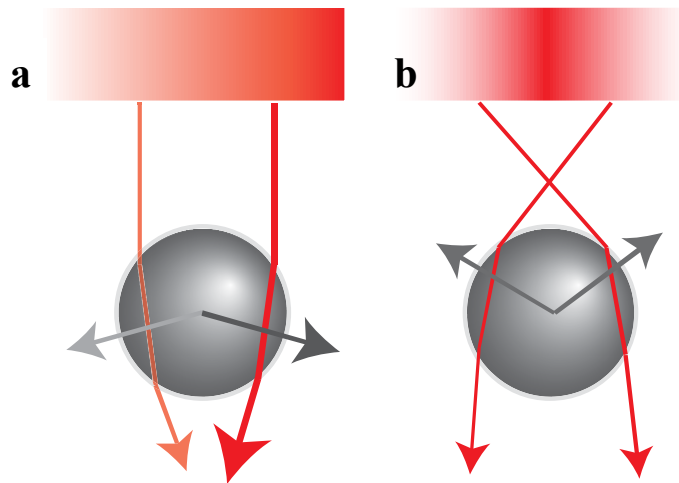


Figure 1-1. Ray optics description of the gradient force. Adapted from Ref. [8]

represented by red lines of different thickness and saturation. The refraction of the rays by the bead changes the momentum of the photons, equal to the change in the direction of the input and output rays. Due to conservation of momentum, the momentum of the bead changes so that it

compensates the changed momentum of light. The net force is denoted by the gray arrows. If one sums up the two grey arrows the resulting forces will point towards higher intensity region and slightly down. To trap stably an object in all 3 dimensions, one must have a gradient along the axial direction as well (**Figure 1-1b**). This is achieved by focusing the beam. If one plots two rays on opposite sides of the bead (represented in red), and calculate the net force exerted on the bead, it will point to the focus. At equilibrium, lateral forces will cancel out while the axial force applied on the bead will cancel out with the scattering force (not shown) which tends to push the bead along the direction of light.

In case the trapped sphere is much smaller than the wavelength of the trapping laser, i.e., $d \ll \lambda$, the Raleigh regime is valid and optical forces can be calculated by treating the particle as a point dipole. For a sphere of radius d , this force is

$$F_{scat} = \frac{I_0 \sigma n_m}{c} \quad (1-1)$$

where σ is the scattering cross section of the sphere,

$$\sigma = \frac{128\pi^5 d^6}{3\lambda^4} \left(\frac{m^2 - 1}{m^2 + 2} \right)^2 \quad (1-2)$$

and where I_0 is the intensity of the incident light, n_m is the index of refraction of the medium, c is the speed of light in vacuum, m is the ratio of the index of refraction of the particle to the index of the medium (n_p/n_m), and λ is the wavelength of the trapping laser. Thus, the scattering force is in the direction of the incident light and is proportional to the intensity. The gradient force arises as a result of the interaction with light in which the laser field polarizes the atom, and the polarized atom experiences a force in the gradient of an electromagnetic field.

$$F_{grad} = \frac{2\pi\alpha}{cn_m^2} \nabla I_0 \quad (1-3)$$

where

$$\alpha = n_m^2 d^3 \left(\frac{m^2 - 1}{m^2 + 2} \right) \quad (1-4)$$

is the polarizability of the sphere. The gradient force is proportional to the intensity gradient, and points up the gradient when $m > 1$. When the dimensions of the trapped particle are comparable to the wavelength of the trapping laser ($d \sim \lambda$), neither of the above approaches are accurate or valid. More complex physical and mathematical approaches are required [70, 71].

The majority of objects that are useful or interesting to trap in biophysics fall into this intermediate size range ($0.1\text{--}10\lambda$). Biological specimens that can be trapped directly, e.g., bacteria, yeast, and organelles of larger cells fall into this range. In addition, it is common to work with objects that can be seen by video microscopy ($\sim 0.1\text{ }\mu\text{m}$). Usually dielectric microspheres with a diameter of $\sim 0.2\text{--}5\text{ }\mu\text{m}$ are used as handles to manipulate biological macromolecules like DNA, RNA, and other biopolymers.

1.1.3 Detection in optical traps

Optical traps are used not only as a technique to manipulate biological macromolecules but also for quantitative measurements. Thus, sensitive position detection within the traps is important for quantitative trapping. Force and position displacement rely on a well calibrated system, which is feasible for only spherical objects such as μm sized beads. One of the methods to detect nanoscale displacements of beads from the focus of the optical trap is based on the interaction of laser light with the beads, called back focal plane interferometry [8, 72] (**Figure 1-2**).

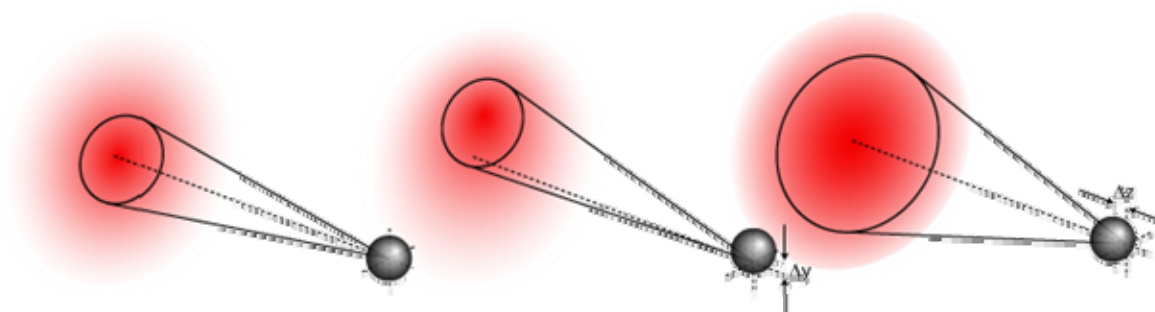


Figure 1-2. Back focal interferometry. Light patterns on a detector depending on position of trapped bead.

This method uses the interference pattern between forward-scattered light from the bead and unscattered light that is monitored by a position sensitive detector. The light pattern on the detector is converted to axial voltage readings. Separation in any axis between the center of the optical trap and the bead changes the interference pattern, which generates a linear response in the voltage read-out. In order to translate or convert these voltages into real displacement, calibration is necessary.

1.1.4 Optical Trap Calibration

As mentioned before the output of data collected from optical trap experiments are voltage readings from detectors. In order to be able to analyze that data one has to calibrate the instrument and beads beforehand. The most important calibrations are the conversion factor ρ from the voltage on the detector into displacement of the bead from the trap, and the stiffness α of the trap which determines force.

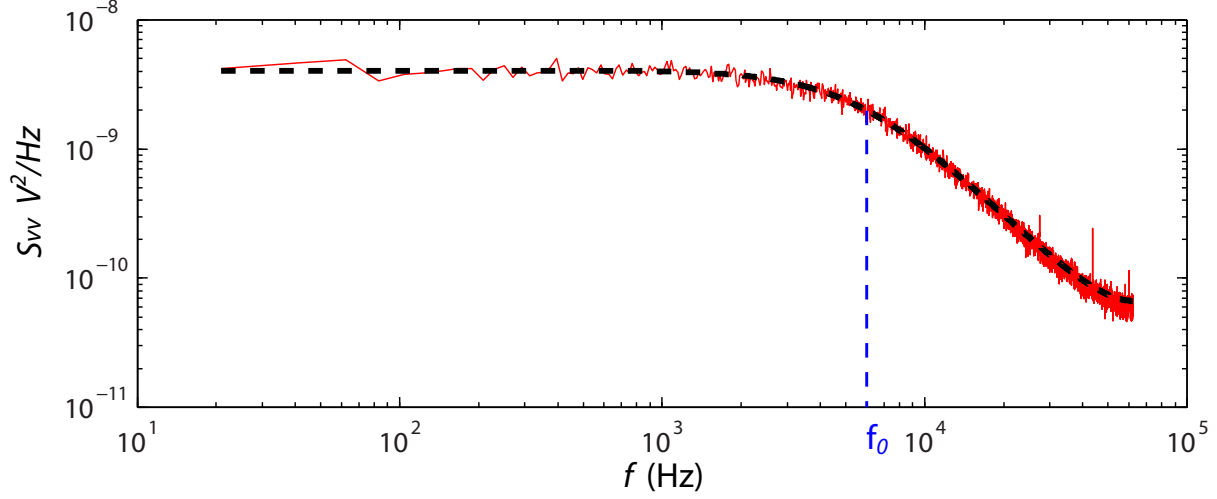


Figure 1-3. Power spectrum of a trapped bead. Raw power spectrum (red) and fit (black dashed line) to a Lorentzian. f_0 is the roll-off frequency.

There are different methods to calibrate the trap. I will focus on only one of them that is typically used in our optical trap. The calibration method we use benefits from the properties of the Brownian motion of a bead [8, 73]. Typically we collect data on a trapped bead with a high-frequency bandwidth of about 125 kHz. Using Matlab code we obtain a one-sided power spectrum for thermal motion (**Figure 1-3**), which should fit to

$$S_{xx}(f) = \frac{k_B T}{\pi^2 \beta (f_0^2 + f^2)} \quad (1-5)$$

where $S_{xx}(f)$ is in units of displacement²/Hz, k_B is Boltzmann's constant, β is the hydrodynamic drag coefficient of the object (e.g., $\beta = 6\pi\eta d$ for Stokes drag on a sphere of radius d in a medium with viscosity η), and f_0 is the roll-off frequency, related to the trap stiffness through $f_0 = \alpha(2\pi\beta)^{-1}$ for a stiffness α .

As mentioned before, the detector measures voltages, thus the spectrum will be $S_{vv}(f)$ in volts²/Hz. $S_{vv}(f)$ is related to the true power spectrum by $S_{vv}(f) = \rho^2 S_{xx}(f)$, where ρ represents the

conversion of the detector in volts/unit distance. $S_{xx}(f)$ asymptotically approaches the limit $k_B T / \pi^2 \beta f_0^2$ for $f \ll f_0$, so the conversion factor can be found by replacing $S_{xx}(f)$ with $S_{vv}(f)/\rho^2$ at low frequencies.

$$\rho = (S_{vv}(f)\pi^2\beta f_0^2/k_B T)^2 \quad (1-6)$$

1.1.5 Trapping geometries

Once properly calibrated, optical traps can be used for quantitative measurements using different tethering approaches. In most trap setups one bead is attached to one end of a molecule of study (ex: DNA, motor protein). That bead is used for manipulation and the other end is usually immobilized to the surface (**Figure 1-4a**) or attached to another bead held by a micropipette [**Figure 1-4b**]. As forces are applied, stretching the tethered molecule, displacements of the trapped bead (Δx , in **Figure 1-4**) report on the actions of the biological system under study. In **Figure 1-4a** a cartoon of an experimental design is shown for a single beam optical trap. In this assay, kinesin, a protein that is responsible for translocation inside

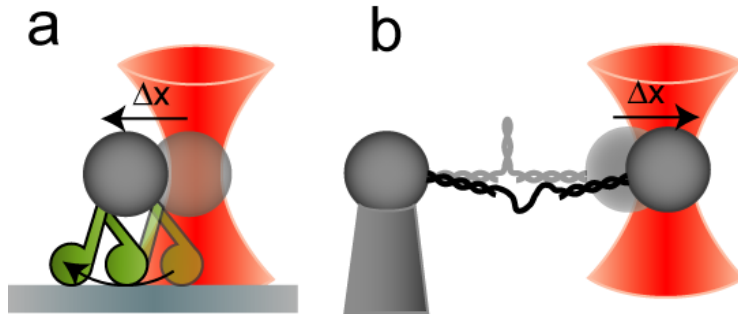


Figure 1-4. Typical examples of OT experimental layouts. a) A surface-based assay of kinesin. b) Micropipette-based assay of DNA hairpin unwinding. Adapted with permission from ref. [1], © 2008 Annual Reviews.

the cell, is attached to a 0.5- μm silica bead, and a microtubule, the track that kinesin walks on, was immobilized on to the surface. Visscher *et al.* [75] used this approach to show that kinesin moves in discrete steps of 8 nm. In **Figure 1-4b** is shown an experimental design where the thermodynamics of RNA hairpin formation was studied under various forces, similar to that used by Liphardt *et al.* [76].

The above tethering approaches have been used to study a variety of systems and have improved our understanding of many processes [55, 75, 77-79]. The major drawback of the above tethering designs is coupling of vibrational noise to the sample stage. This alone limits spatial resolution. In order to overcome this problem several designs have been used, one of which will be described in the next part.

1.2 High resolution optical trapping

1.2.1 Introduction

In the last decade, the necessity for traps that are capable of resolving base pair steps has arisen. Proteins that bind to DNA must interact with their substrates on length scales on the order of several basepairs (1 bp = 3.4Å in duplex DNA). Direct observation of these protein-nucleic acid interactions requires sensitivity to motions on the nanometer and even sub-nanometer scale. One of the shortcomings of a single trap is that it is coupled to a fixed surface, be it a glass surface or a micropipette [80]. Since fixed surfaces drift due to temperature variations and mechanical vibrations, this limits the resolution of the trap. Using a second trap as a substitute was a breakthrough in achieving high resolution optical traps. This is still not enough to resolve base pair steps, due to environmental limitations such as acoustical noise, temperature and air fluctuations etc. In order to overcome these problems, the setup should be placed on an optical table in sound-isolated and temperature-controlled rooms in the basement. The recent technical development of high-resolution optical tweezers [9, 81, 82] has made possible, for the first time, the direct observation of molecular motion on the basepair scale. This advance has stemmed from improved isolation from the environment [8, 83], reducing much of the drift observed in “traditional” designs [9, 81, 82] (ex: air density fluctuation).

Even so, measurements are still affected by Brownian motion of the trapped beads. One can reduce this noise by decreasing temperature, but this is not a viable option when studying biological systems since they require room temperature to be active. This problem has been overcome by the Bustamante lab, where for the first time, a high resolution trap with differential detection was built [9]. The main idea is that the Brownian noise of the two beads is correlated through tethers between the beads, which allows one to subtract part of the noise and improve resolution.

1.2.2 Dual Trap Setup

First I discuss a generic optical trap layout which is shown in **Figure 1-5**, and then I will describe advantages of using a dual optical trap. A laser beam is expanded by a simple telescope (lenses $L1$ and $L2$) to match roughly the objective back aperture. A second telescope in a 1:1

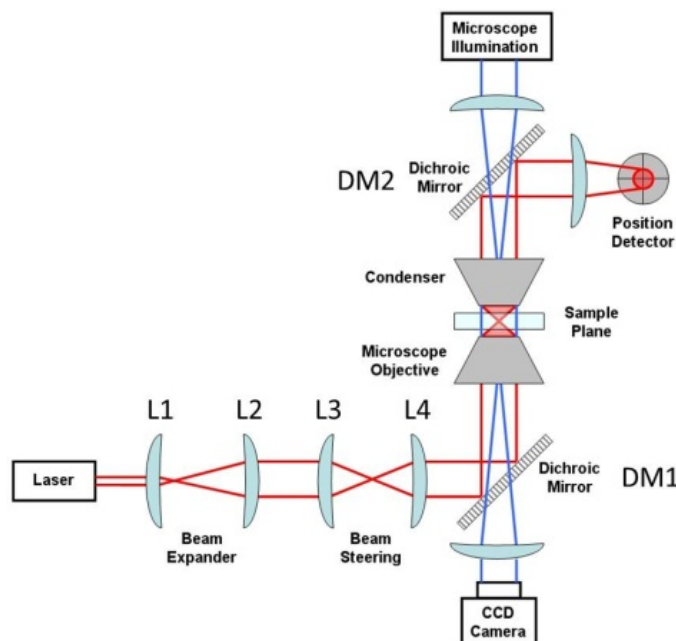


Figure 1-5. A generic optical tweezer diagram. Adapted from Wikipedia

configuration is used to steer the optical trap in the specimen plane. The microscope objective focuses the beam to create a trap, and then forward scattered light is collected by the condenser and coupled to the detector. DM1 and DM2 are dichroic mirrors that reflect the infrared beam to the trap and allow visible light to pass through and illuminate the sample plane. The setup is built so that lens $L3$ (steering lens) and microscope objective are conjugate. As a result, if one changes the position of $L3$ the beam at the aperture will translate in the specimen plane with minimal beam clipping.

As mentioned above the resolution of single optical trap are limited by vibrational and environmental noise coupled to a bead position measurements. In order to overcome this, a second optical trap is necessary. Here I describe one such layouts based on Bustamante design [9] that I closely participated in building. The dual trap located in the basement of Loomis is in a

temperature-controlled room coated with foam for vibration isolation (**Figure 1-6**). All optical components were mounted on vibration isolated table (TMC 14-414-34). The dual traps were formed from orthogonal polarizations of a single laser (a 5-W, 1064-nm diode-pumped solid-state laser, IPG Photonics YLR-5-1064-LP). The beam from an infrared laser is split into two orthogonally polarized beams with the beam splitter PB1, the separation between the two traps was controlled by a piezo-actuated mirror stage SM (Nano-MTA, MadCityLabs). Then, with the beam splitter PB2 they are recombined back and aligned perfectly co-linear. Making the beams overlap is extremely important. Air fluctuations introduce low frequency noise on trap

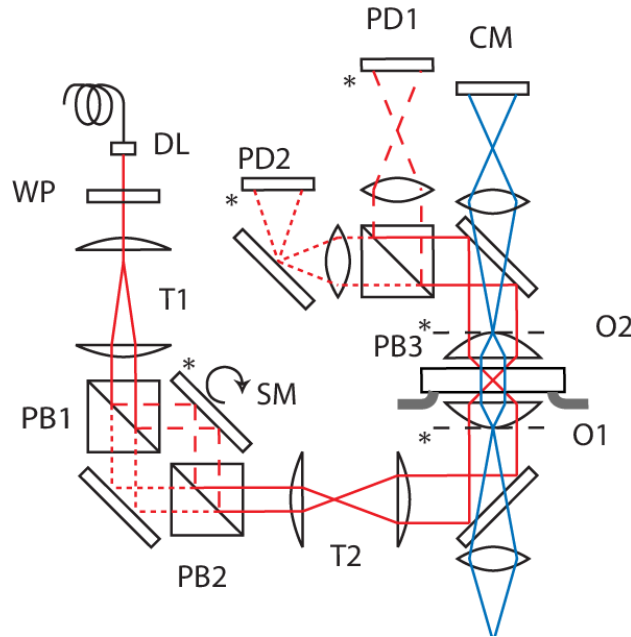


Figure 1-6. Dual trap instrument layout
Adapted from Ref. [9].

positions which will show up in both traps with the same displacement, so differential detection of beads will cancel the noise. The only optical path where the two traps are not co-linear before entering the objective is the space between the two beam splitters, so it is important to minimize this space. The beams are then focused to create two traps in the sample plane between the two high NA objectives O1 and O2 (Nikon CFI Plan Apo VC 60x/1.2 Water Immersion objective from Fryer Company Inc.). The condenser O2 collects the light, then the beam splitter PB3 separates the two orthogonally polarized beams and by additional lenses, the beams are projected onto position detectors. Another important point is that the setup is built so that the steering

mirror SM, the back focal plane of the objectives, and the detector detection plane are conjugate (conjugate planes are denoted as stars). If one changes the angle of the SM, the beam at the aperture of objectives will translate in the specimen plane with minimal beam clipping. The same is true for the position detectors; steering of the trap will not affect the position of the beam on the detector plane.

The detection of laser beams was done using position sensitive detectors (PD1 and PD2). Trap stiffnesses were controlled using two rotary motors from New Focus with mounted half wave plates (WP). All motion controllers and piezo-actuated mirror were manipulated from computer outside of the room using Labview software. Data acquisition was collected using Daq card from National Instrument and saved into computer.

1.2.3 Differential detection improves spatial resolution [9]

A dual trap setup offers a significant resolution advantage over a single trap [9]. Given a signal ΔL due to a change in the DNA tether length from binding or action of a protein, the signal-to-noise ratio of a dual trap for one of the traps is given by

$$SNR_1 = \frac{k_{DNA}\Delta L}{\sqrt{4k_BTB}} \frac{k_2 k_{DNA}}{\sqrt{\gamma_1(k_2 + k_{DNA})^2 + \gamma_2 k_{DNA}^2}} \quad (1-7)$$

where γ_1 and γ_2 are drag coefficients of the two beads, k_1 and k_2 are trap stiffnesses, T is the temperature of medium, B is measurement bandwidth, and k_{DNA} is the DNA stiffness. Changing 1 to 2 gives the signal-to-noise ratio for the second trap. The signal-to-noise ratio for single trap optical tweezers is:

$$SNR_{single} = \frac{k_{DNA}\Delta L}{\sqrt{4k_BTB\gamma_1}} \quad (1-8)$$

Both SNR_1 and SNR_{single} scale similarly with bandwidth and drag coefficient, but SNR_1 saturates with k_{DNA} and $SNR_{single} > SNR_1$. As a result, addition of a second trap increases Brownian noise level. However, if one measures the *position difference* (1 – 2) the signal-to-noise ratio is:

$$SNR_{opt} = \frac{k_{DNA}\Delta L}{\sqrt{4k_BTB\gamma_{eff}}} \quad (1-9)$$

where $\gamma_{eff} = \gamma_1\gamma_2/(\gamma_1 + \gamma_2)$.

Since $\gamma_{eff} < \gamma_1, \gamma_2$, SNR_{opt} is always higher than SNR_1 or SNR_{single} . Thus, differential detection not only helps to improve resolution limited by air fluctuations, but also decrease noise associated with Brownian motion of beads [9]. The brief explanation of this phenomenon can be

easily described if one divides fluctuations of a system into two modes: symmetric and antisymmetric (**Figure 1-7**). In a differential measurement, symmetric fluctuations cancel

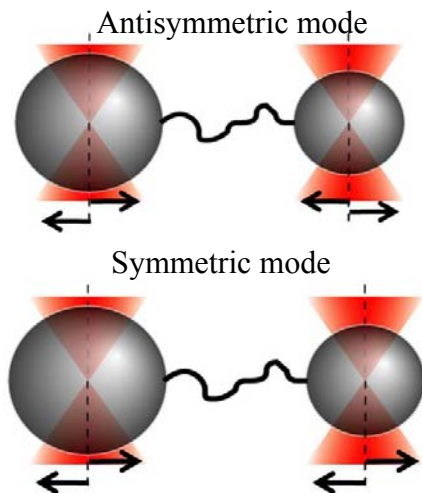


Figure 1-7. Demonstrations of antisymmetric and symmetric modes of fluctuations

out and one only measures antisymmetric fluctuations. Thus by measuring the position difference, all noise not directly relevant to the detection of the signal is rejected and the signal to noise ratio is SNR_{opt} .

Our apparatus can achieve single-basepair resolution, as demonstrated in proof-of-principle

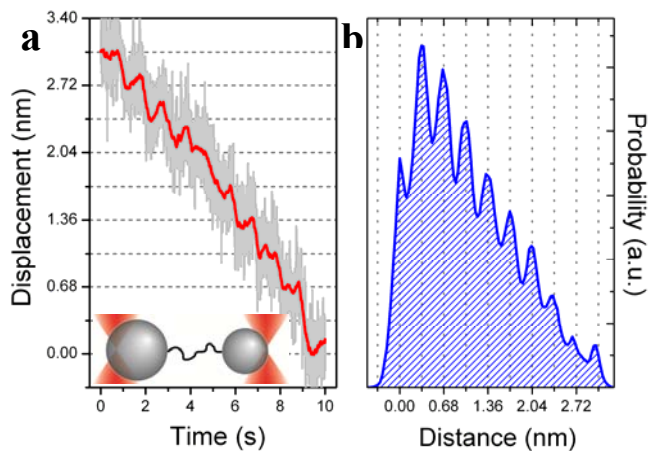


Figure 1-8. Demonstration of 1-basepair resolution with DNA-tethered beads (inset). **a)** Observed bead displacements at 100Hz (gray) and averaged to 10Hz (red). **b)** Corresponding pairwise distribution plots.

experiments in which DNA-tethered beads are held in the dual traps and one trap is displaced relative to the other in steps of 0.34 nm (**Figure 1-8**).

1.2.4 Application of high resolution optical traps

High resolution optical traps provide the cutting edge in sensitivity and are just beginning to be applied to biological questions. These optical traps are used to study molecular motors, proteins that can translocate on the variety of substrates. There are many good examples [84-88] but I will describe only few interesting and important discoveries that have been made using high resolution optical traps. A study of virus packaging motor was done by the Bustamante lab using dual optical trap [86]. They developed an assay where they could study the packaging mechanism of *Bacillus subtilis* bacteriophage $\phi 29$, applying different loading forces and varying ATP concentration. In this study they were able to show that DNA is packaged in 10-bp increments, where each step was composed of four 2.5-bp steps. This was surprising since no one knew or proposed previously in scientific publications that a step size can be a non-integer number.

A very important enzyme was studied by the Block group at Stanford [81]. *E.coli* RNAP is the protein that drives transcription, translocating along DNA while synthesizing messenger RNA from a DNA sequence. As a result of their studies they showed that RNAP takes single base pair steps at a time. Moreover they were able to give insight about the mechanism of translocation of RNAP on a DNA substrate.

Despite these advances, high-resolution OTs have yet to be applied in the context of nucleic-acid binding proteins. This new instrumentation has the potential to go beyond the limitations of previous assays, probing interactions not only at the single-protein level but also at finer length scales.

1.3 References

1. Moffitt, J.R., et al., *Recent advances in optical tweezers*. Annual Review of Biochemistry, 2008. 77: p. 205-228.
2. Ashkin, A. and J.M. Dziedzic, *Optical Trapping and Manipulation of Viruses and Bacteria*. Science, 1987. 235(4795): p. 1517-1520.
3. Min, T.L., et al., *High-resolution, long-term characterization of bacterial motility using optical tweezers*. Nature Methods, 2009. 6(11): p. 831-U71.

4. Ashkin, A. and J.M. Dziedzic, *Observation of Resonances in Radiation Pressure on Dielectric Spheres*. Physical Review Letters, 1977. 38(23): p. 1351-1354.
5. Ashkin, A. and J.M. Dziedzic, *Observation of Optical Resonances of Dielectric Spheres by Light-Scattering*. Applied Optics, 1981. 20(10): p. 1803-1814.
6. Ashkin, A., J.M. Dziedzic, and T. Yamane, *Optical Trapping and Manipulation of Single Cells Using Infrared-Laser Beams*. Nature, 1987. 330(6150): p. 769-771.
7. Ashkin, A. and J.M. Dziedzic, *Internal Cell Manipulation Using Infrared-Laser Traps*. Proceedings of the National Academy of Sciences of the United States of America, 1989. 86(20): p. 7914-7918.
8. Neuman, K.C. and S.M. Block, *Optical trapping*. Rev Sci Instrum, 2004. 75(9): p. 2787-809.
9. Moffitt, J.R., et al., *Differential detection of dual traps improves the spatial resolution of optical tweezers*. Proc Natl Acad Sci U S A, 2006. 103(24): p. 9006-11.
10. Gmachl, C., *High-power directional emission from microlasers with chaotic resonators (vol 280, pg 1556, 1998)*. Science, 1998. 282(5386): p. 49-50.
11. Chu, S., *The manipulation of neutral particles*. Reviews of Modern Physics, 1998. 70(3): p. 685-706.
12. Chu, S., et al., *3-Dimensional Viscous Confinement and Cooling of Atoms by Resonance Radiation Pressure*. Physical Review Letters, 1985. 55(1): p. 48-51.
13. Ketterle, W., *Nobel lecture: When atoms behave as waves: Bose-Einstein condensation and the atom laser*. Reviews of Modern Physics, 2002. 74(4): p. 1131-1151.
14. Nelson, K.E., et al., *Evidence for lateral gene transfer between Archaea and bacteria from genome sequence of Thermotoga maritima*. Nature, 1999. 399(6734): p. 323-9.
15. Svoboda, K. and S.M. Block, *Biological Applications Of Optical Forces*. Annual Review Of Biophysics And Biomolecular Structure, 1994. 23: p. 247-285.
16. Finer, J.T., R.M. Simmons, and J.A. Spudis, *Single Myosin Molecule Mechanics - Piconewton Forces and Nanometer Steps*. Nature, 1994. 368(6467): p. 113-119.
17. Kurachi, M., M. Hoshi, and H. Tashiro, *Buckling of a single microtubule by optical trapping forces: direct measurement of microtubule rigidity*. Cell Motil Cytoskeleton, 1995. 30(3): p. 221-8.
18. Smith, S.B., Y. Cui, and C. Bustamante, *Overstretching B-DNA: the elastic response of individual double-stranded and single-stranded DNA molecules*. Science, 1996. 271(5250): p. 795-9.
19. Ashkin, A., *Acceleration and Trapping of Particles by Radiation Pressure*. Physical Review Letters, 1970. 24(4): p. 156-&.
20. Ashkin, A. and J.M. Dziedzic, *Optical Levitation by Radiation Pressure*. Applied Physics Letters, 1971. 19(8): p. 283-&.
21. Ashkin, A., et al., *Observation of a Single-Beam Gradient Force Optical Trap for Dielectric Particles*. Optics Letters, 1986. 11(5): p. 288-290.
22. Ashkin, A., *History of optical trapping and manipulation of small-neutral particle, atoms, and molecules*. Ieee Journal of Selected Topics in Quantum Electronics, 2000. 6(6): p. 841-856.
23. Chu, S., et al., *Experimental observation of optically trapped atoms*. Physical Review Letters, 1986. 57(3): p. 314-317.
24. Ashkin, A., J.M. Dziedzic, and T. Yamane, *Optical trapping and manipulation of single cells using infrared laser beams*. Nature, 1987. 330(6150): p. 769-71.

25. Bustamante, C., J.C. Macosko, and G.J. Wuite, *Grabbing the cat by the tail: manipulating molecules one by one*. Nat Rev Mol Cell Biol, 2000. 1(2): p. 130-6.
26. Ishii, Y., A. Ishijima, and T. Yanagida, *Single molecule nanomanipulation of biomolecules*. Trends Biotechnol, 2001. 19(6): p. 211-6.
27. Ishijima, A. and T. Yanagida, *Single molecule nanobioscience*. Trends Biochem Sci, 2001. 26(7): p. 438-44.
28. Jeney, S., E.L. Florin, and J.K. Horber, *Use of photonic force microscopy to study single-motor-molecule mechanics*. Methods Mol Biol, 2001. 164: p. 91-108.
29. Khan, S. and M.P. Sheetz, *Force effects on biochemical kinetics*. Annu Rev Biochem, 1997. 66: p. 785-805.
30. Kuo, S.C., *Using optics to measure biological forces and mechanics*. Traffic, 2001. 2(11): p. 757-63.
31. Mehta, A.D., J.T. Finer, and J.A. Spudich, *Use of optical traps in single-molecule study of nonprocessive biological motors*. Methods Enzymol, 1998. 298: p. 436-59.
32. Mehta, A.D., et al., *Single-molecule biomechanics with optical methods*. Science, 1999. 283(5408): p. 1689-95.
33. Simmons, R., *Molecular motors: single-molecule mechanics*. Curr Biol, 1996. 6(4): p. 392-4.
34. Wang, M.D., *Manipulation of single molecules in biology*. Curr Opin Biotechnol, 1999. 10(1): p. 81-6.
35. Bar-Ziv, R., E. Moses, and P. Nelson, *Dynamic excitations in membranes induced by optical tweezers*. Biophys J, 1998. 75(1): p. 294-320.
36. Crocker, J.C. and D.G. Grier, *Microscopic measurement of the pair interaction potential of charge-stabilized colloid*. Physical Review Letters, 1994. 73(2): p. 352-355.
37. Crocker, J.C. and D.G. Grier, *When Like Charges Attract: The Effects of Geometrical Confinement on Long-Range Colloidal Interactions*. Physical Review Letters, 1996. 77(9): p. 1897-1900.
38. Grier, D.G., *Optical tweezers in colloid and interface science*. Current Opinion in Colloid & Interface Science, 1997. 2(3): p. 264-270.
39. Grier, D.G., *A revolution in optical manipulation*. Nature, 2003. 424(6950): p. 810-6.
40. Hough, L.A. and H.D. Ou-Yang, *Correlated motions of two hydrodynamically coupled particles confined in separate quadratic potential wells*. Phys Rev E Stat Nonlin Soft Matter Phys, 2002. 65(2 Pt 1): p. 021906.
41. Korda, P.T., M.B. Taylor, and D.G. Grier, *Kinetically locked-in colloidal transport in an array of optical tweezers*. Physical Review Letters, 2002. 89(12): p. 128301.
42. Lin, B., J. Yu, and S.A. Rice, *Direct measurements of constrained brownian motion of an isolated sphere between two walls*. Phys Rev E Stat Phys Plasmas Fluids Relat Interdiscip Topics, 2000. 62(3 Pt B): p. 3909-19.
43. Allemand, J.F., D. Bensimon, and V. Croquette, *Stretching DNA and RNA to probe their interactions with proteins*. Curr Opin Struct Biol, 2003. 13(3): p. 266-74.
44. Bryant, Z., et al., *Structural transitions and elasticity from torque measurements on DNA*. Nature, 2003. 424(6946): p. 338-41.
45. Bustamante, C., Z. Bryant, and S.B. Smith, *Ten years of tension: single-molecule DNA mechanics*. Nature, 2003. 421(6921): p. 423-7.
46. Bustamante, C., et al., *Single-molecule studies of DNA mechanics*. Curr Opin Struct Biol, 2000. 10(3): p. 279-85.

47. Janshoff, A., et al., *Force Spectroscopy of Molecular Systems-Single Molecule Spectroscopy of Polymers and Biomolecules*. Angew Chem Int Ed Engl, 2000. 39(18): p. 3212-3237.
48. Liphardt, J., et al., *Reversible unfolding of single RNA molecules by mechanical force*. Science, 2001. 292(5517): p. 733-7.
49. Onoa, B., et al., *Identifying kinetic barriers to mechanical unfolding of the T. thermophila ribozyme*. Science, 2003. 299(5614): p. 1892-5.
50. Perkins, T.T., et al., *Relaxation of a single DNA molecule observed by optical microscopy*. Science, 1994. 264(5160): p. 822-6.
51. Perkins, T.T., D.E. Smith, and S. Chu, *Direct observation of tube-like motion of a single polymer chain*. Science, 1994. 264(5160): p. 819-22.
52. Perkins, T.T., et al., *Stretching of a single tethered polymer in a uniform flow*. Science, 1995. 268(5207): p. 83-7.
53. Pope, L.H., M.L. Bennink, and J. Greve, *Optical tweezers stretching of chromatin*. J Muscle Res Cell Motil, 2002. 23(5-6): p. 397-407.
54. Wang, K., J.G. Forbes, and A.J. Jin, *Single molecule measurements of titin elasticity*. Prog Biophys Mol Biol, 2001. 77(1): p. 1-44.
55. Wang, M.D., et al., *Stretching DNA with optical tweezers*. Biophys J, 1997. 72(3): p. 1335-46.
56. Ashkin, A., *Optical trapping and manipulation of neutral particles using lasers*. Proc Natl Acad Sci U S A, 1997. 94(10): p. 4853-60.
57. Garces-Chavez, V., et al., *Simultaneous micromanipulation in multiple planes using a self-reconstructing light beam*. Nature, 2002. 419(6903): p. 145-7.
58. MacDonald, M.P., et al., *Creation and manipulation of three-dimensional optically trapped structures*. Science, 2002. 296(5570): p. 1101-3.
59. McGloin, D., V. Garces-Chavez, and K. Dholakia, *Interfering Bessel beams for optical micromanipulation*. Optics Letters, 2003. 28(8): p. 657-9.
60. Paterson, L., et al., *Controlled rotation of optically trapped microscopic particles*. Science, 2001. 292(5518): p. 912-4.
61. Brouhard, G.J., H.T. Schek, 3rd, and A.J. Hunt, *Advanced optical tweezers for the study of cellular and molecular biomechanics*. IEEE Trans Biomed Eng, 2003. 50(1): p. 121-5.
62. Molloy, J.E., *Optical chopsticks: digital synthesis of multiple optical traps*. Methods Cell Biol, 1998. 55: p. 205-16.
63. Visscher, K. and S.M. Block, *Versatile optical traps with feedback control*. Methods Enzymol, 1998. 298: p. 460-89.
64. Fallman, E. and O. Axner, *Design for fully steerable dual-trap optical tweezers*. Applied Optics, 1997. 36(10): p. 2107-2113.
65. Lang, M.J., et al., *An automated two-dimensional optical force clamp for single molecule studies*. Biophysical Journal, 2002. 83(1): p. 491-501.
66. Rice, S.E., T.J. Purcell, and J.A. Spudich, *Building and using optical traps to study properties of molecular motors*. Biophotonics, Pt B, 2003. 361: p. 112-133.
67. Smith, S.B., Y.J. Cui, and C. Bustamante, *Optical-trap force transducer that operates by direct measurement of light momentum*. Biophotonics, Pt B, 2003. 361: p. 134-162.
68. Felgner, H., O. Muller, and M. Schliwa, *Calibration of Light Forces in Optical Tweezers*. Applied Optics, 1995. 34(6): p. 977-982.

69. Wright, W.H., G.J. Sonek, and M.W. Berns, *Radiation Trapping Forces on Microspheres with Optical Tweezers*. Applied Physics Letters, 1993. 63(6): p. 715-717.
70. Zemanek, P., A. Jonas, and M. Liska, *Simplified description of optical forces acting on a nanoparticle in the Gaussian standing wave*. Journal of the Optical Society of America A-Optics Image Science and Vision, 2002. 19(5): p. 1025-1034.
71. Almaas, E. and I. Brevik, *Radiation forces on a micrometer-sized sphere in an evanescent field*. Journal of the Optical Society of America B-Optical Physics, 1995. 12(12): p. 2429-2438.
72. Allersma, M.W., et al., *Two-dimensional tracking of ncd motility by back focal plane interferometry*. Biophys J, 1998. 74(2 Pt 1): p. 1074-85.
73. Berg-Sorensen, K. and H. Flyvbjerg, *Power spectrum analysis for optical tweezers*. Review of Scientific Instruments, 2004. 75(3): p. 594-612.
74. Wuite, G.J., et al., *An integrated laser trap/flow control video microscope for the study of single biomolecules*. Biophys J, 2000. 79(2): p. 1155-67.
75. Visscher, K., M.J. Schnitzer, and S.M. Block, *Single kinesin molecules studied with a molecular force clamp*. Nature, 1999. 400(6740): p. 184-9.
76. Liphardt, J., et al., *Reversible unfolding of single RNA molecules by mechanical force*. Science, 2001. 292(5517): p. 733-737.
77. Felgner, H., R. Frank, and M. Schliwa, *Flexural rigidity of microtubules measured with the use of optical tweezers*. Journal of Cell Science, 1996. 109: p. 509-516.
78. Tskhovrebova, L., et al., *Elasticity and unfolding of single molecules of the giant muscle protein titin*. Nature, 1997. 387(6630): p. 308-312.
79. Mihardja, S., et al., *Effect of force on mononucleosomal dynamics*. Proceedings of the National Academy of Sciences of the United States of America, 2006. 103(43): p. 15871-15876.
80. Nugent-Glandorf, L. and T.T. Perkins, *Measuring 0.1-nm motion in 1 ms in an optical microscope with differential back-focal-plane detection*. Optics Letters, 2004. 29(22): p. 2611-2613.
81. Abbondanzieri, E.A., et al., *Direct observation of base-pair stepping by RNA polymerase*. Nature, 2005. 438(7067): p. 460-5.
82. Carter, A.R., Y. Seol, and T.T. Perkins, *Precision surface-coupled optical-trapping assay with one-basepair resolution*. Biophys J, 2009. 96(7): p. 2926-34.
83. Bustamante, C., Y.R. Chemla, and J.R. Moffitt, *High resolution dual trap optical tweezers with differential detection*, in *Single-Molecule Techniques: A Laboratory Manual*, P. Selvin, T.J. Ha, Editor. 2007, Cold Spring Harbor Laboratory Press: Woodbury, New York.
84. Perkins, T.T., et al., *Forward and reverse motion of single RecBCD molecules on DNA*. Biophysical Journal, 2004. 86(3): p. 1640-1648.
85. Dumont, S., et al., *RNA translocation and unwinding mechanism of HCV NS3 helicase and its coordination by ATP*. Nature, 2006. 439(7072): p. 105-8.
86. Moffitt, J.R., et al., *Intersubunit coordination in a homomeric ring ATPase*. Nature, 2009. 457(7228): p. 446-50.
87. Yu, H., et al., *Direct observation of multiple misfolding pathways in a single prion protein molecule*. Proc Natl Acad Sci U S A, 2012. 109(14): p. 5283-8.
88. Xi, Z., et al., *Single-molecule observation of helix staggering, sliding, and coiled coil misfolding*. Proc Natl Acad Sci U S A, 2012. 109(15): p. 5711-6.

Chapter 2. Introduction to *E. coli* SSB protein

2.1 Historical perspective

Single stranded DNA binding proteins (SSBs) are accessory proteins involved in replication, recombination, and repair [1, 2]. These proteins protect single-stranded DNA intermediates from chemical and nucleolytic attacks in the cell by binding selectively to single stranded regions of DNA in a sequence-independent manner [4]. The first single stranded DNA binding protein – the bacteriophage T4 gene 32 protein – was discovered and characterized in the laboratory of Bruce Albert in the late 1960s [5]. Soon after, *E. coli* SSB (also referred to as *Eco* SSB) was isolated in 1972 [6]. Since then other prokaryotic SSBs have been identified in bacteria [7], conjugative bacterial plasmids [8-10] and bacteriophages [11-13]. SSBs in eukaryotes that are functionally similar to prokaryotic SSBs were identified as well: nuclear SSBs (RPA and RFA) in human and yeast. Interestingly, this class of proteins was initially referred to with names suggesting their role in the DNA-unwinding process: including “DNA-unwinding proteins” [6, 14], “DNA-melting proteins” and “helix-destabilizing proteins” [15, 16]. However, with time they have come to be known as single stranded DNA binding proteins since their major role *in vivo* is to assist in various DNA-modifying processes by binding to transient single stranded regions of DNA. By virtue of these properties, *Eco* SSB has served as the prototype for the study of DNA-protein interactions since its discovery. While a great wealth of literature on various aspects of *Eco* SSB already exists, the role and mechanism of SSB-mediated stimulation of various DNA processes is still under debate [1, 2].

2.2 *E. coli* SSB and its Binding Modes

The *Escherichia coli* SSB protein consists of four monomers (~19 kDa each) that oligomerize into a functional homotetramer ~50 Å in dimension (**Figure 2-1**). Each monomer contains an oligonucleotide/oligosaccharide binding (OB) fold that binds to ssDNA [2, 3, 17, 18], which gives the tetramer four potential ssDNA binding sites. *Eco* SSB has been reported to be present in high concentrations *in vivo* with estimates ranging from 300 to 2000 tetramers per cell, equivalent to 0.05 µM to 0.35 µM [4, 19]. The monomer has a 177-amino acid chain with high glycine content (one out of seven amino acids) and a single histidine (implicated in subunit

interactions) residue, and lacks any cysteines. The N-terminus contains the ssDNA binding site of *Eco* SSB in residues 1-115. Two tryptophans, Trp 40 and Trp 54, are believed to form base stacking interactions with the bases of the ssDNA [20, 21]. It has been shown that Phe 60 is also involved in DNA binding [22, 23]. In addition, acetylation of Lys 43, Lys 62, Lys 73, or Lys 87 is greatly reduced upon ssDNA binding [24, 25], suggesting an electrostatic interaction of Lys residues with the backbone of DNA. The C-terminus, on the other hand, is characterized by the presence of highly acidic amino acids. Residues between these two stretches are

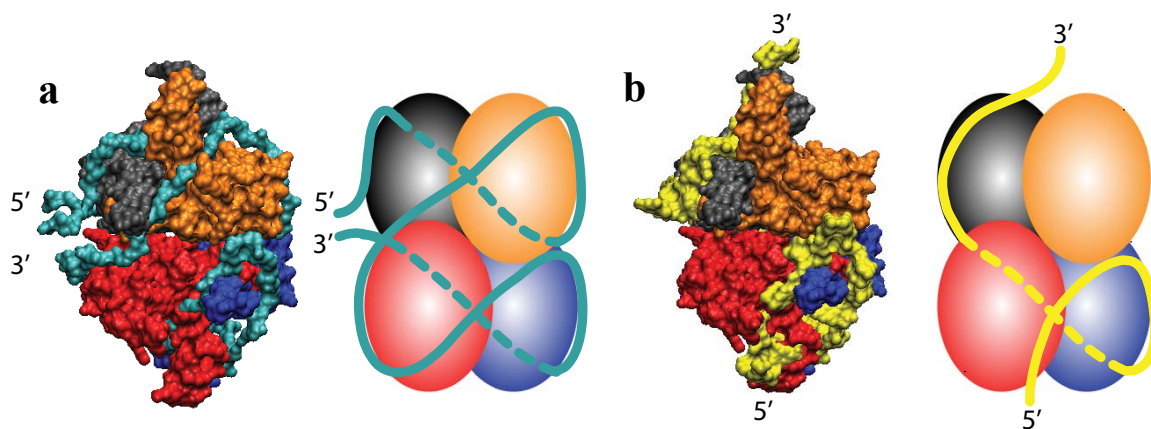


Figure 2-1. *E. coli* SSB. Structural model and schematic representation of SSB homotetramer (red, black, blue, and grey) and ssDNA (cyan and yellow) in the **a)** (SSB)₆₅ and **b)** (SSB)₃₅ wrapping conformation. PDB's from Ref.[3]

mostly characterized as random coils with high glycine, proline and glutamine content.

Different studies using various techniques have shown that there are two major binding modes of SSB to ssDNA which involves wrapping of 65 ± 3 nucleotides to all four subunits of the tetramer and 35 ± 3 nucleotides to two diagonally opposite subunits of the tetramer [26, 27]. Electron microscopy studies by Griffith and co-workers in the 1980's suggested different binding characteristics of SSB to ssDNA depending upon the protein to DNA ratio [28, 29]. Under low protein to DNA ratios, nucleosome-like beaded structures were observed that formed small clusters spaced by protein-free linkers with a decrease in the contour length of the DNA. When the protein to DNA ratio was increased, the frequency of these beaded structures increased until the entire DNA was observed to be in the beaded form. Upon increasing the protein to DNA ratio further, the contour length of DNA increased abruptly and the DNA-protein complex was found to have a smooth-contoured form. Subsequently, these observations have been explained by

reports of multiple binding modes of *Eco* SSB to ssDNA by Lohman and co-workers [2, 30, 31]. Work from the Lohman lab showed that the SSB tetramer can bind long ssDNA in a variety of binding modes depending on solution conditions, especially salt concentration and type [2, 29-33]. At low monovalent salt concentrations (<10mM NaCl) and high protein to DNA ratios, a SSB tetramer binds to ssDNA with high inter-tetramer cooperativity using only two out of four subunits on average, and gets wrapped by ~35 nucleotides (nt) of ssDNA. This binding mode is referred to as the (SSB)₃₅ mode [34], and has been shown to exhibit “unlimited” cooperativity, where SSBs associate to each other and can form long protein filaments [2]. Cooperativity is a phenomenon whereby an SSB tetramer has a higher affinity for a polynucleotide to which an SSB is already bound than to one lacking SSB. However, at higher salt concentrations (>0.2M NaCl), a SSB tetramer binds to ssDNA using all four subunits with approximately 65 nt wrapped around the tetramer to form the (SSB)₆₅ mode [2, 3]. This binding mode exhibits low cooperativity, and formation of SSB filaments has not been observed [2]. Techniques like nuclease digestion, protein fluorescence quenching and electron spin resonance spectroscopy under a wide variety of conditions [26-28, 30, 33, 35, 36] reported formation of such a 65-nucleotide binding conformation as well.

Several crystal structures of single stranded DNA binding protein from different sources have been reported over the years. These carry the characteristic DNA binding OB (oligomer-binding) fold [17, 37-42]. Homotetrameric structures of *Eco* SSB and analogous human mitochondrial SSB (hmtSSB) were determined independently by the Waksman group and Yang *et. al.* in 1997 [17, 42]. Both SSBs had similar structures and carried the well-characterized ssDNA binding OB-fold. The structure of the monomer revealed a β barrel spanning one side and a small helix on the other. Trp40, Trp54 and Phe60 already implicated in DNA binding by biochemical studies were clustered and indicated the likely binding track of the DNA. More recently, the Waksman group reported the DNA-bound structure of a truncated *Eco* SSB (a C-terminal truncation of 42 residues; called SSBc) carrying the DNA binding domain [3]. A model for SSB bound to ssDNA in its (SSB)₆₅ binding mode has been suggested based on this structure of a tetramer of SSBc bound to two molecules of (dC)₃₅. In this mode ~65 nt of ssDNA interact with all four SSB subunits with a topology approximating the stitches around a baseball (**Figure 2-1a**). In this topology, the entry and exit sites of a 65 nt ssDNA are in close proximity. A more

speculative structural model for the (SSB)₃₅ binding mode was also proposed (**Figure 2-1b**) [3]. The transition between these binding modes is reversible [30, 43].

2.3 Interaction with Other Proteins

Beyond the role of protection from chemical and nucleolytic attacks, SSB proteins have a second, less well-appreciated role in cellular genome maintenance machinery in which they interact directly with other genome-maintenance enzymes. The acidic tail (high Asp density) of *Eco* SSB at its C-terminus is believed to be responsible for these interactions, since mutations within the C-terminus (Asp-Phe-Asp-Asp-Asp-Ile-Pro-Phe) have a negative impact on cell survival [44-48]. One of the mutations results in the loss of DNA replication under nonstandard growth conditions [44, 45], and displays sensitivity to the DNA damage under standard conditions (permissive conditions). Other mutations similarly impair cell viability [46, 47]. Deletion of a highly conserved region among the bacterial SSB (the last 10 amino acids from the C-terminus) also makes cells unviable [48].

SSB's interaction with DNA plays a role in the replication process, particularly in assembly of the replication machinery [47]. In DNA recombination SSB has been shown to stimulate DNA helicase activity through direct interaction [49-51], and influence exonuclease activity [52]. Additionally, SSB stimulates helicase activity in DNA replication restart [53] and exonuclease activity in DNA repair [54, 55].

2.4 Influence of DNA Binding Modes on SSB Function

Though several binding modes of *Eco* SSB to ssDNA have been observed by various methods one must consider whether any particular mode is selectively chosen for different metabolic processes in *E. coli*. No direct evidence for the effect of binding modes on SSB function *in vivo* exist, though several indirect pieces of evidence suggest that (SSB)₆₅ binding mode might be associated with recombination processes under conditions where RecA protein stimulates DNA strand exchange *in vitro* [32]. On the other hand, (SSB)₃₅ binding has been proposed to function in DNA replication [2, 56]. *In vitro*, SSB has been known to stimulate RecA filament formation and strand exchange in high salt (~10mM MgCl₂), while inhibiting the same process in low salt (~1mM MgCl₂) [29, 57]. This suggests that the high salt binding mode (SSB)₆₅ must be involved in assisting the RecA action. It was shown that the *ssbW54S* (gene)

mutant is defective in both replication and UV repair *in vivo* [58]. However the most dramatic effect of this mutation is that the mutant SSB favorably bound ssDNA in the (SSB)₃₅ binding mode even in high salt concentrations [30, 31]. This also supports the idea that (SSB)₆₅ mode is critical to the SSB function. On the other hand, DNA replication occurs at high speeds of 1000 bps/s which would require rapid saturation of the ssDNA generated in the lagging strand, which has to have transient long ssDNA intermediates for polymerization during DNA replication. This could be accomplished with the help of the (SSB)₃₅ mode with its “unlimited cooperativity” [2].

Moreover, in replication pathways, specifically in the *G4oric* replication system, two SSBs bind near the *oric* region that generate a free region of DNA and serve as the *E. coli* primase recognition target [59]. This could be explained by low cooperativity of (SSB)₆₅ mode that has its effect on the DNA availability for interaction with other proteins [25, 26]. In this mode SSB proteins bind DNA discretely (and independently), forming protein bound regions separated by single stranded DNA stretches [28]. This binding mode provides the opportunity for other proteins to get access to the DNA at the free regions and may explain why stimulation effects are observed (instead of inhibition with (SSB)₃₅ mode due to its high cooperativity). Such a mechanism of SSB binding that gives room for other protein factors and initiates the genomic maintenance machinery might be a common path of the SSB protein that requires binding in the (SSB)₆₅ mode. It has also been shown that the (SSB)₃₅ mode is efficient in undergoing “direct transfer” from one strand to another strand of DNA, which can serve as an extremely useful asset to achieve rapid recycling of the SSB protein during replication [19]. However further studies are required to find out the role of the binding modes in biological function of this protein.

2.5 Previous studies

The interactions of *E. coli* SSB with ssDNA have been examined structurally [3, 60], thermodynamically [24, 56, 61-67] (reviewed in [2]) and kinetically [19, 68, 69]. At low salt conditions, binding of SSB to ssDNA is rapid, at a rate of 10^8 - 10^9 M⁻¹s⁻¹ which is very close to the diffusion controlled collision rate [19, 70]. On the other hand, the rate of protein dissociation is estimated to be extremely low (< 1 s⁻¹ at room temperature and only ~ 400 s⁻¹ even at 35-40°C in 2M NaBr) [19, 70]. To increase dissociation rates, biochemical studies have been performed under very high salt conditions. As a result it has only been possible to measure kinetic and thermodynamic constants at high, non-physiological salt concentrations.

Recent single-molecule fluorescence studies [43, 71, 72] have investigated SSB dynamics in complex with ssDNA. Single-molecule FRET (fluorescence resonance energy transfer) in particular is a powerful tool that can detect protein interactions with DNA at the single-protein level and serves as a molecular ruler to measure molecular distances [73, 74]. Using this technique for the first time direct evidence for fluctuations between the two wrapping modes has been shown [43]. Interestingly, this study also showed that the SSB binding conformation is very dynamic and capable of alternating wrapping topologies without protein dissociation. Other FRET studies have shown recently that *E. coli* SSB can diffuse on ssDNA to facilitate formation of RecA filaments [71].

Fluorescence readouts are limited in quantitative information content; they can relay the presence or absence of a protein [71, 75], or uncalibrated, relative (and not absolute) changes in distances [43, 72, 76]. An ideal measurement technique would allow one to distinguish not only the presence of a protein but also measure the conformational state of the nucleoprotein complex (i.e. how much DNA is wrapped). Recently, the effect of forces applied on a system with SSB and ssDNA was studied by using a hybrid instrument consisting of single optical trap and fluorescence techniques. It was shown that SSB gradually unwraps from ssDNA starting at 1 pN and dissociates at forces of about 10 pN [72]. A model for diffusive behavior of SSB has been proposed as well [72]. Due to low resolution of optical trap it was not possible to get detailed information about conformational state of SSB/ssDNA complex. In order to achieve this, high resolution optical traps have to be used, and will be the main technique to study this system in the following Chapters.

2.6 References

1. Shereda, R.D., et al., *SSB as an organizer/mobilizer of genome maintenance complexes*. Crit Rev Biochem Mol Biol, 2008. 43(5): p. 289-318.
2. Lohman, T.M. and M.E. Ferrari, *Escherichia coli single-stranded DNA-binding protein: multiple DNA-binding modes and cooperativities*. Annu Rev Biochem, 1994. 63: p. 527-70.
3. Raghunathan, S., et al., *Structure of the DNA binding domain of E. coli SSB bound to ssDNA*. Nat Struct Biol, 2000. 7(8): p. 648-52.
4. Meyer, R.R. and P.S. Laine, *The single-stranded DNA-binding protein of Escherichia coli*. Microbiol Rev, 1990. 54(4): p. 342-80.

5. Alberts, B.M. and L. Frey, *T4 bacteriophage gene 32: a structural protein in the replication and recombination of DNA*. Nature, 1970. 227(5265): p. 1313-8.
6. Sigal, N., et al., *DNA-Unwinding Protein Isolated from Escherichia-Coli - Its Interaction with DNA and with DNA Polymerases*. Proceedings of the National Academy of Sciences of the United States of America, 1972. 69(12): p. 3537-3541.
7. Devries, J. and W. Wackernagel, *Cloning and Sequencing of the Serratia-Marcescens Gene Encoding a Single-Stranded DNA-Binding Protein (Ssb) and Its Promoter Region*. Gene, 1993. 127(1): p. 39-45.
8. Golub, E.I. and K.B. Low, *Conjugative plasmids of enteric bacteria from many different incompatibility groups have similar genes for single-stranded DNA-binding proteins*. J Bacteriol, 1985. 162(1): p. 235-41.
9. Howland, C.J., et al., *The ssb gene of plasmid Collb-P9*. J Bacteriol, 1989. 171(5): p. 2466-73.
10. Ruvolo, P.P., et al., *Single-stranded DNA binding proteins (SSBs) from prokaryotic transmissible plasmids*. Proteins, 1991. 9(2): p. 120-34.
11. Martin, G. and M. Salas, *Characterization and cloning of gene 5 of Bacillus subtilis phage phi 29*. Gene, 1988. 67(2): p. 193-201.
12. Lindberg, G., et al., *Purification and characterization of the coliphage N4-coded single-stranded DNA binding protein*. Journal of Biological Chemistry, 1989. 264(21): p. 12700-8.
13. Scherzinger, E., F. Litfin, and E. Jost, *Stimulation of T7 DNA polymerase by a new phage-coded protein*. Molecular & General Genetics, 1973. 123(3): p. 247-62.
14. Molineux, I.J., S. Friedman, and M.L. Gefter, *Purification and Properties of Escherichia-Coli Deoxyribonucleic Acid Unwinding Protein - Effects on Deoxyribonucleic-Acid Synthesis In vitro*. Journal of Biological Chemistry, 1974. 249(19): p. 6090-6098.
15. Alberts, B. and R. Sternglanz, *Recent excitement in the DNA replication problem*. Nature, 1977. 269(5630): p. 655-61.
16. Coleman, J.E. and J.L. Oakley, *Physical chemical studies of the structure and function of DNA binding (helix-destabilizing) proteins*. CRC Crit Rev Biochem, 1980. 7(3): p. 247-89.
17. Raghunathan, S., et al., *Crystal structure of the homo-tetrameric DNA binding domain of Escherichia coli single-stranded DNA-binding protein determined by multiwavelength x-ray diffraction on the selenomethionyl protein at 2.9-A resolution*. Proc Natl Acad Sci U S A, 1997. 94(13): p. 6652-7.
18. Theobald, D.L., R.M. Mitton-Fry, and D.S. Wuttke, *Nucleic acid recognition by OB-fold proteins*. Annu Rev Biophys Biomol Struct, 2003. 32: p. 115-33.
19. Kozlov, A.G. and T.M. Lohman, *Kinetic mechanism of direct transfer of Escherichia coli SSB tetramers between single-stranded DNA molecules*. Biochemistry, 2002. 41(39): p. 11611-11627.
20. Curth, U., et al., *Multiple binding modes of the single-stranded DNA binding protein from Escherichia coli as detected by tryptophan fluorescence and site-directed mutagenesis*. Biochemistry, 1993. 32(10): p. 2585-91.
21. Khamis, M.I., et al., *Investigation of the role of individual tryptophan residues in the binding of Escherichia coli single-stranded DNA binding protein to single-stranded polynucleotides. A study by optical detection of magnetic resonance and site-selected mutagenesis*. Journal of Biological Chemistry, 1987. 262(23): p. 10938-45.

22. Casas-Finet, J.R., et al., *Tryptophan 54 and phenylalanine 60 are involved synergistically in the binding of E. coli SSB protein to single-stranded polynucleotides*. FEBS Lett, 1987. 220(2): p. 347-52.
23. Bayer, I., et al., *Modulation of the affinity of the single-stranded DNA-binding protein of Escherichia coli (E. coli SSB) to poly(dT) by site-directed mutagenesis*. Eur J Biochem, 1989. 179(2): p. 399-404.
24. Bujalowski, W. and T.M. Lohman, *Negative co-operativity in Escherichia coli single strand binding protein-oligonucleotide interactions. II. Salt, temperature and oligonucleotide length effects*. Journal of Molecular Biology, 1989. 207(1): p. 269-88.
25. Overman, L.B., W. Bujalowski, and T.M. Lohman, *Equilibrium binding of Escherichia coli single-strand binding protein to single-stranded nucleic acids in the (SSB)₆₅ binding mode. Cation and anion effects and polynucleotide specificity*. Biochemistry, 1988. 27(1): p. 456-71.
26. Lohman, T.M. and M.E. Ferrari, *Escherichia coli single-stranded DNA-binding protein: multiple DNA-binding modes and cooperativities*. Annual Review of Biochemistry, 1994. 63: p. 527-70.
27. Meyer, R.R. and P.S. Laine, *The Single-Stranded DNA-Binding Protein of Escherichia-Coli*. Microbiological Reviews, 1990. 54(4): p. 342-380.
28. Chrysogelos, S. and J. Griffith, *Escherichia-Coli Single-Strand Binding-Protein Organizes Single-Stranded-DNA in Nucleosome-Like Units*. Proceedings of the National Academy of Sciences of the United States of America-Biological Sciences, 1982. 79(19): p. 5803-5807.
29. Griffith, J.D., L.D. Harris, and J. Register, *Visualization of Ssb-Ssdna Complexes Active in the Assembly of Stable RecA-DNA Filaments*. Cold Spring Harbor Symposia on Quantitative Biology, 1984. 49: p. 553-559.
30. Lohman, T.M. and L.B. Overman, *Two binding modes in Escherichia coli single strand binding protein-single stranded DNA complexes. Modulation by NaCl concentration*. Journal of Biological Chemistry, 1985. 260(6): p. 3594-603.
31. Bujalowski, W. and T.M. Lohman, *Escherichia coli single-strand binding protein forms multiple, distinct complexes with single-stranded DNA*. Biochemistry, 1986. 25(24): p. 7799-802.
32. Bujalowski, W., L.B. Overman, and T.M. Lohman, *Binding Mode Transitions of Escherichia-Coli Single-Strand Binding Protein-Single-Stranded DNA Complexes - Cation, Anion, Ph, and Binding Density Effects*. Journal of Biological Chemistry, 1988. 263(10): p. 4629-4640.
33. Lohman, T.M., W. Bujalowski, and L.B. Overman, *Escherichia-Coli Single-Strand Binding-Protein - a New Look at Helix-Destabilizing Proteins*. Trends in Biochemical Sciences, 1988. 13(7): p. 250-255.
34. Ferrari, M.E., W. Bujalowski, and T.M. Lohman, *Cooperative Binding of Escherichia-Coli Ssb Tetramers to Single-Stranded-DNA in the (Ssb)₍₃₅₎ Binding Mode*. Journal of Molecular Biology, 1994. 236(1): p. 106-123.
35. Bobst, E.V., et al., *An Epr Study to Determine the Relative Nucleic-Acid Binding-Affinity of Single-Stranded DNA-Binding Protein from Escherichia-Coli*. Biochimica Et Biophysica Acta, 1991. 1078(2): p. 199-207.

36. Boidotforget, M., et al., *Single-Strand Binding-Proteins from Phage-T4 and Escherichia-Coli Form Higher-Order Structures with Poly(Dt)*. Biochimie, 1986. 68(9): p. 1129-1134.
37. Bernstein, D.A., et al., *Crystal structure of the Deinococcus radiodurans single-stranded DNA-binding protein suggests a mechanism for coping with DNA damage*. Proc Natl Acad Sci U S A, 2004. 101(23): p. 8575-80.
38. Hollis, T., et al., *Structure of the gene 2.5 protein, a single-stranded DNA binding protein encoded by bacteriophage T7*. Proc Natl Acad Sci U S A, 2001. 98(17): p. 9557-62.
39. Matsumoto, T., et al., *Roles of functional loops and the C-terminal segment of a single-stranded DNA binding protein elucidated by x-ray structure analysis*. Journal of Biochemistry, 2000. 127(2): p. 329-335.
40. Ollis, D., et al., *Crystals of Escherichia-Coli Single-Strand DNA-Binding Protein Show That the Tetramer Has D2 Symmetry*. Journal of Molecular Biology, 1983. 170(3): p. 797-800.
41. Thorn, J.M., et al., *Crystallization and Low-Temperature Diffraction Studies of the DNA-Binding Domain of the Single-Stranded-DNA Binding-Protein from Escherichia-Coli*. Journal of Molecular Biology, 1994. 240(4): p. 396-399.
42. Yang, C., et al., *Crystal structure of human mitochondrial single-stranded DNA binding protein at 2.4 Å resolution*. Nat Struct Biol, 1997. 4(2): p. 153-7.
43. Roy, R., et al., *Dynamic structural rearrangements between DNA binding modes of E. coli SSB protein*. J Mol Biol, 2007. 369(5): p. 1244-57.
44. Chase, J.W., et al., *Characterization of the Escherichia coli SSB-113 mutant single-stranded DNA-binding protein. Cloning of the gene, DNA and protein sequence analysis, high pressure liquid chromatography peptide mapping, and DNA-binding studies*. Journal of Biological Chemistry, 1984. 259(2): p. 805-14.
45. Wang, T.C. and K.C. Smith, *Effects of the ssb-1 and ssb-113 mutations on survival and DNA repair in UV-irradiated delta uvrB strains of Escherichia coli K-12*. J Bacteriol, 1982. 151(1): p. 186-92.
46. Kelman, Z., et al., *Devoted to the lagging strand-the subunit of DNA polymerase III holoenzyme contacts SSB to promote processive elongation and sliding clamp assembly*. EMBO J, 1998. 17(8): p. 2436-49.
47. Yuzhakov, A., Z. Kelman, and M. O'Donnell, *Trading places on DNA--a three-point switch underlies primer handoff from primase to the replicative DNA polymerase*. Cell, 1999. 96(1): p. 153-63.
48. Curth, U., et al., *In vitro and in vivo function of the C-terminus of Escherichia coli single-stranded DNA binding protein*. Nucleic Acids Res, 1996. 24(14): p. 2706-11.
49. Shereda, R.D., D.A. Bernstein, and J.L. Keck, *A central role for SSB in Escherichia coli RecQ DNA helicase function*. Journal of Biological Chemistry, 2007. 282(26): p. 19247-58.
50. Umez, K. and H. Nakayama, *RecQ DNA helicase of Escherichia coli. Characterization of the helix-unwinding activity with emphasis on the effect of single-stranded DNA-binding protein*. Journal of Molecular Biology, 1993. 230(4): p. 1145-50.
51. Lecointe, F., et al., *Anticipating chromosomal replication fork arrest: SSB targets repair DNA helicases to active forks*. EMBO J, 2007. 26(19): p. 4239-51.
52. Han, E.S., et al., *RecJ exonuclease: substrates, products and interaction with SSB*. Nucleic Acids Res, 2006. 34(4): p. 1084-91.

53. Cadman, C.J. and P. McGlynn, *PriA helicase and SSB interact physically and functionally*. Nucleic Acids Res, 2004. 32(21): p. 6378-87.
54. Lu, D. and J.L. Keck, *Structural basis of Escherichia coli single-stranded DNA-binding protein stimulation of exonuclease I*. Proc Natl Acad Sci U S A, 2008. 105(27): p. 9169-74.
55. Genschel, J., U. Curth, and C. Urbanke, *Interaction of E. coli single-stranded DNA binding protein (SSB) with exonuclease I. The carboxy-terminus of SSB is the recognition site for the nuclease*. Biol Chem, 2000. 381(3): p. 183-92.
56. Overman, L.B. and T.M. Lohman, *Linkage of pH, anion and cation effects in protein-nucleic acid equilibria. Escherichia coli SSB protein-single stranded nucleic acid interactions*. Journal of Molecular Biology, 1994. 236(1): p. 165-78.
57. Kowalczykowski, S.C., et al., *Effects of the Escherichia coli SSB protein on the binding of Escherichia coli RecA protein to single-stranded DNA. Demonstration of competitive binding and the lack of a specific protein-protein interaction*. Journal of Molecular Biology, 1987. 193(1): p. 81-95.
58. Carlini, L.E., et al., *Viability and preliminary in vivo characterization of site-directed mutants of Escherichia coli single-stranded DNA-binding protein*. Mol Microbiol, 1993. 10(5): p. 1067-75.
59. Sun, W. and G.N. Godson, *Structure of the Escherichia coli primase/single-strand DNA-binding protein/phage G4oric complex required for primer RNA synthesis*. Journal of Molecular Biology, 1998. 276(4): p. 689-703.
60. Savvides, S.N., et al., *The C-terminal domain of full-length E. coli SSB is disordered even when bound to DNA*. Protein Sci, 2004. 13(7): p. 1942-7.
61. Bujalowski, W., L.B. Overman, and T.M. Lohman, *Binding mode transitions of Escherichia coli single strand binding protein-single-stranded DNA complexes. Cation, anion, pH, and binding density effects*. J Biol Chem, 1988. 263(10): p. 4629-40.
62. Kozlov, A.G. and T.M. Lohman, *Calorimetric studies of E. coli SSB protein-single-stranded DNA interactions. Effects of monovalent salts on binding enthalpy*. J Mol Biol, 1998. 278(5): p. 999-1014.
63. Bustamante, C., et al., *Entropic elasticity of lambda-phage DNA*. Science, 1994. 265(5178): p. 1599-600.
64. Kozlov, A.G. and T.M. Lohman, *Adenine base unstacking dominates the observed enthalpy and heat capacity changes for the Escherichia coli SSB tetramer binding to single-stranded oligoadenylates*. Biochemistry, 1999. 38(22): p. 7388-97.
65. Kozlov, A.G. and T.M. Lohman, *Effects of monovalent anions on a temperature-dependent heat capacity change for Escherichia coli SSB tetramer binding to single-stranded DNA*. Biochemistry, 2006. 45(16): p. 5190-205.
66. Kozlov, A.G., M.M. Cox, and T.M. Lohman, *Regulation of single-stranded DNA binding by the C termini of Escherichia coli single-stranded DNA-binding (SSB) protein*. J Biol Chem, 2010. 285(22): p. 17246-52.
67. Lohman, T.M. and W. Bujalowski, *E. coli SSB Protein: Multiple Binding Modes and Cooperativities*. CRC Press, 1990: p. 131-168.
68. Kozlov, A.G. and T.M. Lohman, *Stopped-flow studies of the kinetics of single-stranded DNA binding and wrapping around the Escherichia coli SSB tetramer*. Biochemistry, 2002. 41(19): p. 6032-44.

69. Kuznetsov, S.V., et al., *Microsecond dynamics of protein-DNA interactions: direct observation of the wrapping/unwrapping kinetics of single-stranded DNA around the E. coli SSB tetramer*. J Mol Biol, 2006. 359(1): p. 55-65.
70. Kuznetsov, S.V., et al., *Microsecond dynamics of protein-DNA interactions: Direct observation of the wrapping/unwrapping kinetics of single-stranded DNA around the E. coli SSB tetramer*. Journal of Molecular Biology, 2006. 359(1): p. 55-65.
71. Roy, R., et al., *SSB protein diffusion on single-stranded DNA stimulates RecA filament formation*. Nature, 2009. 461(7267): p. 1092-7.
72. Zhou, R., et al., *SSB functions as a sliding platform that migrates on DNA via reptation*. Cell, 2011. 146(2): p. 222-32.
73. Clegg, R.M., *Fluorescence Resonance Energy-Transfer and Nucleic-Acids*. Methods in Enzymology, 1992. 211: p. 353-388.
74. Selvin, P.R., *The renaissance of fluorescence resonance energy transfer*. Nature Structural Biology, 2000. 7(9): p. 730-734.
75. van Mameren, J., et al., *Counting RAD51 proteins disassembling from nucleoprotein filaments under tension*. Nature, 2009. 457(7230): p. 745-8.
76. Joo, C., et al., *Real-time observation of RecA filament dynamics with single monomer resolution*. Cell, 2006. 126(3): p. 515-27.

Chapter 3. Observing binding of *E. coli* SSB using optical trap

In this work, we present optical trap measurements of SSB interacting with a 70-nt oligodeoxythymidylate (dT)₇₀—a substrate to which SSB binds with highest affinity [1]—with single-protein resolution. Ensemble measurements of the binding affinity of SSB to (dT)₇₀ have only been feasible in buffers with very high salt concentrations (NaBr > 0.8 M) needed to lower the stability of the nucleoprotein complex [2, 3]. In order to overcome this problem and make measurements under more biologically relevant conditions, a new approach is necessary: optical traps. Due to such tight binding of SSB to ssDNA, the question that arises is how SSB is removed from ssDNA? What kinds of forces are needed to disrupt a SSB-DNA complex? Can the DNA unwrap (partially) from the protein? And if so at what forces does this occur? All these questions can be answered by probing SSB/ssDNA interaction with applied force using optical traps. Although some of these measurements have been done to some extent [4] using high resolution optical traps, enabled us to determine details of ssDNA wrapping around SSB and obtain the free energy landscape for SSB/ssDNA interaction.

3.1 Experimental Design

The main goal of the work presented in Chapter 3 is to detect nucleic-acid and ssDNA binding protein interactions at high spatial and temporal resolution. To achieve these aim we will use an experimental system involving: optical traps, described in Chapter 1 with the resolution to detect binding of individual SSBs and to distinguish different partially wrapped intermediates; a microfluidic flow chamber, to manipulate the buffer conditions rapidly (ex: protein concentration) and in arbitrary fashion; and a DNA construct, to investigate the dynamics of SSB/ssDNA complex. Below we outline the technical details of our approach and methods we used for experiments.

3.1.1 DNA construct design

To achieve our goal of observing SSB-ssDNA interactions with single protein resolution, we designed a ssDNA substrate that can accommodate an individual protein and that can be tethered between beads in our dual optical trap instrument.

The SSB-binding construct consisted of three separate fragments that were ligated together (**Figure 3-1**): 1) a 1.5-kbp dsDNA “Right Handle” (RH), 2) a 70-nt ssDNA SSB protein

“Binding Site” (BS), and 3) a 1.7-kbp dsDNA “Left Handle” (LH). The handles served as functionalized linkers that bound to trapped beads through biotin-streptavidin and digoxigenin-anti-digoxigenin linkages and spatially separated the beads from the protein binding site. RH and LH were synthesized from PCR amplification of different regions of a plasmid using 5’

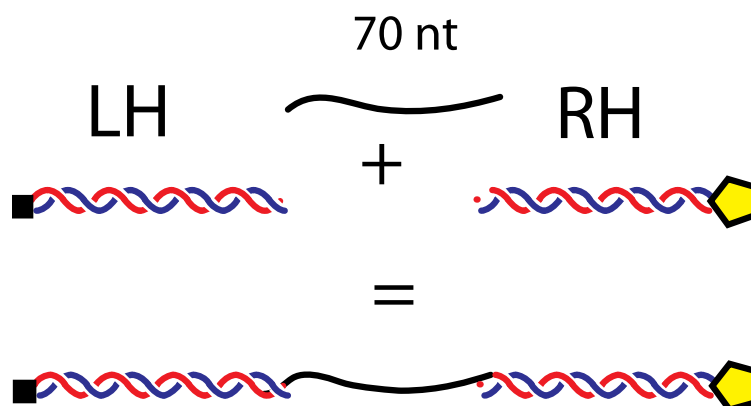


Figure 3-1. DNA Construct dsDNA handles (LH and RH) that are functionalized with biotin (black squares) and digoxigenin (yellow star) to inserts (black) containing SSB binding sites

biotin-labeled and 5’ digoxigenin-labeled primers (Integrated DNA Technologies, Coralville, IA), respectively. RH was digested with the PspGI restriction enzyme (New England Biolabs, Ipswich, MA) and gel purified to yield ~1.5-kbp dsDNA with a 5-nt 5’overhang. LH was digested with the TspRI restriction enzyme and gel purified, resulting in ~1.7-kbp dsDNA with a 9-nt 3’ overhang. The last fragment of the construct, BS, consisted of a 70-nt poly-dT oligodeoxyribonucleotide flanked by sequences complementary to the overhangs left by digestion of RH and LH. The restriction sites were designed to have non-palindromic sequences to eliminate self-ligation of RH and LH and produce a high yield of the correct three-fragment construct. The fully ligated construct thus consisted of a 70-nt SSB protein binding site flanked by functionalized dsDNA handles labeled with biotin and digoxigenin moieties at each end to allow attachment to streptavidin- and anti-digoxigenin-antibody coated beads, respectively (SpheroTech, 860 nm and 790 nm diameters, respectively).

3.1.2 Flow chamber

As mentioned above we needed the ability to change buffer condition rapidly. In order to do that we designed a flow chamber that was made by melting patterned parafilm (Nescofilm, Karlan Research Products Corporation) between two glass coverslips. One coverslip had inlet holes cut into it using laser engraver system (VLS2.30 Versa laser from Universal laser systems Inc.) to allow different buffers to be flowed through. We constructed chambers with four separate inlets into three channels separated by parafilm. Top and bottom channels contained buffers with beads coated with streptavidin and anti-digoxigenin, respectively (**Figure 3-2**),

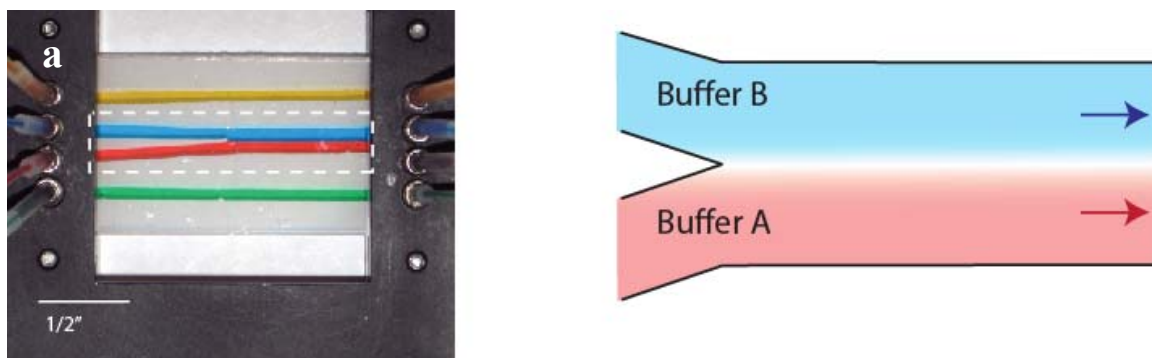


Figure 3-2. Laminar flow cell a) Image of the flow cell used to create the flow streams. b) Cartoon image of the two merging streams

and these were connected to a central channel through thin glass capillaries (OD 100 μm , ID 25 μm) to allow flow of both bead types into the trapping region. A syringe pump (Harvard Apparatus, PHD2000) was used to inject two separate buffers merging in the central channel (**Figure 3-2b**). Though the streams merged, the flow cell dimensions and flow rates ensured that laminar flow was established, forming a stationary profile with minimal mixing between the two streams. Similar laminar flow chamber designs have been used in single-molecule studies of DNA-protein interactions [5]. The flow chamber could be displaced relative to the two traps in all directions by a motorized three-axis translational stage (CMA 12CCCL) and controller (ESP3000) from New Port. Thus, rapid exchange of buffer conditions was possible by moving the stage relative to the traps across the narrow laminar flow interface. We tested the effect of laminar flow on our optical trap resolution. Provided the flow rates were small ($<100 \mu\text{m/s}$) and differential detection of the dual traps was used to subtract common mode noise [6], the effects of flow on resolution were minimal.

3.1.3 Single-stranded DNA protein purification

E. coli SSB protein was expressed and purified as described in [7] with the addition of a double-stranded DNA cellulose column to remove a minor exonuclease contaminant. SSB protein concentrations were determined spectrophotometrically in Tris buffer (pH 8.1, 0.2 M NaCl) using an extinction coefficient of $\epsilon_{280} = 1.13 \times 10^5 \text{ M}^{-1} \text{ (tetramer) cm}^{-1}$ [8].

3.1.4 Buffer conditions

Experiments were performed in a “trapping buffer” containing 100 mM Tris-HCl, 10 mM NaCl, and 0.1 mM EDTA, supplemented with an oxygen scavenging system (400 µg/ml glucose oxidase, 80 µg/ml catalase, 0.8% glucose) to increase tether lifetime [9] and 0.1 mg/ml human serum albumin (HSA) to eliminate non-specific sticking of the protein to our experimental chamber and tubing. In addition, our chambers were flushed with buffer containing 0.1 mg/ml bovine serum albumin (BSA) to inhibit any non-specific interactions before each experiment. Protocols for preparing scavenging system and BSA are provided in the Protocols section of the thesis.

3.1.5 Tether formation

DNA samples were incubated with streptavidin beads (see Protocol section). In the dual trap setup typically we would first position the trap within ~10 µm of the capillary tube connecting the bottom channel (green **Figure 3-2**) to the middle channel (red **Figure 3-2**). A small but steady flow through this capillary produces a small flow of beads from the bottom channel, containing digoxigenin antibody coated beads. Once one of these beads is trapped in one of the optical traps, the flow cell is moved to a position close to another capillary tube that connected the top (yellow **Figure 3-2**) and central channels (blue **Figure 3-2**). This time a small but steady flow produces a constant flow of DNA-coated beads. When one of these beads is captured in the second trap, the flow cell is then moved so that the traps are positioned far enough upstream from the capillary tubes. One should take care not to catch another bead with trap already occupied with a digoxigenin antibody coated bead. We work far enough from the capillaries to avoid dilution of the reaction buffer due to small leakage from capillaries and to avoid any other beads falling into the trap. Once the two beads are trapped we would repeatedly move one of the trap relative to another or ‘fish’ trying to form a single tether until force signal is detected. Each

time the tether formed one should double check for single tether by taking F-x curve and fit it to predicted theoretical plot (**Figure 3-4**).

3.2 Gradual unwrapping of SSB as a function of force

To test single SSB association (**Figure 3-3**), force-extension curves (F-x curves) of our constructs were obtained by increasing the trap separation at a rate ~ 12 nm/sec, with data collection at a rate of 100 Hz. The F-x curve is a plot of force measured versus stretched DNA length. The polymer properties of our tethers were determined by fitting the F-x curves to the extensible worm-like chain model [10]. Parameters for dsDNA were obtained from 3.4-kbp “calibration” dsDNA molecules prepared by PCR amplification (see Protocols) of a section of phage lambda DNA using 5' biotin-labeled and 5' digoxigenin-labeled primers (Integrated DNA Technologies, Coralville, IA). These molecules were pulled in the same buffer used for the SSB experiments and yielded a persistence length of 49 nm and stretch modulus of 960 pN (assuming 0.34 nm/bp contour length per base pair), consistent with previous measurements under

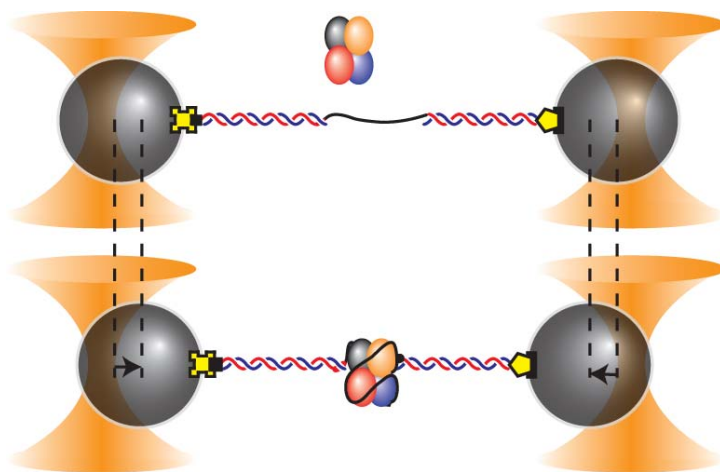


Figure 3-3. Schematic of optical trap experiment. A DNA molecule containing a (dT)₇₀ ssDNA SSB binding site flanked by functionalized dsDNA ends is tethered between beads held in dual optical traps (top). Upon binding and wrapping of one SSB, the DNA molecule extension decreases (bottom).

similar solution conditions [10]. F-x curves of the bare ss-dsDNA hybrid molecule (the SSB-binding construct without protein) were modeled by summing the extensions of the ds- and

ssDNA sections of the construct. Using the known lengths for these sections and the fixed dsDNA parameters obtained from the “calibration” molecule, ssDNA polymer parameters were obtained from fits of the F-x curves. This procedure yielded a persistence length of 1.7 nm for ssDNA, consistent with previous measurements (assuming 0.7 nm/nt contour length per nucleotide and stretch modulus of 960 pN [11-13]). In our flow cell, we formed a DNA tether in a laminar stream containing no protein and ensured that we had a single tether by measuring its extension as a function of the force exerted by the dual optical traps. The force-extension (F-x) behavior of molecules in the absence of protein (red curve, **Figure 3-4**) is in excellent agreement with that theoretically predicted from the models of dsDNA and ssDNA elasticity (black curve, **Figure 3-4**) [10, 14, 15], confirming the correct construction of the molecule. When the trapped bead-DNA-bead complex was moved to a laminar stream containing SSB, the DNA molecule condensed, as seen by its slightly decreased extension at low forces relative to the bare tether (blue curve, **Figure 3-4**). As tension in the molecule was increased beyond ~10 pN, a “break” (inset, **Figure 3-4**) was observed and the F-x curve overlapped with that of the bare ssDNA tether. Breaks occurred at an average force 10.1 ± 0.2 pN (**Figure 3-4**) and always in one step,

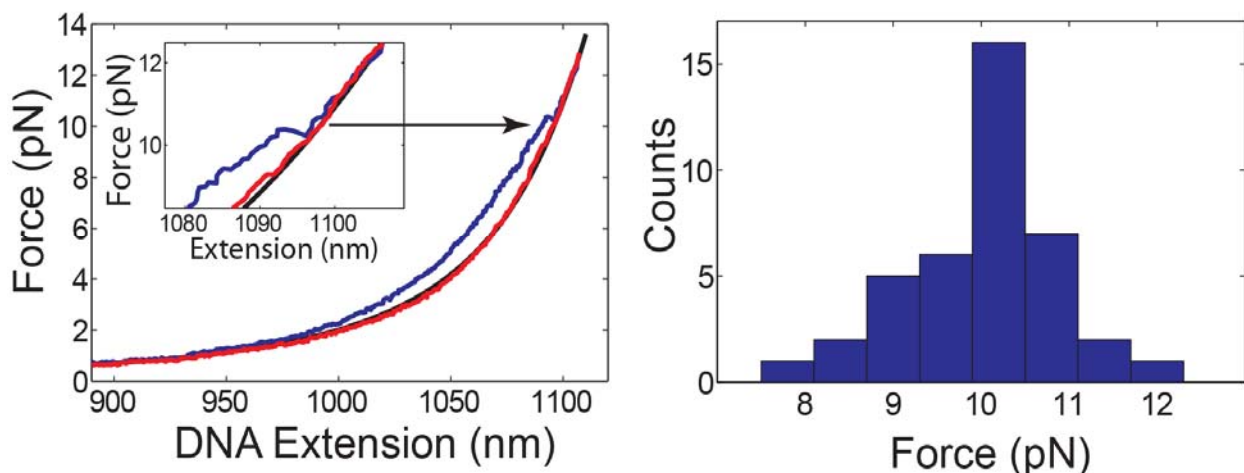


Figure 3-4. Representative force-extension behavior of bare DNA molecule (red) and SSB-bound molecule (blue). Inset: close-up of SSB dissociation event at ~10 pN. The bare DNA molecule force-extension is fit by the model of elasticity described in the text (black line). Distribution of dissociation forces ($N = 40$).

indicating the dissociation of an individual SSB from the construct. This interpretation was corroborated by moving a tether with bound SSB back into a stream with no protein and

observing its F-x behavior. Within a short time of stretching the molecule (<1 s), the F-x curve discretely reverted back to its bare form, indicating that the SSB had indeed dissociated. These results demonstrate our ability to detect wrapping of ssDNA by a single SSB tetramer.

3.3 Tension and its effect on SSB-ssDNA conformation

The ability to detect the presence of an individual SSB on our construct and to use tension to make it dissociate allowed us to characterize very accurately the change in tether extension due to DNA wrapping. This extension change, Δx , provides information on the change in the wrapping conformation of the nucleoprotein complex. In order to investigate this dependence further, we determined Δx from the difference in tether extension between the bare DNA and SSB-bound DNA F-x curves (**Figure 3-4**) at each force. The ability to measure the F-x behavior with and without protein from the *same* tether allowed us to eliminate any effects from tether and bead variability that could have obscured some of the observed features. **Figure 3-5** displays the extension change Δx for a selection of individual tethers (gray curves) and the average from all tethers (red circles). As tension is increased, Δx sharply increases from zero, plateaus at a fairly constant value of ~ 10 - 12 nm, and decreases as the dissociation force is approached.

To measure the extension change upon SSB binding Δx vs. tension (**Figure 3-5**) F-x curves were obtained at fast pulling speeds of $1 \mu\text{m/s}$ and data were collected at 1 kHz. This procedure was used to reduce inaccuracies in Δx observed at slower pulling speeds due to dissociation kinetics. Tethers were pulled at speeds faster than dissociation of the protein, ensuring that the SSB remained bound over the full range of tensions 0 - 15 pN, yet slower than the wrapping/unwrapping kinetics of the SSB-ssDNA complex. Pulling and relaxing curves showed negligible hysteresis confirming the measurement of the actual SSB-ssDNA conformation. The extension change Δx from F-x curves taken at fast ($1 \mu\text{m/s}$) and slow pulling speeds (12 nm/s) were identical at most forces and only exhibited discrepancies only near the dissociation force, as expected.

Moreover, the force dependence of Δx reveals the effect of tension on the wrapping state. Interpreting the change in tether extension with regards to the wrapping state of the SSB tetramer requires a model. Two competing effects should contribute to Δx : (i) on one hand the number of nucleotides N_w that are wrapped around the protein no longer contribute to the elasticity of the

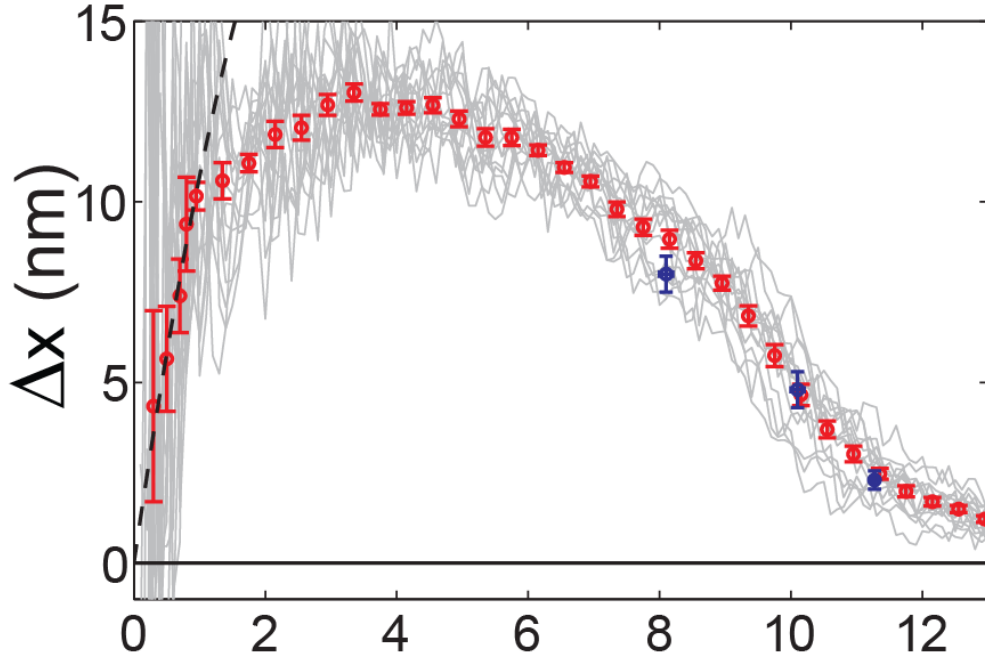


Figure 3-5. Conformation of SSB-DNA complex under mechanical tension. Extension change, Δx , upon SSB binding vs. tension. Individual traces (gray; $N = 15$ traces) were binned and averaged to yield the mean Δx (red circles). The extension change determined from individual binding/unbinding time traces exhibits good agreement (blue circles). The model for Δx (black dotted line) assumes 65 nt remain wrapped around the protein.

tether, but (ii) the ends of the ssDNA bound to the SSB are now separated by a distance that is dependent on the wrapping geometry (**Figure 3-6**). The change in extension (in nm) upon binding one SSB is the difference of those two contributions:

$$\Delta x = \xi_{ss}(F)N_w h_{ss} - x_{SSB}(N_w) \quad (3-1)$$

where ξ_{ss} is the extension of one ssDNA nucleotide at a tension F according to the worm-like chain model of elasticity, h_{ss} is the 0.7-nm contour length per nucleotide of ssDNA [11-13], and x_{SSB} is a geometrical factor that accounts for the distance between the wrapped ssDNA ends on the SSB.

The dashed black line in **Figure 3-5** is a prediction for Δx based on this expression, assuming the protein remains in the (SSB)₆₅ mode at all tensions ($N_w = 65$ nt) and that x_{SSB} is zero; i.e. the ends of the wrapped ssDNA exit the protein next to each other, as indicated by the model for the (SSB)₆₅ wrapping mode derived from the crystal structure [16]. Though this prediction is in reasonable agreement with the data at low forces (<1 pN), it overshoots significantly at larger

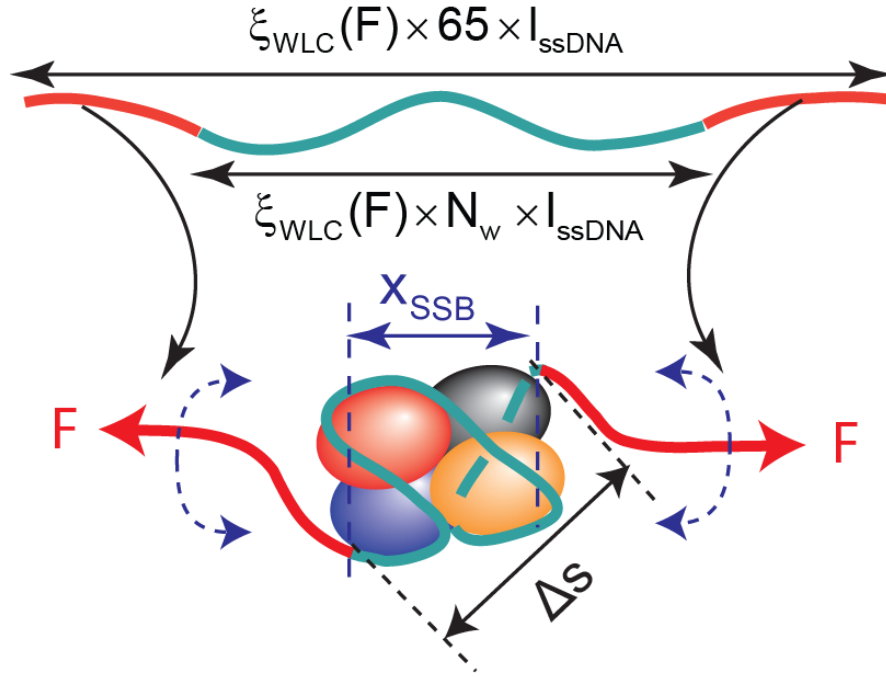


Figure 3-6. Schematic representation of Δx . Top: Bare 65-nt ssDNA and its extension based on the model of elasticity described in the text. Bottom: SSB-bound ssDNA, showing N_w (< 65) nucleotides wrapped (cyan) and the remainder unwrapped (red). Δx is the difference between the end-to-end extension of N_w bare nucleotides (top, cyan) and the separation between the wrapped ssDNA ends on the SSB, x_{SSB} (bottom, cyan), accounting for rotational diffusion of the protein (bottom, blue dotted lines).

tensions. Our data thus suggest that ssDNA is gradually unwrapped from the SSB at forces of 1-8 pN until complete dissociation. This would indicate that tension shifts the protein from the canonical (SSB)₆₅ mode to a different wrapping configuration.

In principle, Eq. (3-1) can be used to extract how the number of wrapped nucleotides N_w depends on tension. The factors in the first term, ζ_{ss} and h_{ss} , that depend on the elastic and structural properties of ssDNA are well determined [11-13] and are consistent with our own fits to the bare tether F-x curves. The second term, x_{SSB} , requires knowing the configuration of ssDNA around the SSB at each tension. As shown in **Figure 3-7a**, we modeled this in two ways: (i) from a “toy” model in which the SSB was approximated as a cylinder with ssDNA wrapped around its circumference (blue curve), and (ii) from the crystal structures of the protein in the (SSB)₆₅ mode (red curve) [16]. In the toy picture, we assumed that 65 nt of ssDNA wraps around the full circumference of the SSB such that its ends exit the protein at the same point. It is

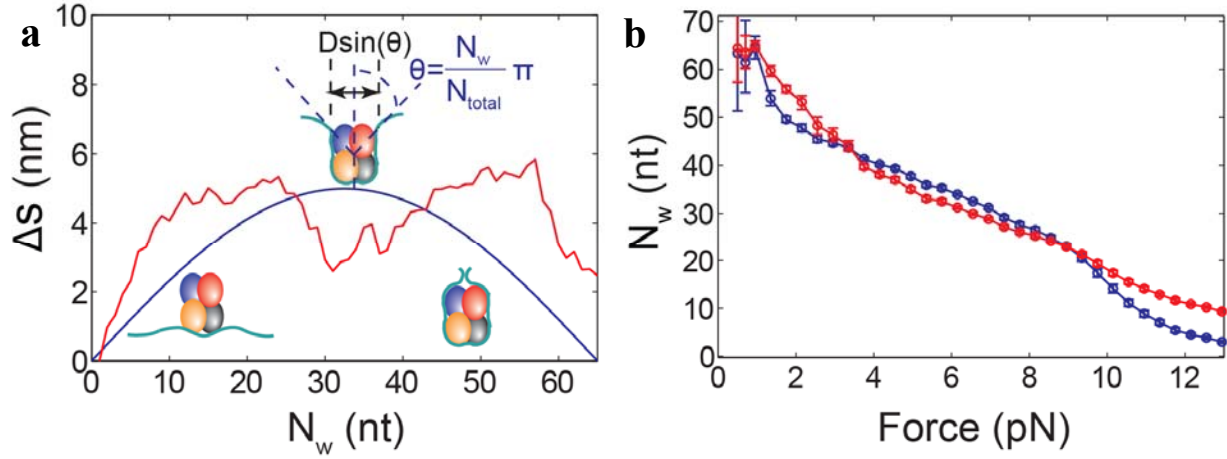


Figure 3-7. (a) Δs vs. N_w based on a “toy” model approximating SSB as a cylinder with ssDNA wrapped around its circumference (blue) and based on the crystal structure of the protein in (SSB)₆₅ wrapping mode (red). Inset: schematic for Δs vs. N_w in the “toy” model. (b) Wrapping conformation (N_w) vs. tension (F) based on the “toy” (blue) and structural (red) models of Δs . Error bars are s.e.m.

easy to show from geometry that the separation between the ends of the wrapped ssDNA, Δs (which is related to x_{SSB} , as discussed below), is given by $\Delta s = D \sin(\pi N_w / N_{tot})$. Here, D is the “effective” diameter of the protein (taken to be ~ 50 Å based on the SSB structure), and $N_{tot} = 65$ nt is the total number of nucleotides available to wrap. This function (blue curve, **Figure 3-7a**) is zero when the SSB is both fully wrapped and unwrapped, and it reaches a maximum when the exiting ends of the ssDNA are on opposite ends of the protein. Our alternate model utilizes the (SSB)₆₅ crystal structure as a starting point for estimating the wrapping geometry at different tensions. Here we calculate the separation Δs between wrapped ssDNA ends as we remove one nucleotide at a time from each end in the structure, maximizing their separation in response to the force applied (this implicitly assumes identical contacts are made by each nucleotide to the protein). Qualitatively, this function, plotted vs. N_w (red curve, **Figure 3-7a**), resembles that of the toy model, though differences emerge from the structural details.

The geometrical factor x_{SSB} in Eq. (3-1) does not depend solely on the end-to-end wrapped ssDNA separation Δs . Another factor contributing to x_{SSB} is the fact that the nucleoprotein complex can diffuse rotationally. At very low tensions, in fact, we expect that the contribution of Δs on the tether extension to be negligible because the protein-DNA complex can reorient itself completely by thermal fluctuations, such that x_{SSB} averages to zero. As force F is exerted,

however, a torque is applied to the complex dependent on the end-to-end separation Δs , orienting it along the direction of tension. Therefore, only the component of Δs tangent to the tether axis (along the tension F) contributes to the measured extension change Δx (**Figure 3-6**). One can show that this component is given by

$$x_{SSB}(N_w) = L(F\Delta s/k_B T)\Delta s(N_w) \quad (3-2)$$

where $L(z) \equiv \coth(z) - 1/z$, is the Langevin function [17], derived from the alignment of a particle undergoing Brownian rotational motion to an external torque (Appendix B). (In Eq. (3-2), N_w implicitly depends on force F .) The effect of this factor is to suppress the contribution from the wrapping geometry on the measured extension change Δx at low tensions.

Using Eqs. (3-1) and (3-2), we extracted N_w from the measured extension change Δx at each tension F . The results of this procedure are shown in the plot of N_w vs. F in **Figure 3-7b** for both configuration models (blue circles for the toy model, red circles for the structure-based model). N_w exhibits a gradual decrease from ~ 65 nt as tension increases from 1-10 pN. Moreover, the trends for both curves are nearly identical, indicating that the details of the geometrical factor x_{SSB} are largely unimportant. Thus, the effect of tension on the SSB-ssDNA complex is to unwrap the protein *gradually*; importantly we see no evidence for discrete changes in wrapping states with tension.

3.4 Discussion

The measurements of the extension change Δx vs. tension (**Figure 3-5**) allow us to form a picture of the energy landscape governing SSB-ssDNA complex formation. From Δx and the two geometrical models for the SSB-ssDNA complex conformation we estimated the number of nucleotides wrapped at each tension, $N_w(F)$. Though the details of the two models differ, the overall trends are duplicated. The data indicate that the protein remains fully wrapped ($N_w \approx 65$ nt) only for tensions < 1 pN, then *gradually* unwraps as tension is increased from 1-8 pN. One observation is that at forces > 6 pN, enough ssDNA is presumably available to bind a second protein. However, experiments at those forces surprisingly provide no evidence for more than a single SSB binding or dissociation event, even at elevated protein concentrations (44 nM; data not shown). These results suggest the bound SSB may be too diffusive on ssDNA to allow a second protein to wrap the limited—though technically sufficient—ssDNA available. Indeed,

we observe multiple binding (or unbinding) events only on longer substrates (175-nt poly-dT; data not shown).

These observations allow us to propose an energy landscape for SSB-ssDNA interactions as plotted schematically in **Figure 3-8** against the number of wrapped nucleotides N_w . The minimum in the free energy curve corresponds to a particular wrapping conformation. The effect of tension on DNA is to tilt the free energy surface along the mechanical reaction coordinate [18], shifting this minimum. At zero tension the nucleoprotein complex resides inside a shallow potential well near its canonical (SSB)₆₅ conformation. The energy barrier around this well is likely quite low (of order $\sim 1 k_B T$) since a small tension of only ~ 1 pN is sufficient to

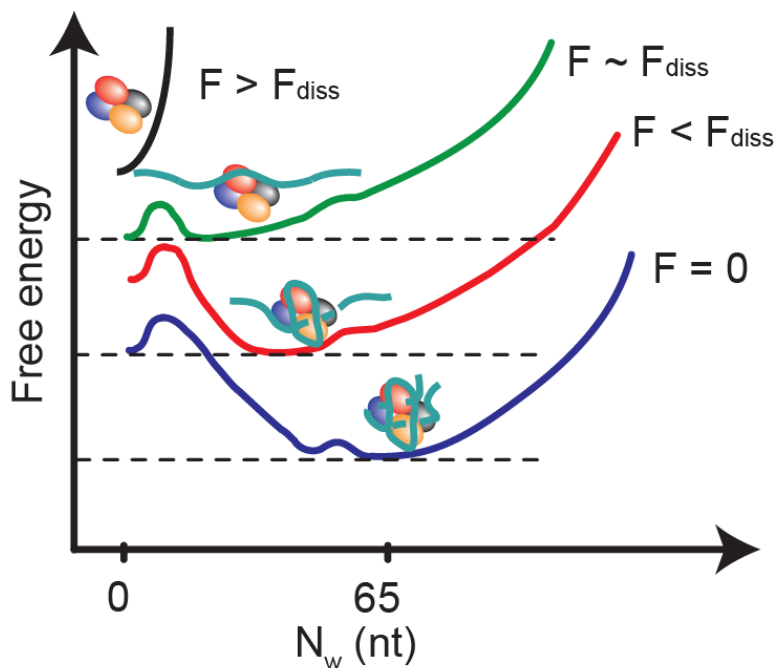


Figure 3-8. Proposed energy landscape for SSB-ssDNA interactions. Free energy surfaces are plotted vs. the number of wrapped nucleotides N_w for different forces. At zero force (blue), the SSB exists in its canonical (SSB)₆₅ wrapping mode. Force tilts the free energy surface, shifting the equilibrium to a less wrapped state (red). At the dissociation force (green), the SSB is mostly unwrapped and dissociation occurs through thermal activation over a final energy barrier, leading to a discrete change in N_w . Above the dissociation force (black) the SSB only engages with ssDNA loosely without wrapping the molecule.

begin unwrapping the protein. As tension is increased beyond 1 pN, the gradual unwrapping indicates that the energy landscape of the complex is quite shallow and smooth in these

intermediate wrapping conformations ($N_w \approx 65\text{-}20$ nt). This landscape cannot exhibit large energy barriers since these would lead to discrete transitions in the extension, which were not observed until complete dissociation. As shown schematically in **Figure 3-8**, as tension is increased, tilting the free energy surface, the energy minimum is shifted gradually. Finally, discrete $\sim 8\text{-}4$ nm-sized transitions are observed for forces of 8-10 pN, where the ssDNA unwraps completely from the protein in one step and dissociates. These events indicate a larger free energy barrier in the near-minimal wrapping conformation ($N_w \leq 20$ nt).

3.5 Summary

Together these findings suggest a very dynamic picture of SSB-ssDNA interactions. In intermediate wrapping conformations ($N_w \approx 65\text{-}20$ nt), the protein is free to wrap and unwrap significant lengths of ssDNA with little free energy cost. This transient wrapping/unwrapping may provide a mechanism for the observed diffusive motion of SSB along ssDNA [19, 20]. This energy landscape may also explain how genome maintenance translocases (e.g. polymerases, helicases) can cause SSB to be displaced along ssDNA. Our observations suggest that these motor proteins need only generate very low forces (of order ~ 1 pN) to disrupt the (SSB)₆₅ structure and begin unwrapping ssDNA. Once partially unwrapped, diffusion can be biased by motor translocation to displace the SSB. Finally, only 10 pN of force are needed for the protein to dissociate completely, within the range of motor forces observed.

3.6 References

1. Lohman, T.M. and W. Bujalowski, *E. coli SSB Protein: Multiple Binding Modes and Cooperativities*. CRC Press, 1990: p. 131-168.
2. Kozlov, A.G. and T.M. Lohman, *Calorimetric studies of E. coli SSB protein-single-stranded DNA interactions. Effects of monovalent salts on binding enthalpy*. J Mol Biol, 1998. 278(5): p. 999-1014.
3. Bujalowski, W. and T.M. Lohman, *Negative co-operativity in Escherichia coli single strand binding protein-oligonucleotide interactions. II. Salt, temperature and oligonucleotide length effects*. Journal of Molecular Biology, 1989. 207(1): p. 269-88.
4. Zhou, R., et al., *SSB functions as a sliding platform that migrates on DNA via reptation*. Cell, 2011. 146(2): p. 222-32.
5. Brewer, L.R. and P.R. Bianco, *Laminar flow cells for single-molecule studies of DNA-protein interactions*. Nat Methods, 2008. 5(6): p. 517-25.

6. Moffitt, J.R., et al., *Differential detection of dual traps improves the spatial resolution of optical tweezers*. Proc Natl Acad Sci U S A, 2006. 103(24): p. 9006-11.
7. Bujalowski, W. and T.M. Lohman, *Escherichia coli single-strand binding protein forms multiple, distinct complexes with single-stranded DNA*. Biochemistry, 1986. 25(24): p. 7799-802.
8. Lohman, T.M. and L.B. Overman, *Two binding modes in Escherichia coli single strand binding protein-single stranded DNA complexes. Modulation by NaCl concentration*. J Biol Chem, 1985. 260(6): p. 3594-603.
9. Landry, M.P., et al., *Characterization of photoactivated singlet oxygen damage in single-molecule optical trap experiments*. Biophys J, 2009. 97(8): p. 2128-36.
10. Wang, M.D., et al., *Stretching DNA with optical tweezers*. Biophysical Journal, 1997. 72(3): p. 1335-46.
11. Murphy, M.C., et al., *Probing single-stranded DNA conformational flexibility using fluorescence spectroscopy*. Biophysical Journal, 2004. 86(4): p. 2530-7.
12. Mills, J.B., E. Vacano, and P.J. Hagerman, *Flexibility of single-stranded DNA: use of gapped duplex helices to determine the persistence lengths of poly(dT) and poly(dA)*. Journal of Molecular Biology, 1999. 285(1): p. 245-57.
13. Rivetti, C., C. Walker, and C. Bustamante, *Polymer chain statistics and conformational analysis of DNA molecules with bends or sections of different flexibility*. Journal of Molecular Biology, 1998. 280(1): p. 41-59.
14. Bustamante, C., et al., *Entropic elasticity of lambda-phage DNA*. Science, 1994. 265(5178): p. 1599-600.
15. Zhang, Y., H. Zhou, and Z.C. Ou-Yang, *Stretching single-stranded DNA: interplay of electrostatic, base-pairing, and base-pair stacking interactions*. Biophysical Journal, 2001. 81(2): p. 1133-43.
16. Raghunathan, S., et al., *Structure of the DNA binding domain of E. coli SSB bound to ssDNA*. Nat Struct Biol, 2000. 7(8): p. 648-52.
17. Kittel, C., *Introduction to solid state physics*. 3rd ed. 1966, New York,: Wiley. 387-389.
18. Bustamante, C., et al., *Mechanical processes in biochemistry*. Annu Rev Biochem, 2004. 73: p. 705-48.
19. Roy, R., et al., *Dynamic structural rearrangements between DNA binding modes of E. coli SSB protein*. J Mol Biol, 2007. 369(5): p. 1244-57.
20. Roy, R., et al., *SSB protein diffusion on single-stranded DNA stimulates RecA filament formation*. Nature, 2009. 461(7267): p. 1092-7.

Chapter 4. Binding Dynamics of (SSB)₆₅ Binding Mode

4.1 Introduction

In the previous chapter we showed that ssDNA can be gradually unwrapped from ssDNA with force. By probing SSB/ssDNA interactions with force we showed that we can dissociate SSB with forces above 10 pN. The ability to disrupt the complex with mechanical force applied to the ssDNA allows us to obtain thermodynamic parameters associated with this interaction under lower salt concentrations where such information is difficult to obtain by ensemble methods which require very high salt concentrations [1-4]. Here we present optical trap measurements to study SSB kinetics and thermodynamics under more biologically relevant conditions. In measurements of SSB dynamics, mechanical force allows us to distinguish between the binding and DNA wrapping kinetics of the protein. With this method, we are able to determine the kinetics of binding and DNA wrapping, the free energy of protein dissociation. These findings not only provide insight into the interaction between SSB and DNA, but also into the mechanism by which SSB diffuses along ssDNA and by which it can be displaced by the genomic machinery [5, 6].

4.2 Experimental results

The ability to detect the presence of an individual SSB on our construct and to use tension to make it dissociate allowed us to characterize very accurately the binding and unbinding kinetics of the protein. Briefly, we held a tether at a tension higher than the dissociation force (>10 pN) in a buffer with SSB, then suddenly dropped the tension to a range permissive for binding (<10 pN) (**Figure 4-1a**). After a short time, we observed a stepwise increase in the tension on the molecule corresponding to DNA condensation from SSB binding (**Figure 4-1b**).

With this “force-jump” technique we were able to detect individual binding events with high temporal resolution (~0.1 s). Moreover, by repeating the force-jump cycle the same tether could be recycled many times, allowing us to collect extensive statistics (~50 binding events per tether, typically) and determine the distributions of binding times, τ_{bind} , for a number of conditions.

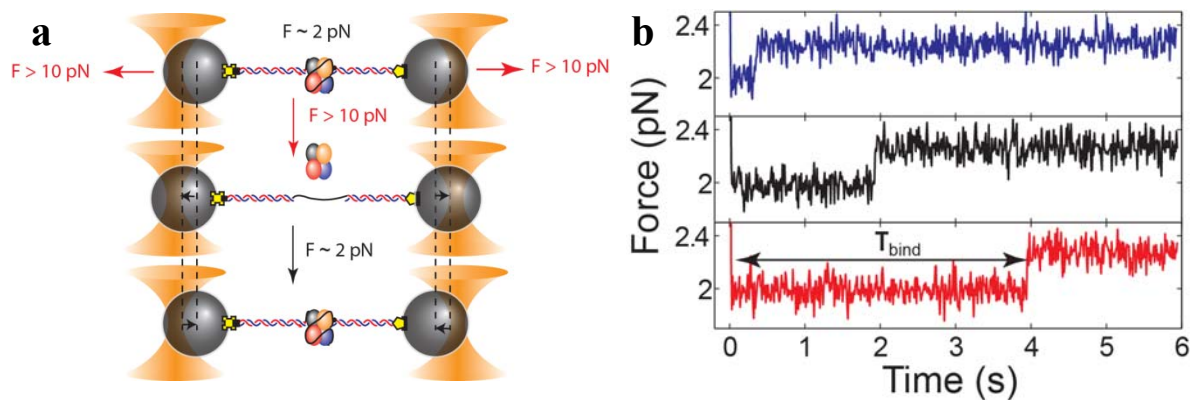


Figure 4-1. Kinetics of SSB binding and unbinding under mechanical tension. **(a)** At $t = 0$, the tension is decreased from $F > 10$ pN to ~ 2 pN; SSB binding leads to an observed increase in force at τ_{bind} . **(b)** Representative time traces of force-jump measurements to determine binding time τ_{bind} .

4.2.1 Diffusion limited binding process

In a first experiment, we measured SSB binding kinetics as a function of protein concentration ($[\text{SSB}] = 0.44\text{--}1.32$ nM tetramer), jumping from a high tension >10 pN to a low force of 2.5 ± 0.4 pN, constant across the range of concentrations. As shown in **Figure 4-2a**, binding time distributions determined at varying SSB levels were exponential, indicative of a single rate-limiting kinetic event.

These distributions were fit to an exponential function (**Figure 4-2a**),

$$P(\tau_{\text{bind}}) = k \cdot \exp(-k\tau_{\text{bind}}) \quad (4-1)$$

to determine the average binding rate, k . As shown in **Figure 4-2b**, k increased linearly with SSB concentration, as expected for a bimolecular reaction. The slope of this line yields a second-order binding rate constant $k_{\text{bind}} = 6.4 \times 10^8 \text{ M}^{-1}\text{s}^{-1}$, which approaches the value of a diffusion-limited bimolecular collision. Our value for k_{bind} is in good agreement with estimates from bulk stopped-flow kinetic measurements under similar buffer conditions [2] suggesting that the tethering geometry and the low tension in these single-molecule measurements do not disrupt the SSB binding process significantly.

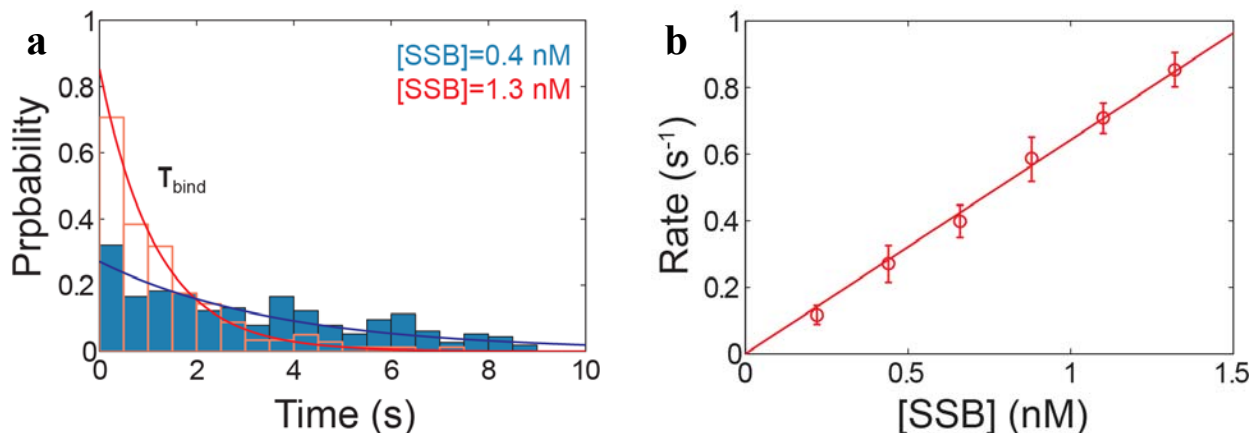


Figure 4-2. SSB binding kinetics **(a)** Representative binding time distributions and fits to exponential at $[SSB] = 0.4$ nM (blue) and 1.3 nM (red) at a tension $F = 2$ pN. **(b)** Average binding rate vs. $[SSB]$ and fit to line with slope $k_{bind} = 6.4 \times 10^8 \text{ M}^{-1} \text{ s}^{-1}$ ($N = 200 - 300$).

4.2.2 Force spectroscopy of binding rates

Since higher tensions eventually lead to dissociation of the protein, we investigated further the role of force on SSB-(dT)₇₀ binding kinetics. The force-jump experiment described above was repeated in a different manner, varying the force to which the tether was dropped (2-8 pN) while maintaining a constant SSB concentration (0.88 nM). Under this range of conditions, the binding time distributions were also single-exponential (data not shown), and the average binding rate k was affected only slightly by tension ($F < 8$ pN, red circles, **Figure 4-4**). This result indicates that for a wide range of tensions SSB binding kinetics are unaffected. At forces of 8 pN and larger, however, the behavior changed noticeably and we observed both protein binding and unbinding events. Rather than utilize the force-jump technique, we characterized these events by maintaining a constant tension on the tether, operating the optical tweezers in force feedback [7]. **Figure 4-3a** displays typical time traces of the tether extension obtained at different forces. Here protein binding was observed as a decrease in extension due to condensation of the tether and protein dissociation as an increase in extension. The time traces in **Figure 4-3a** exhibit a characteristic two-state hopping pattern between low extension or “condensed” state (offset to 0 for clarity), corresponding to SSB-bound DNA, and high extension (4-8 nm, depending on tension), corresponding to the bare DNA tether. As force on the DNA increases, the equilibrium can be seen to shift gradually to the unbound state.

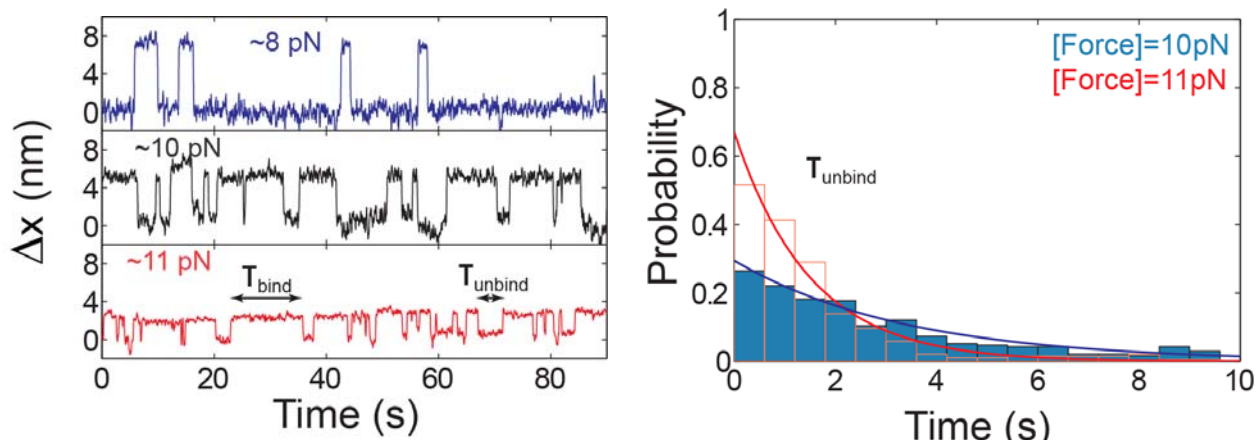


Figure 4-3. Binding rate force spectroscopy. (a) Representative time traces of force-feedback measurements at tensions $F = 7$ pN (blue), 9 pN (black), and 10 pN (red) at a concentration $[SSB] = 0.88$ nM. Hopping between bare (high) and SSB-bound (low) states determines the binding and unbinding times τ_{bind} and τ_{unbind} , respectively. (b) Representative unbinding time distributions and fits to exponential at $F = 10$ pN (blue) and 11 pN (red) at a concentration $[SSB] = 0.88$ nM.

From these traces, we were able to measure individual binding and dissociation times, τ_{bind} and τ_{unbind} , at high tensions (>8 pN), and collect sufficient statistics to compile probability distributions. As shown in **Figure 4-3b**, unbinding time distributions were single exponential at those forces, indicating a single rate-limiting kinetic event. The average rates determined from these distributions together with those obtained at low forces from force-jump experiments are plotted against tension in **Figure 4-4**. Above 8 pN, both binding (red circles) and unbinding (blue triangles) exhibit a force dependence, crossing at a force of ~ 10 pN. At this force the tethers spend half their time in the SSB-bound state and half in the bare state on average.

The force dependence of the binding/unbinding kinetics reveals important features of nucleoprotein complex formation. Since wrapping of ssDNA by the SSB condenses the tether against the tension applied by the optical traps, we expect that wrapping (and the reverse reaction, unwrapping) should be strongly force-dependent. In contrast, any process that does not affect the extension of the DNA molecule should not display tension sensitivity. Thus, force provides a useful probe to distinguish kinetic steps that affect DNA conformation from those that do not. In **Figure 4-4**, the average binding rate (red curve) displays a biphasic behavior, largely independent of tension from 2 - 6 pN, and force-dependent from 8 - 10 pN. This observation suggests that two different kinetic events may be involved at different tensions. To test this idea, the binding rates were fit to a model where binding occurs in two successive kinetic steps

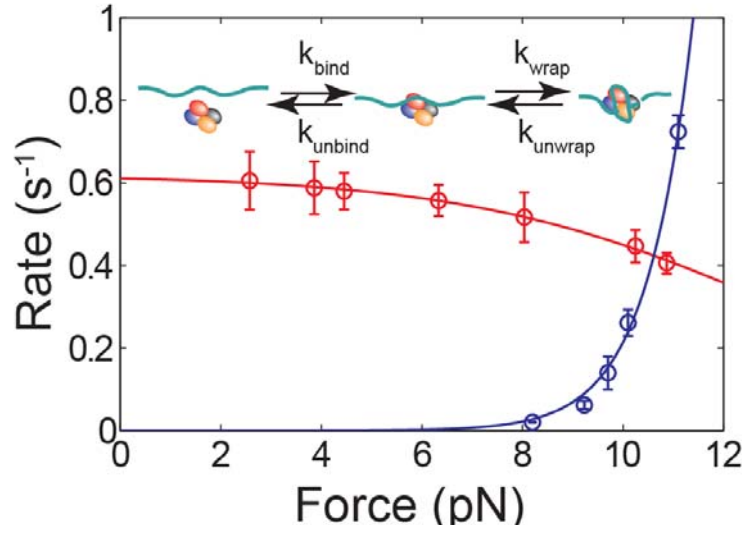


Figure 4-4. Average binding (red) and unbinding (blue) rates vs. tension ($N = 100 - 200$). Inset: schematic of two-step kinetic model for binding and wrapping. The data are well fit by the kinetic model (red and blue lines). Error bars are s.e.m.

(**Figure 4-4**, inset): (i) a tension-independent, second-order process where the SSB come into loose contact with ssDNA, followed by (ii) a tension-dependent first-order step in which the ssDNA is wrapped. A similar mechanism was proposed previously based on ensemble kinetic results [2]. Based on this model, the observed binding rate is given by the following expression:

$$\frac{1}{k_{bind,obs}} = \frac{1}{k_{bind}[SSB]} + \frac{1}{k_{wrap}^0 e^{-F\Delta x_b / k_B T}} \left(1 + \frac{k_{unbind}}{k_{bind}[SSB]} \right) \quad (4-2)$$

where k_{bind} is the second-order binding rate constant from the unbound to loosely bound state, k_{unbind} is the unbinding rate from this loosely bound conformation, and k_{wrap}^0 is the force-dependent wrapping rate at zero tension. The wrapping process is assumed to be driven by thermal activation over a free energy barrier [8], leading to the exponential force dependence. Here, Δx_b is the distance to the barrier in the free energy landscape of SSB-DNA interactions along the mechanical reaction coordinate of the experiment. A similar expression is obtained for the observed unbinding time:

$$\frac{1}{k_{unbind,obs}} = \frac{1}{k_{unbind}} \left(1 + \frac{k_{wrap}^0 e^{-F\Delta x_b / k_B T}}{k_{unwrap}^0 e^{F\Delta x_u / k_B T}} \right) + \frac{1}{k_{unwrap}^0 e^{F\Delta x_u / k_B T}} \quad (4-3)$$

where k_{unwrap}^0 is the unwrapping rate at zero tension, and Δx_u is the distance along the mechanical coordinate between the wrapped state and the free energy barrier for dissociation.

The diffusion limit places an upper bound on the binding rate k_{bind} in Eq. (4-2). Thus, at the SSB concentration assayed, 0.88 nM, $k_{bind}[\text{SSB}]$ must be of order $\sim 1 \text{ s}^{-1}$. This is consistent with the fact that the observed binding rate is independent of force at low tensions, i.e. that the rate-limiting step is likely k_{bind} . Conversely, the observed unbinding rate displays a strong force dependence, increasing from a negligibly small value at low forces (no unbinding events were detected at tensions $< 7 \text{ pN}$), to a value exceeding that of the binding rate at high forces. This indicates that the unwrapping step is rate-limiting. It follows that k_{unbind} in Eq. (4-3) must be much larger than the maximum observed unbinding rate in the experiments, $\sim 1 \text{ s}^{-1}$. As a result, $k_{unbind} \gg k_{bind}[\text{SSB}]$. This observation simplifies Eq. (4-2) since the rightmost term in the parentheses dominates, and Eq. (4-3) since the first term is negligibly small. The fit of Eq. (4-2) to the binding data is excellent (red curve **Figure 4-4**) and yields values of $k_{bind} = (7 \pm 0.3) \times 10^8 \text{ M}^{-1} \text{ s}^{-1}$, $k_{wrap}^0/k_{unbind} = \sim 10^2 \text{ s}^{-1}$, and $\Delta x_b = 1.4 \pm 0.3 \text{ nm}$. The fit of Eq. (4-3) to the unbinding data (blue curve **Figure 4-4**) yields values of $k_{unwrap}^0 = \sim 10^{-3} \text{ s}^{-1}$ and $\Delta x_u = 2.8 \pm 0.5 \text{ nm}$. The small value for k_{unwrap}^0 indicates that dissociation is a very rare event at forces less than 7 pN, which is consistent with what we observe experimentally.

Thus, according to the data and model the binding/unbinding and wrapping/unwrapping rates for 0.88 nM SSB and zero tension are ordered as follows: $k_{wrap}^0 \gg k_{unbind} \gg k_{bind}[\text{SSB}] \gg k_{unwrap}^0$. These results indicate that the loosely bound state is a short-lived intermediate; at low tension (where $k_{wrap}^0 > k_{unbind}$), the SSB-ssDNA complex is driven kinetically to the wrapped state, and at tensions close to 10 pN (where $k_{wrap}(F) < k_{unbind}$) it is driven to dissociation.

4.3 Discussion

Our measurements of single SSB-ssDNA complexes under tension provide insight into the dynamics, energetics of nucleoprotein complex formation and dissociation as well as the wrapping topology. The characterization of binding/dissociation kinetics by force-jump and force-feedback experiments strongly suggests that SSB-ssDNA complexes form in two successive steps, as depicted in the inset to **Figure 4-4**. In our simple model used to fit the data

in **Figure 4-4**, we assumed an exponential form for the rate dependence on tension (Eqs. (4-2) and (4-3)). From these fits, the distances to the transition state along the mechanical reaction coordinate, Δx_b and Δx_u for binding and dissociation, sum to $1.4+2.8 = 4.2$ nm. This value is in excellent agreement with the extension change $\Delta x = 4.4$ nm measured upon SSB binding near the dissociation force ~ 10 pN (**Figure 3-5**, red points determined from the force-extension behavior, and blue points from constant force binding/unbinding transitions), a tension where the rate dependence on force is most pronounced and detectable. This observation corroborates our interpretation that the force-dependent step involves the transition from the loosely bound to the fully wrapped state. In this picture, the distance to the transition state for binding, Δx_b , corresponds to the “minimal” ssDNA interaction length required to wrap the protein. A distance Δx_b of 1.3 nm equates to 5-6 nt at a force of 10 pN, based on our conversion from extension to number of wrapped nucleotides in **Figure 3-5** (i.e. at 10 pN, 15 nt of wrapped ssDNA corresponds to 4 nm in extension change).

The rate constants determined from the fits of our kinetic data to the two-step model allow us, in principle, to calculate the equilibrium constant for SSB-(dT)₇₀ binding under our solution conditions. The force-dependent equilibrium constant is related to the rate constants by the expression

$$K_{eq}(F) = \frac{k_{bind}}{k_{unbind}} \frac{k_{wrap}^0 e^{-F\Delta x_b / k_B T}}{k_{unwrap}^0 e^{F\Delta x_u / k_B T}} = \frac{k_{bind} k_{wrap}^0}{k_{unbind} k_{unwrap}^0} e^{-F\Delta x / k_B T} = K_{eq}^0 e^{-F\Delta x / k_B T} \quad (4-4)$$

where K_{eq}^0 is the equilibrium constant at zero force, and $\Delta x = \Delta x_b + \Delta x_u$ is the extension change between unwrapped and wrapped states. Based on Eq. (4-4), our fitted rates lead to an estimate of $K_{eq}^0 \sim 10^{14} \text{ M}^{-1}$, corresponding to a standard binding free energy (at zero force) of $\Delta G^0 \sim 30 k_B T$. However, one should exercise caution with this estimate. Though the force-dependent rates in Eqs. (4-2), (4-3), and (4-4) are valid in the vicinity of the dissociation force where the data were fit (~ 10 pN), extrapolating these expressions to zero force implicitly assumes that the extension change Δx is constant. However, it is evident from **Figure 3-5** that this assumption is not justified; $\Delta x(F)$ decreases as tension increases from 2-10 pN, and extrapolation based on a value of Δx near 10 pN will underestimate the true equilibrium binding constant.

One can show (Appendix A) that a force-dependent extension change $\Delta x(F)$ can be accounted for by modifying the expression for the equilibrium constant to

$$K_{eq}(F) = K_{eq}^0 \exp\left(-\int_0^F dF' \Delta x(F') / k_B T\right) \quad (4-5)$$

Note that the integral in the exponential is simply the area under the Δx vs. force curve in **Figure 3-5**, and thus can be obtained directly from our measurements. Using Eq. (4-5) to properly extrapolate $K_{eq}(F)$ near the dissociation force to 0 pN yields a better estimate of $K_{eq}^0 \sim 10^{19} \text{ M}^{-1}$, corresponding to a free energy of $\Delta G^0 \sim 45 k_B T$. It should be noted that the very high affinity of SSB to ssDNA (dT)₇₀ and the competitive effects of the different binding modes has made measurements of the equilibrium constant at low salt concentrations difficult in bulk studies [9]. To date, accurate measurements for SSB binding to (dT)₇₀ have been made only under very high salt concentrations (even requiring NaBr rather than NaCl), solution conditions that lower the equilibrium binding constant to $K_{eq} < 10^9 \text{ M}^{-1}$ ($K_{eq} = 4 \times 10^9 \text{ M}^{-1}$ in 0.8 M [NaBr], pH 8.1, 25°C) [9, 10]. The ability to use force to disrupt SSB interactions to ssDNA allows us for the first time to make reasonable estimates thermodynamic properties under lower salt conditions (10 mM NaCl).

4.4 Summary

We carried out measurements of SSB binding/unbinding and wrapping/unwrapping kinetics as a function of mechanical force with our optical trap assay. The data indicate a two-step mechanism where: 1) SSBs bind to ssDNA in a fast, diffusion-limited step and adopt a short-lived “loosely bound” mode where the protein is in contact with ssDNA but does not wrap it, and 2) SSBs wrap the available ssDNA in a fast, tension dependent step. Dissociation with force occurs in part because of the slight decrease in wrapping rate with tension, but mostly because of a large increase in unwrapping rate. Fitting the kinetic data allowed us to estimate individual rates for these two steps, and these yield equilibrium constants consistent with the thermodynamics measurements.

4.5 References

1. Lohman, T.M. and M.E. Ferrari, *Escherichia coli single-stranded DNA-binding protein: multiple DNA-binding modes and cooperativities*. Annu Rev Biochem, 1994. 63: p. 527-70.

2. Kozlov, A.G. and T.M. Lohman, *Stopped-flow studies of the kinetics of single-stranded DNA binding and wrapping around the Escherichia coli SSB tetramer*. Biochemistry, 2002. 41(19): p. 6032-44.
3. Kuznetsov, S.V., et al., *Microsecond dynamics of protein-DNA interactions: direct observation of the wrapping/unwrapping kinetics of single-stranded DNA around the E. coli SSB tetramer*. J Mol Biol, 2006. 359(1): p. 55-65.
4. Kozlov, A.G. and T.M. Lohman, *Kinetic mechanism of direct transfer of Escherichia coli SSB tetramers between single-stranded DNA molecules*. Biochemistry, 2002. 41(39): p. 11611-11627.
5. Joo, C., et al., *Real-time observation of RecA filament dynamics with single monomer resolution*. Cell, 2006. 126(3): p. 515-27.
6. Hobbs, M.D., A. Sakai, and M.M. Cox, *SSB protein limits RecOR binding onto single-stranded DNA*. J Biol Chem, 2007. 282(15): p. 11058-67.
7. Visscher, K. and S.M. Block, *Versatile optical traps with feedback control*. Methods Enzymol, 1998. 298: p. 460-89.
8. Bustamante, C., et al., *Mechanical processes in biochemistry*. Annu Rev Biochem, 2004. 73: p. 705-48.
9. Kozlov, A.G. and T.M. Lohman, *Calorimetric studies of E. coli SSB protein-single-stranded DNA interactions. Effects of monovalent salts on binding enthalpy*. J Mol Biol, 1998. 278(5): p. 999-1014.
10. Bujalowski, W. and T.M. Lohman, *Negative co-operativity in Escherichia coli single strand binding protein-oligonucleotide interactions. II. Salt, temperature and oligonucleotide length effects*. Journal of Molecular Biology, 1989. 207(1): p. 269-88.

Chapter 5. Interaction of *E.coli* SSB with long ssDNA

5.1 Introduction

As described in the introduction Chapter 2 *E. coli* SSB is unique among ssDNA-binding proteins in that it can bind its substrate in two distinct modes: (SSB)₆₅ and (SSB)₃₅, which bind to 65 and 35 nucleotides, respectively [1]. In (SSB)₆₅ binding mode ssDNA wraps around all four monomers (shown schematically in **Figure 2-1**). In contrast, the (SSB)₃₅ mode likely involves interactions of ssDNA with only two monomers at diagonal ends of the tetramer [2] (**Figure 2-1**). Two types of cooperative binding to ssDNA, referred to as “limited” and “unlimited”, have been observed for *Eco* SSB [3, 4], and these yield complexes with quite different properties *in vitro* [4-6]. Although the mechanism of forming clusters is not clear, it is clear that the (SSB)₆₅ binding mode displays a “limited” type of cooperativity [3, 5, 7] in which SSB filaments appear to be limited to the formation of dimers of SSB tetramers (octamers), which are seen as “beads” in the EM [8]; long nucleoprotein filaments of SSB tetramers do not form along ssDNA in this mode [4]. However in the “unlimited” cooperativity mode long clusters of SSB can form which appears to be correlated with the (SSB)₃₅ binding mode [4, 9].

In this study, we will try to address the following issues: What are the energetics and dynamics of SSB oligomerization? How do these differ from the single-protein behavior, and do the differences reflect protein-protein interactions? Are filaments uniformly composed of SSBs in the same binding mode? What is the minimal protein cluster size competent to nucleate filaments? In order to do this we needed to design DNA substrates that had multiple binding sites for SSB proteins. We achieved this in two ways: 1) one substrate had 175 nucleotides so that at least two SSBs could bind in “65” binding mode, which we named “dT175”, 2) a very long ssDNA that had up to 1700 nucleotides, named “dN1700”, where multiple binding events could be observed.

5.2 Experimental procedures

5.2.1 Medium length ssDNA construct

Our DNA construct design described in Chapter 3 gives us the flexibility to interchange the protein binding site fragment with substrates of varying length, sequence, or secondary structure.

We have main results on a poly-dT, 70-nt ssDNA site (to detect the binding of a single SSB in (SSB)₆₅ mode or two in (SSB)₃₅ mode). We have adapted this approach to make a poly-dT, 175-nt site to accommodate two proteins in (SSB)₆₅ mode or five in (SSB)₃₅ mode.

5.2.2 Long construct

We have also designed a long (>1 kb) ssDNA substrate to allow binding of tens of SSB. Due to difficulties in synthesizing ssDNA oligomers of such length to ligate into our modular construct, we have adopted a different procedure. Here, our basic approach is to utilize an exonuclease to digest one strand of a dsDNA molecule, then ligate functionalized dsDNA handles to this molecule in order to form tethers in our traps (**Figure 5-1**). Briefly, we use a nicking enzyme to introduce one lesion into the bottom strand of a circular plasmid at one position. The exonuclease ExoIII (New England Biolabs) then digests the bottom strand beginning at the nick, moving in the 3'-5' direction at a rate of ~0.5 kb per minutes at 37°C. The plasmid is then cut with two restriction enzymes and ligated to complementary biotinylated

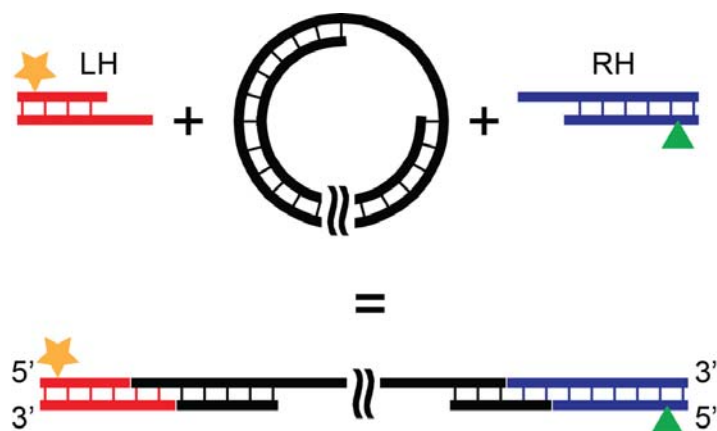


Figure 5-1. SSB binding constructs. Construction involves ligating dsDNA handles (LH and RH) that are functionalized with biotin (green triangle) and digoxigenin (yellow star) to an exonuclease-digested plasmid (black).

and digoxigenated dsDNA handles at each end. The complete constructs are remarkably uniform, consisting of a 1700-nt ssDNA substrate flanked by 1.3-kb biotinylated and 1.8-kb digoxigenated dsDNA.

5.3 Protein clustering on 175nt poly-dT

To investigate nucleoprotein filament formation, we first performed preliminary tests with our “dT175” construct containing a 175-nt binding sites. F-x curves of this molecule are similar to those of the single-protein “dT70” substrate, with an expectedly larger transition region (**Figure 5-2a**, and inset). Importantly, the dissociation force (~ 10 pN) is identical in both constructs, suggesting that the presence of additional protein does not increase the stability of the SSB-ssDNA interaction (more on this point below). Probing the extension of the tether under force feedback as it is moved into a laminar stream containing SSB (4.4 nM), we typically detect 3 or more individual binding steps, as shown in **Figure 5-2b**, inconsistent with all the proteins being in (SSB)₆₅ mode ($65 \times 3 > 175$). The measured step sizes are generally consistent with the single-protein data at the various tensions, though more variability is observed (9-12 nm). In

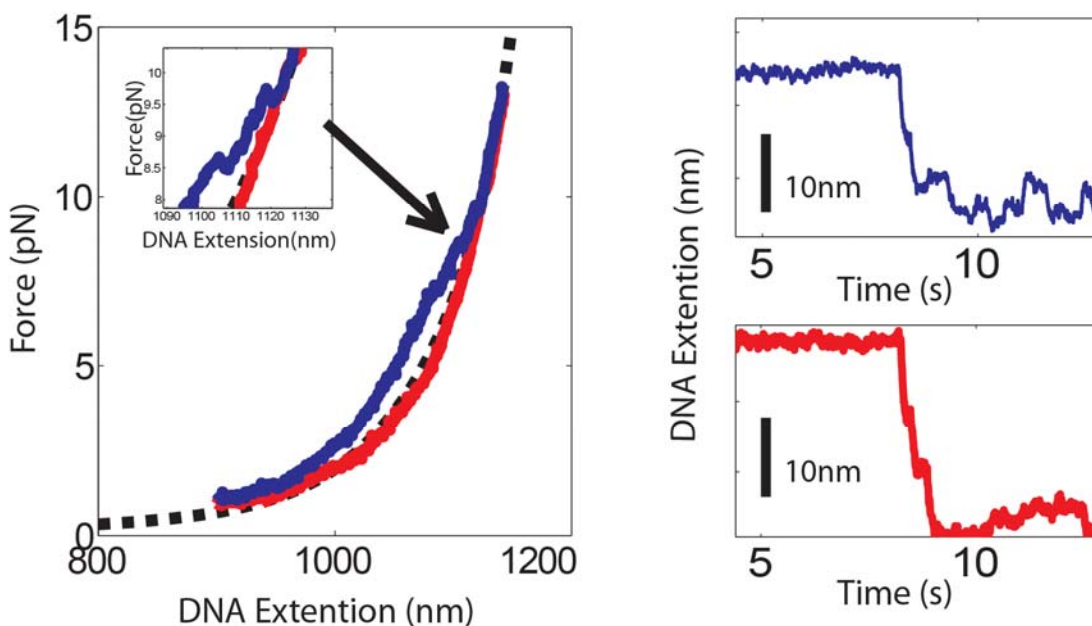


Figure 5-2. Binding of multiple SSB. (a) F-x behavior for “dT-175” ssDNA construct with (red) and without (blue) protein. Black dotted line is a fit. (b) Representative binding time traces. $F=8$ pN.

particular, richer dynamics are commonly detected, in which the ssDNA extension varies by large distances (>5 nm) on relatively slow (~ 0.1 -1 s) timescales (**Figure 5-2b**). These results may indicate that some proteins are in intermediate wrapping states and are transiently wrapping and unwrapping from their substrates.

5.4 Binding dynamics of SSB to Kbps of random sequence DNA

We also tested our “dN1700” construct with a 1700-nt long ssDNA site. In the presence of SSB, this molecule exhibits a different F-x behavior compared to the shorter constructs (**Figure 5-3a**). At low forces (2-15 pN), the molecule is compacted due to wrapping by the SSBs, then smoothly transitions to that of the bare tether at high forces (> 20 pN). As expected, there is more compaction (~ 300 nm at 7 pN) relative to the shorter constructs since there is more available ssDNA for SSBs to bind. More importantly, whereas dissociation of the protein is observed at a force of only 10 pN in the “dT70” and “dT175” constructs, here we must pull to 20 pN for the F-x curves of the SSB-bound molecule and bare molecule to overlap (**Figure 5-3a**). (Moreover, we have never observed dissociation of even one individual SSB from the tether at 10 pN). If the SSBs were independent, non-interacting proteins, we would expect that the

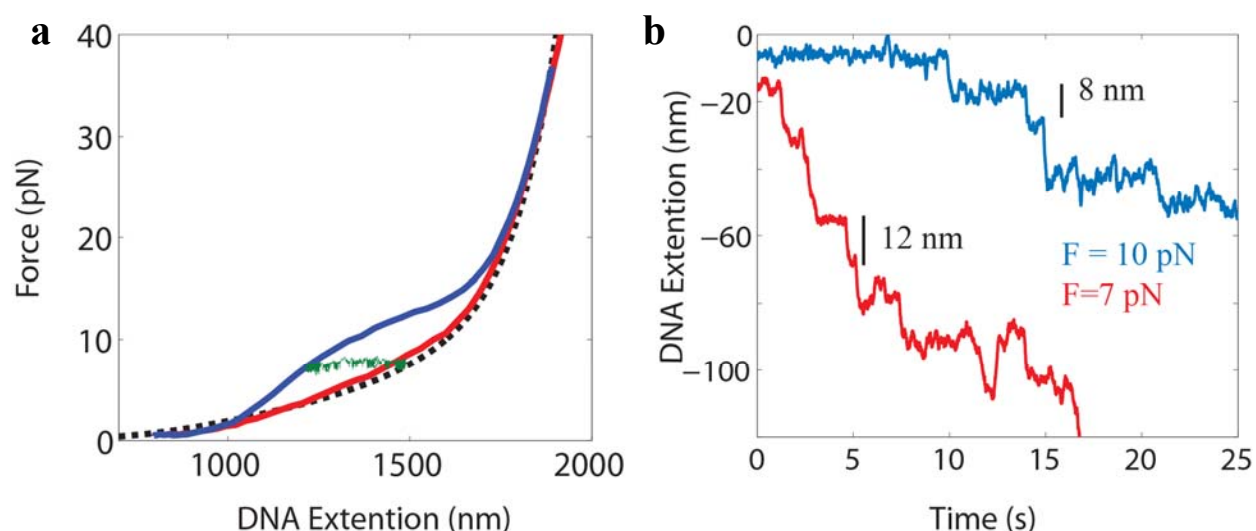


Figure 5-3. Binding of multiple SSB. F-x behavior for **a)** “dN1700” constructs with (blue) and without (red) protein. Black dotted lines are fits; green trace shows compaction at a constant tension. **b)** Representative binding time traces in.

same tension would be required to dissociate several proteins as for an individual protein. Our result may thus represent a direct manifestation of interactions between SSBs, expected for a cooperative binding mode.

As in the other constructs, force feedback experiments (green trace, **Figure 5-3a**) reveal compaction in steps; typically, in the range of ~ 20 transitions (close-up, **Figure 5-3b**). The

predominant step size is consistent with the single-protein data (9-12 nm at tensions of 7-10 pN), though wrapping/unwrapping dynamics are prevalent and variability is also observed, as can be seen directly in sample time traces (**Figure 5-3b**, dotted lines indicate steps). This variability suggests a non-homogeneous SSB-ssDNA filament, composed of proteins in various binding states. Our high-resolution measurements allow us to detect this detailed nucleoprotein filament structure for the first time.

5.5 Discussion

Although the F-x curves for bare and SSB-bound DNA overlap at forces >20 pN, we have evidence that the proteins remain bound at these comparatively high tensions. Taking advantage of our laminar flow cell setup, we place our tether in a region containing a high concentration of SSB (4.4 nM) to saturate it with protein, then move the molecule to a region with no protein. Despite the absence of SSB, the F-x curves (pulling to >20 pN) remain almost identical to those in the presence of protein for an extended period of time. It takes an excess of 8 s at a high tension of ~ 30 pN to observe complete dissociation of the SSB from the construct, in stark contrast to our measurements of the single SSB. These results suggest that the proteins remain bound to the DNA, albeit in a “loose” configuration in which ssDNA is not wrapped. Moreover, they indicate that the transition regions (~ 20 pN) in the F-x curves do not represent unbinding of the protein, but rather unwrapping to a “loose”, but still DNA-bound state. We suspect that this is the same loose binding mode observed in the single-protein measurements. However, our data surprisingly suggest that even this unwrapped mode is less prone to dissociation with tension when present in cluster, perhaps pointing to protein-protein interactions at this level.

5.6 Summary

We carried out measurements of SSB interaction with long and medium length ssDNA binding substrates as a function of mechanical force using our optical trap assay. The data indicate that 1) for a DNA substrate that can accommodate 2 to 3 SSBs does not effect on dissociation force whatsoever, and 2) SSBs bound to longer stretches of ssDNA bound much tighter, probably due to nucleoprotein filament formation. Furthermore, we have evidence that SSB can bind to ssDNA in intermediate wrapping states and are transiently wrapping and unwrapping from their substrates.

5.7 References

1. Lohman, T.M. and M.E. Ferrari, *Escherichia coli single-stranded DNA-binding protein: multiple DNA-binding modes and cooperativities*. Annu Rev Biochem, 1994. 63: p. 527-70.
2. Raghunathan, S., et al., *Structure of the DNA binding domain of E. coli SSB bound to ssDNA*. Nat Struct Biol, 2000. 7(8): p. 648-52.
3. Lohman, T.M., W. Bujalowski, and L.B. Overman, *Escherichia-Coli Single-Strand Binding-Protein - a New Look at Helix-Destabilizing Proteins*. Trends in Biochemical Sciences, 1988. 13(7): p. 250-255.
4. Lohman, T.M., L.B. Overman, and S. Datta, *Salt-dependent changes in the DNA binding co-operativity of Escherichia coli single strand binding protein*. J Mol Biol, 1986. 187(4): p. 603-15.
5. Bujalowski, W. and T.M. Lohman, *Limited co-operativity in protein-nucleic acid interactions. A thermodynamic model for the interactions of Escherichia coli single strand binding protein with single-stranded nucleic acids in the "beaded", (SSB)65 mode*. J Mol Biol, 1987. 195(4): p. 897-907.
6. Ferrari, M.E., W. Bujalowski, and T.M. Lohman, *Co-operative binding of Escherichia coli SSB tetramers to single-stranded DNA in the (SSB)35 binding mode*. J Mol Biol, 1994. 236(1): p. 106-23.
7. Overman, L.B. and T.M. Lohman, *Linkage of pH, anion and cation effects in protein-nucleic acid equilibria. Escherichia coli SSB protein-single stranded nucleic acid interactions*. J Mol Biol, 1994. 236(1): p. 165-78.
8. Martin, G. and M. Salas, *Characterization and cloning of gene 5 of Bacillus subtilis phage phi 29*. Gene, 1988. 67(2): p. 193-201.
9. Sigal, N., et al., *DNA-Unwinding Protein Isolated from Escherichia-Coli - Its Interaction with DNA and with DNA Polymerases*. Proceedings of the National Academy of Sciences of the United States of America, 1972. 69(12): p. 3537-3541.

Chapter 6. Enhancing Rep helicase activity

6.1 Introduction

In the previous chapters we studied the direct interaction of a protein with DNA. In this chapter, we explore whether protein conformation, specifically orientation of different domains within a single protein, can enhance its activity. As an example of such a protein we studied a particular type of helicase called Rep from *E. coli*. Helicases are motor proteins that use energy from NTP binding and/or hydrolysis to unwind dsDNA into two complementary strands. DNA unwinding is essential for a variety of biological processes like DNA replication, recombination, and repair. DNA helicases can unwind dsDNA in the absence of other replication machinery *in vitro*, some of them with high processivity and with unwinding rates up to 500 bp/sec [4]. (Processivity is defined as the length of DNA that can be unzipped at once without dissociation). Helicases physically translocate along DNA, and do so by going through conformational changes caused by a chemical reaction (binding/hydrolysis of NTP) and release of the subsequent product (NDP + Pi) [5-9]. Many helicases are believed to function as oligomers, generally as dimers or hexamers. Oligomerization may provide helicases with multiple DNA binding sites, which is required for helicase function [6-8].

DNA helicases play a central role in DNA metabolism. Mutations in helicases result in a number of human genetic diseases; including xeroderma pigmentosum (XP), Bloom's syndrome, Werner's syndrome, and α -thalassemia [10]. For example, XP is a human disease that increases the risk of skin cancers and can also contribute to neurological problems. Mutations in helicases XPB and XPD that are responsible for repairing DNA result in deficiencies in nucleotide excision repair. Furthermore, mutations in XPB and XPD genes are also linked to two other rare diseases, Cockayne's syndrome and trichothiodystrophy. Both of these diseases result in problems associated with cell development, but without subsequent risk of cancer. The genes linked to Bloom's syndrome and Werner's syndrome also have been shown to encode DNA helicases that have sequence similarity to *E. coli* RecQ DNA helicase [11, 12]. Mutations in these two genes result in a high risk of cancer and chromosomal problems, and in the case of Werner's syndrome, premature aging. However, the biological function of either helicase is not yet clear [10].

The general existence of helicases in prokaryotes, eukaryotes, and viruses demonstrate their importance in nucleic acid metabolism. Almost all organisms possess multiple helicase

genes. In *E. coli* for example, at least 12 different DNA helicases have been identified [8], where each of them may play a role at different DNA metabolism processes. Due to their importance in DNA metabolism and their association with human genetic diseases, helicases have been a wide subject of research in the scientific community and are potential targets for drug development.

6.1.1 SF-I helicases

Helicases have been divided into a number of families and superfamilies (SF1, SF2, SF3, F4 and F5) based on amino acid sequence [13]. The first two and largest superfamilies are defined by seven conserved regions of primary structure or helicase motifs (**Figure 6-1**). Motifs I-VI and Ia [13] are involved in either nucleotide and/or DNA binding sites, motifs I and IV generally interact with ADP. ATP interacts with residues within almost all motifs with the exception of Ia. SF1 contains *B. stearothermophilus* PcrA, *E. coli* Rep (which we will investigate in this chapter), UvrD, RecB, RecD, TraI (F-plasmid), phage T4 Dda, Herpes simplex virus type 1 UL5. SF2 contains *E. coli* PriA, UvrB, RecG, yeast RAD3, eIF-4A, Hepatitis C virus NS3 helicases. SF3 helicases are defined by three conserved regions. Hexameric helicases are classified separately into two small families, the F4 and F5 helicases. The F4 helicases contain 5 distinct conserved motifs and are associated with DNA primase activity. The F5 helicase family is based on sequence similarity to proton-transporting F-1 ATPase [13].

Crystal structures of three SF1 DNA helicases have been solved, including *B. stearothermophilus* PcrA [14, 15], *E. coli* Rep [3] (**Figure 6-1**), and *E. coli* UvrD [16, 17]. The structures of these three proteins are homologous: they consist of two domains that are separated by a cleft, and each of these two domains is further separated into two subdomains (subdomains A and B).

6.1.2 Oligomeric nature of most helicases.

Although some helicases function as hexameric ring structures, some helicases that are monomeric in the absence of NTP or DNA have to oligomerize in order to unwind DNA [18, 19]. The *E. coli* helicases Rep, UvrD and PcrA helicase from *B. stearothermophilus* can form dimers. Furthermore, the main *E. coli* replication helicase DnaB, bacteriophage T7 gene 4 helicase/primase and many others can form ring-like toroidal hexamers [20]. *E. coli* Rep helicase is monomeric in the absence of DNA at concentrations below 8 μ M, but dimerizes upon

binding to DNA [21, 22]. Moreover, Rep dimerization is essential for unwinding DNA *in vitro* [23].

Oligomerization is clearly important for helicase activity of SF1 helicases [19, 24-26]. However some studies investigated the possibility that some SF1 helicases may function as a monomer. In fact, studies of *B. stearrowthermophilus* PcrA helicase suggest that PcrA monomers are the functional form of the helicase [15, 27, 28]. PcrA is very close structurally and in amino-acid sequence to *E. coli* Rep and UvrD helicases [3, 14]. A study of UvrD helicase also proposed that this helicase may function as a monomeric helicase [29]. Truncated form of Rep (Rep Δ 2B see description of a study below) has been shown to have unwinding ability as a monomer [30]. These seemingly independent observations on SF1 helicases' possible unwinding activity as a monomer demonstrate the need for further careful and thorough investigations. In this chapter we will try to explore these discrepancies, and discuss the processivity of these kinds of helicases as well. But first we give some background on Rep helicase that we will study as a prototype for SF-1 helicases.

6.1.3 *E. coli* Rep DNA helicase

The biological function of Rep helicase in *E. coli* is not clear, because it is non-essential under laboratory growth conditions. The *E. coli rep* gene has 673 amino acids ($M_r = 76.4$ kD) [31-33]. Rep has been shown to be present *in vivo* at about 50 copies per wild type cell [34]. Although it is not essential for *E. coli* replication under laboratory conditions, Rep is essential for rolling circle replication by a number of small DNA phages (ϕ X174, S18, the G phages) and filamentous phages (P22, M13, f1, fd) that infect *E. coli* [35].

The deletion of the *rep* gene results in a slower rate of *E. coli* replication fork movement and initiation of an increased number of replication forks [33, 36, 37]. Furthermore, unlike the essential DnaB helicase, Rep can easily bypass Lac repressors bound on its substrate DNA [38]. These observations may explain the frequent pauses of the replication fork in *E. coli rep* mutants when the replication fork encounters protein-DNA complexes [38]. It has been proposed that Rep helps the movement of the replication fork by dissociating DNA-bound proteins [39, 40]. *Rep* mutations increase sensitivity to thymine starvation, ultraviolet light and X-ray radiation, and reduce recombination frequency [37, 41, 42]. Interestingly, simultaneous deletion of *rep*, *uvrD*, and *recBC* genes involved in DNA repair pathways is lethal [40, 43, 44], although their individual deletions result in viable cells. These results from gene deletion experiments suggest

that Rep may function in both replication and DNA repair pathways in *E. coli* [33].

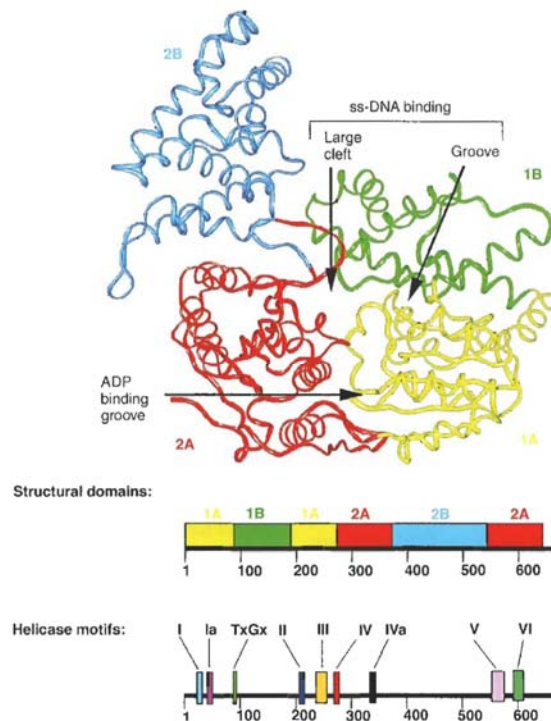


Figure 6-1. The domain structure of *E. coli* Rep monomer. The positions of the subdomains and the helicase motifs within the primary structure of Rep are also shown. Adapted with permission from ref.[1], © 2004 Elsevier

Rep helicase is essential for phage ϕ X174 replication *in vivo* [45]. The life cycle of ϕ X174 has three stages. First, circular ssDNA converted into double stranded DNA “replication form” (RF) DNA. Second, RF is replicated through a rolling circle mechanism. Lastly DNA is encapsulated into the phage capsid [46]. For ϕ X174 replication *in vitro*, the following four kinds of enzymes are required: the CisA protein, Rep helicase, single stranded DNA binding protein (SSB), and DNA polymerase III holoenzyme [46]. After ssDNA has been replicated by polymerase into dsDNA, CisA nicks RF DNA at the origin of replication and forms a covalent complex with the 5'-end. The free 3'-end at the nick is used as the primer for DNA synthesis by polymerase. The CisA protein then recruits a Rep helicase molecule and the dsDNA ahead of the replication complex is unwound by Rep [47]. Here CisA protein serves as a processivity factor, enabling Rep molecule to be a very efficient helicase [48]. It is quite possible that CisA protein locks Rep helicase into one of the conformations (see next part) that it can adopt.

6.1.4 Structure of *E. coli* Rep

The crystal structures of Rep protein in a complex with ssDNA & ADP was determined and is shown in **Figure 6-2** [3]. Rep consists of two domains (1 and 2); each can be divided further into two structural subdomains (A and B). Rep shares ~40% sequence similarity with *B. stearothermophilus* PcrA and *E. coli* UvrD helicases [14, 16].

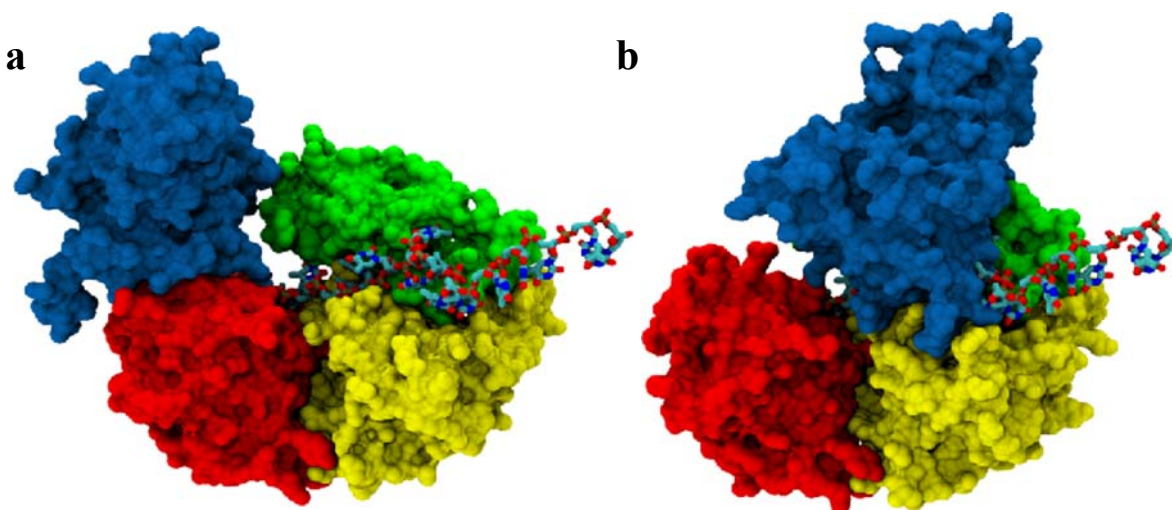


Figure 6-2. Crystal structures: **a)** “open” and **b)** “closed” forms of Rep helicase. Adapted from [3]. Blue is 2B domain, red is 1B domain, yellow 1A domain and green is 1B domain.

The observed contacts of ssDNA with Rep protein include residues in motifs Ia, III, IVa, and V, and some regions outside the conserved motifs (**Figure 6-3**). Two types of interaction are present in Rep-ssDNA complex. One includes residues from motifs Ia (T56, N57), III (Y248), IVa (R350, G351, and N352), and V (H558, T556) that interact with the DNA backbone only. The second type of interaction is the stacking interaction by aromatic residues (W250 of motif III and F183, outside consensus motifs), and the hydrogen-bond interaction between the residues (R251 of motif III, H85 of TxGx motif, and non-motif residues H580 and S582).

Rep can adopt two conformations that differ from each other with respect to the orientation of the 2B domain relative to the other three subdomains (**Figure 6-2**). These two conformations have been called the “open” and “closed” forms, which correspond to a swiveling

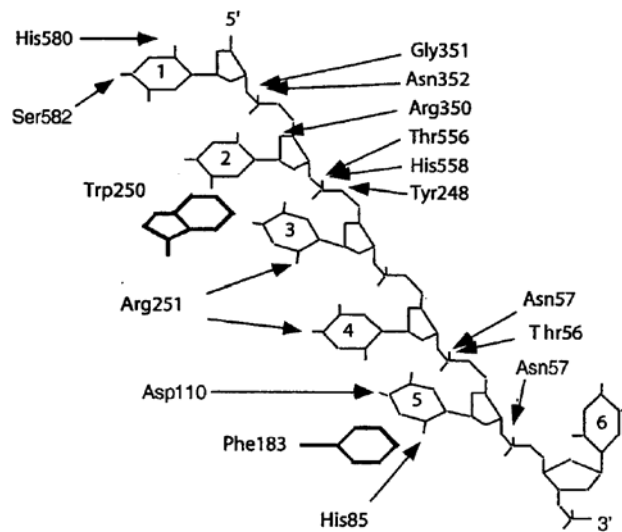


Figure 6-3. Amino acids within the Rep monomer that appear to contact the ss-DNA. Adapted with permission from ref. [2], © 2003 Elsevier.

motion of the 2B domain by 130° about a hinge region. Residues involved in DNA binding and the orientation of the ssDNA in both conformations are identical. The 2B domain is the only domain that does not contain any of the conserved amino acids that comprise the seven helicase motifs that define the SFI helicase superfamily. It was hypothesized that the 2B domain might be involved in dimerization of the Rep protein [3]. In order to test the biological relevance of the 2B domain, this functional domain was deleted from the rep gene and replaced by three glycines to form Rep Δ 2B protein [49]. This change in Rep protein can support ϕ X174 replication *in vivo*, and retain helicase activity *in vitro*. Rep Δ 2B shows an unwinding rate that is as fast as the wild type Rep, but also shows higher extent of unwinding (higher processivity) and higher affinity for ssDNA. Moreover, studies using stopped-flow and quenched-flow techniques showed limited Rep Δ 2B helicase activity as a monomer *in vitro* [30, 49]. These observations suggest that Rep helicase has a potential to unwind dsDNA as a monomer. This remains controversial, as other observations have shown that Rep helicase requires oligomerization for helicase activity *in vitro* [18, 23] and is unable to either start or preserve unwinding activity as a monomer. The possible monomeric helicase activity of Rep and importance of the 2B domain will be a major subject of exploration in this chapter.

6.2 Cross-linking 2B domain activates unwinding ability of Rep helicase

As described above Rep helicase has two distinct conformations named “closed” and “open”. Early studies indicated that upon ssDNA binding, a site within Rep becomes very sensitive to cleavage by trypsin [50]. It is now known that this site lies within the hinge region of Rep [3]. This suggested that some motion of the 2B domain occurs upon ssDNA binding of Rep, which may indicate that movements of the 2B domain are functionally relevant for Rep’s helicase activity. Moreover it was shown that Rep helicase exhibits conformational changes as it approaches dsDNA junction during translocation on ssDNA, with direct evidence that the helicase is in the “closed” conformation at a ds-ssDNA junction [51]. It was further proposed that the 2B domain might be involved in dimerization of the Rep protein [3]. The essential functionality of the 2B domain is still under debate even today.

In order to examine the functional importance of the 2B domain in Rep, our collaborators (Professor Taekjip Ha and graduate student Sinan Arslan) have successfully crosslinked 2B and 1B domains very close to the “closed” form. Two cysteine residues were strategically introduced in each of the 2B and 1B domains, where positions were picked such that upon crosslinking of cysteines, the conformation would mimic the “closed” form as much as possible.

Using single molecule FRET, our collaborators observed crosslinked Rep (“Rep-X”) monomer unwinding of short dsDNA. Single molecule fluorescence resonance energy transfer (smFRET) is a technique where one fluorophore, a donor, can transfer energy to another fluorophore, an acceptor, provided they are not far from each other (1-10 nm). By exciting the donor, some energy is transferred to the acceptor and one can measure relative emission of donor and acceptor (or the FRET efficiency). This provides information the distance between the two molecules. They used an 18-bp dsDNA substrate with a 20-nt long poly-dT 3’ overhang for initial protein binding. Donor/acceptor (Cy3/Cy5) FRET pair were located on the opposite ends of the DNA duplex. N-terminal hexa-histidine tagged Rep-X monomers were tethered to a PEG-coated quartz slide surface via biotin/streptavidin and anti-penta histag antibody linkages (**Figure 6-4a**). Sudden appearance of Cy3 and Cy5 **Figure 6-4b** (green and red traces; emission of Cy3 and Cy5 respectively at 130 seconds) signals indicated that Rep-X monomer ‘caught’ the DNA substrate (**Figure 6-4a** second cartoon) by binding to the 3’ overhang (**Figure 6-4b**; emission of Cy5 indicates FRET; blue trace at 130 seconds). Initiation of unwinding was indicated by a FRET increase (**Figure 6-4a** third cartoon). As unwinding occurs, the average

distance between Cy3 and Cy5 decreased and FRET increased (**Figure 6-4b**), since ssDNA

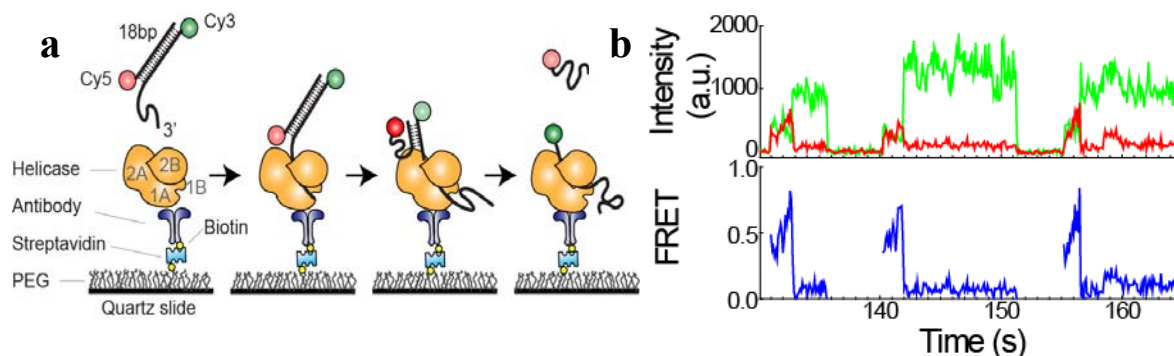


Figure 6-4. Rep-X smFRET study assay. **a)** Rep-X tethered on to polymer coated surface catches disabled DNA with pair of FRET pairs. **b)** Typical three smFRET traces.

is more compact and has shorter end-to-end distance compared to the stiffer dsDNA of the same length. The displaced Cy5-carrying DNA strand dissociated (**Figure 6-4a** fourth cartoon) from the Rep-X-DNA complex after a certain high FRET value was reached, as indicated by a sudden drop in the Cy5 signal and recovery of the Cy3 signal (**Figure 6-4b**). After a while, Cy3 strand also dissociated from Rep-X monomer as the signal completely disappeared. This kind of behavior could not be observed if Rep-X was just translocating on ssDNA. For the first time our collaborators have shown that at least one of the SF1 helicases can unwind DNA as a monomer, provided the 2B domain is locked in the “closed” form.

As mentioned above it has been shown that in complex with CisA protein, Rep is highly processive and is able to unwind the entire phage genome (>6 kbp) [47]. This observation together with the FRET results may indicate a mechanism where the CisA accessory protein locks the 2B domain in the “closed” state. This would mean that the 2B domain acts like a conformational switch that is regulated in the cell. To test this idea, we measured the processivity of Rep-X. Since FRET cannot detect long unzipping events due to the limited range of energy transfer of ~10 nm (30 bp), we decided to use the optical trap.

6.3 Observing DNA unwinding by Rep-X using optical trap

SmFRET experiments are limited to detecting unzipping of only short dsDNA. In order to measure the processivity of Rep-X helicase without accessory protein we used dual optical traps. The main advantage of optical trap over smFRET is that it is possible to track unwinding activity over thousands of base pairs. This will be the main discussion point for the remainder of this chapter.

6.3.1 Experimental design

To achieve our goal of observing Rep-X's ability to unwind long dsDNA, we designed a DNA substrate that had a short ssDNA binding site for Rep-X, followed by a long dsDNA to test whether Rep-X can successfully start and continue unwinding.

DNA construct design

The Rep-X-binding construct (**Figure 6-5**) consisted of two separate DNA fragments that were ligated together: a 6-kbp dsDNA “Unwinding Substrate” (US) with a 15-nt 5' ssDNA overhang that is complementary to the 5' end of a 15-nt ssDNA plus 15(polydT) ssDNA Rep-X protein “Binding Site” (BS). The dsDNA served as a functionalized linker that bound to a trapped bead through the biotin-streptavidin linkage and served as a DNA unwinding substrate.

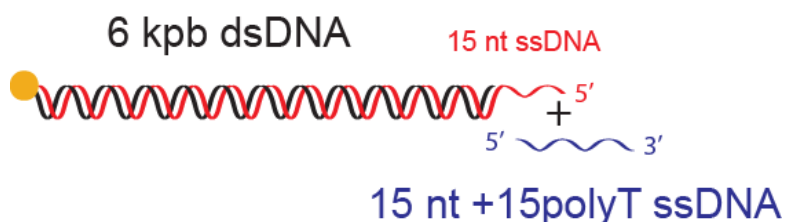


Figure 6-5. Rep-X DNA construct. Biotin labeled on blunt end of DNA and 3' ssDNA overhang a binding site for Rep-X helicase on the other end.

“US” was synthesized from autosticky PCR amplification of Lambda DNA with a 5' biotin-labeled primer and a 5' primer with an abasic site in the middle to create a 5' overhang (Integrated DNA Technologies, Coralville, IA). The oligonucleotide fragment of the construct, BS, consisted of a DNA sequence complementary to the 5' overhang of “US” and 15-nt poly-dT

oligonucleotide. Presence of an abasic site on “US” required an extra dT addition at the 5’ end of the oligomer for more effective ligation.

Rep-X immobilization on beads

Rep-X protein was incubated with biotinylated anti-penta histidine tag from Qiagen in 50mM Tris HCl pH 8.0, 100mM NaCl, 20% (v/v) glycerol, 1mM EDTA buffer at 0 °C for an hour. Then biotin labeled Rep-X was mixed with streptavidin functionalized beads for an hour at 0 °C in the same buffer.

6.3.2 Processive unwinding of Rep helicase

To measure Rep-X processivity we used optical traps (**Figure 6-6**). We constructed a dsDNA substrate 6 kbp in length. We trapped each bead with DNA substrate and Rep-X protein separately. Then we repeatedly moved one of the traps relative to another until we formed a tether (**Figure 6-6**). As soon as we formed a DNA tether in a solution containing 1 mM ATP,

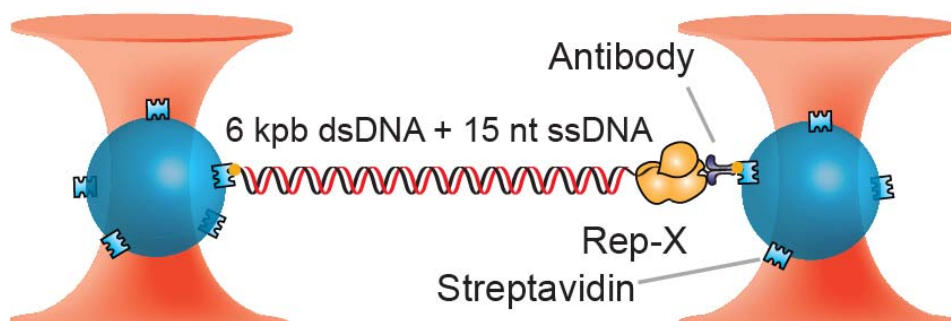


Figure 6-6. Schematic of optical trap experiment. A DNA molecule containing a 6 kbp duplex DNA with bound Rep monomer is tethered between beads held in dual optical traps.

we observed unwinding activity of Rep-X in force feedback mode at 10 pN (**Figure 6-8**). Importantly, our DNA construct could only accommodate binding of a single Rep-X protein via the 15-poly-dT overhang. These results constitute the first observation of processive unwinding activity of a Rep mutant at the single molecule level.

Next we aimed to form stalled complexes of Rep-X-DNA, such that Rep-X’s unwinding activity could be restarted at will upon introduction of saturating amounts of ATP. To achieve this goal we looked for the best condition to form stalled complexes. First, in the absence of

ATP we were unable to form any tethers, which suggested that ATP was needed for the protein to bind stably to DNA. Next, instead of ATP we tried to form tethers in the presence of ATP- γ S, an ATP analog which is non-hydrolyzable. Using ATP- γ S, we started to see tether formation. However the tether lifetime was very short and did not allow enough time to take any reasonable amount of data. The combination of 100 μ M ATP and 100 μ M ATP- γ S was the best condition for stable stalled complex formation. Under this buffer condition the Rep-X-DNA complex neither exhibited unwinding activity nor had a limited tether lifetime.

The ability to detect the unwinding activity of an individual Rep-X on our construct and to use tension to oppose it allowed us to characterize unwinding kinetics of the protein. In our flow cell (**Figure 6-7**), we formed DNA tethers in a laminar stream containing the buffer favoring stalled complexes (100 μ M ATP, 100 μ M ATP- γ S, and no protein), and ensured that we had a single tether by measuring its extension at 10 pN exerted by the dual optical traps. When the trapped bead-DNA-bead complex was moved to a laminar stream containing only 1 mM

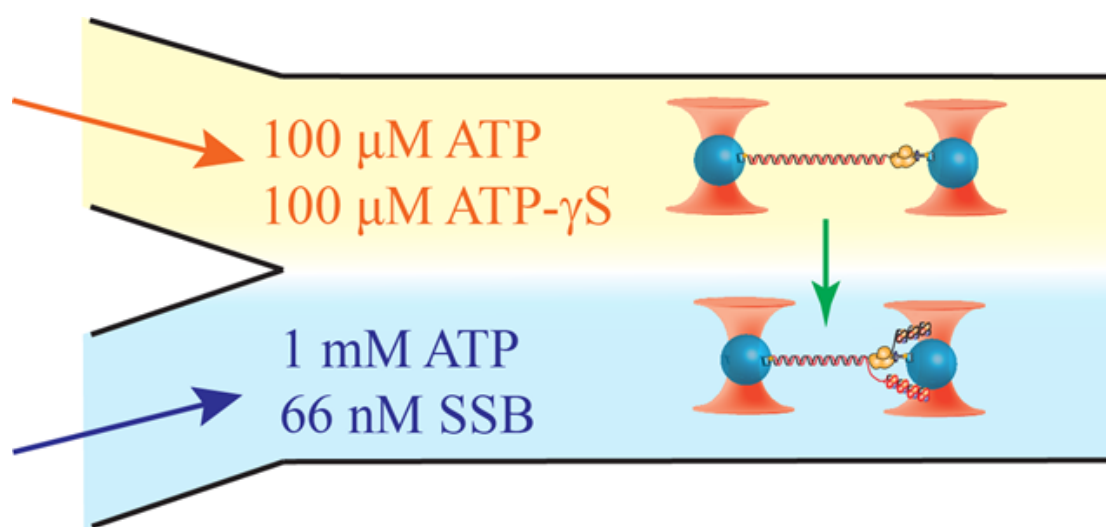


Figure 6-7. Schematic representation of the two merging streams with different solution conditions and schematics of buffer exchange by moving chamber relative to dual trap positions. In the bottom flow channel, as Rep-X unwinds dsDNA ssDNA is coated with SSB. As a result further attachment of free ssDNA to other Rep-X is inhibited.

ATP and no ATP- γ S, the DNA molecule condensed, as seen by its decreased extension over time in force feedback mode (**Figure 6-8**). This observation alone showed direct evidence that Rep helicase in “closed” form can unwind processively, and this conformation is an active form of the helicase. In the latter buffer, 66 nM SSB in addition to saturating concentration of ATP was

present in order to prevent any subsequent attachment of unwound single-stranded DNA to other Rep-X proteins on the bead surface (**Figure 6-7**).

As a control, we wanted to test if we could observe helicase activity of wild-type Rep using the same approaches and conditions. As expected, we formed many short lived tethers with very occasional processive unwinding events (in 3% of formed tethers; data not shown). This is consistent with results of smFRET experiments conducted separately using 18 bp duplex DNA. Thus, wildtype Rep cannot unwind dsDNA as a monomer, but Rep-X not only unwinds, but is highly processive.

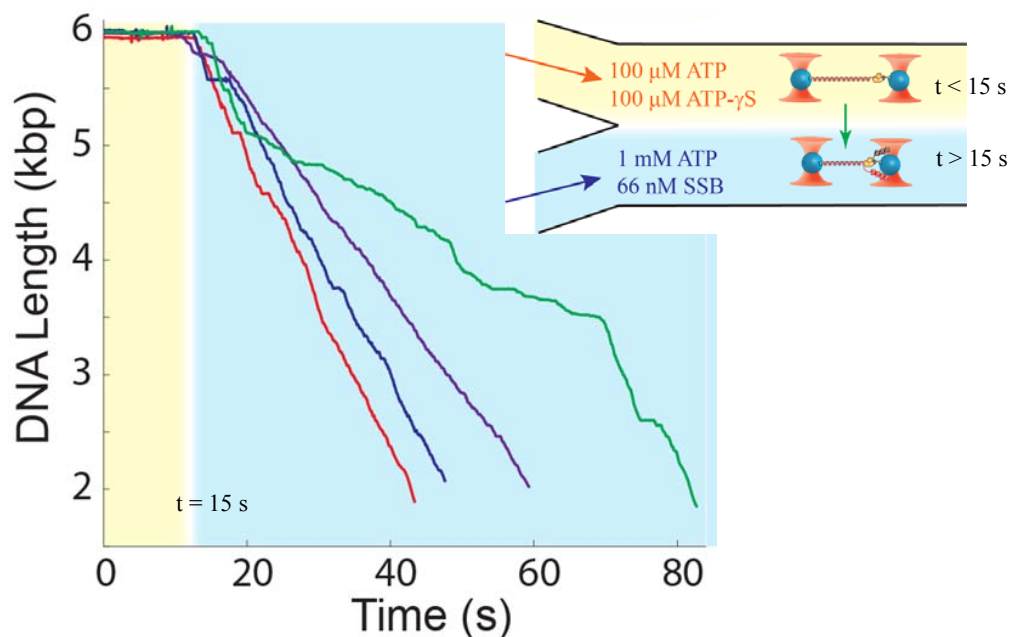


Figure 6-8. Duplex DNA unwinding example traces at force feedback of 10pN. First 15 sec (yellow background) represent Rep-X-DNA stalled complex (no unwinding observed). At 15 sec (inset) buffer conditions change to saturating ATP concentration followed by rapid unwinding activity (blue background).

Separately, we ran control experiments to test if SSB actually inhibited formation of additional Rep-X-DNA tethers. SSB cannot stably bind to 15 nt long ssDNA, so instead we prepared a DNA construct with 75 nucleotides. In this case we could also successfully form Rep-X-DNA tethers and register helicase activity. However, no tethers could be formed once SSB was present at relatively high concentrations (66 nM), confirming that SSB inhibited Rep-X binding to ssDNA. This is in contrast to the 15 nt ssDNA case where we could still form tethers

in the presence of SSB, and more than 95% of tethers showed processive unwinding (**Figure 6-8**).

6.3.3 Heterogeneity of unwinding rates

In **Figure 6-9**, we show example traces of Rep-X helicase activity. In **Figure 6-9** (grey trace) a single Rep-X molecule moved unidirectional at a nearly constant speed of 200 bp/sec. Other molecules moved at different velocities. Velocity varied not only from protein to protein, but also within the unwinding activity of a single protein (**Figure 6-9** green trace). The average unwinding speed of 140 bp/sec is in agreement with other biochemical studies [24].

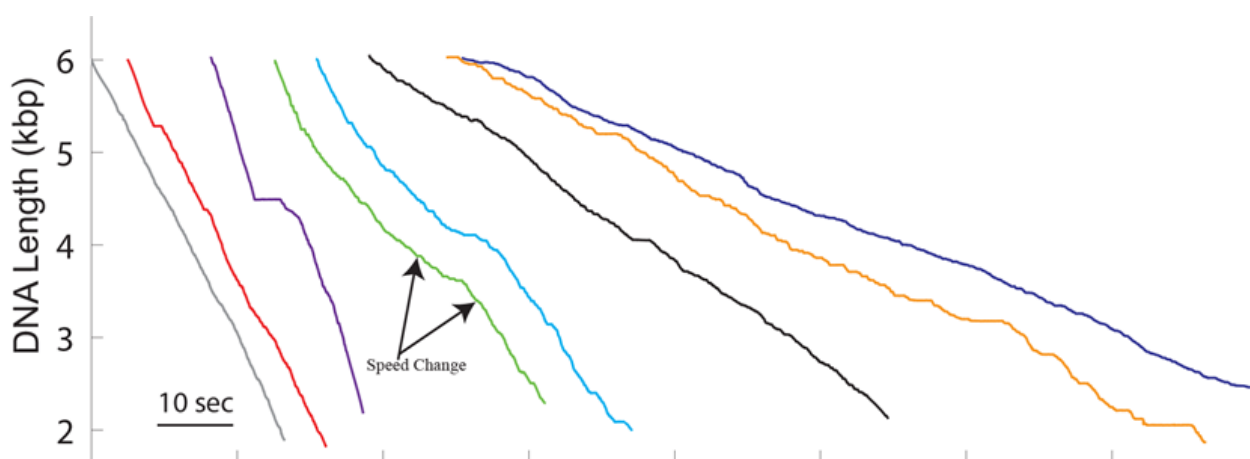


Figure 6-9. Example traces of DNA length change versus time at 10 pN force and 1 mM ATP. Different unwinding rates as well as pause position are observed

Some helicases unwound at nearly uniform speeds for all 4 kbps (**Figure 6-9** grey, red, and blue traces), and others unwound with fluctuating speeds (**Figure 6-9** green and cyan traces). To calculate the unwinding rates we excluded pauses that are a longer than 1 second and calculated the average unwinding speeds. A speed distribution is shown in **Figure 6-10**. Interestingly, the unwinding rates are very heterogeneous. This heterogeneity is not only observed in this helicase, but also in some other proteins like RecBCD [52]. Some fluctuations in speed can arise simply from the stochastic nature of translocation kinetics [53]. However this does not account for the abrupt and persistent changes in rates observed in individual traces (**Figure 6-9** green trace). We also observed frequent pauses, which did not occur at the same place for every molecule (**Figure 6-9** red, black, and yellow traces), but rather randomly during unwinding, suggesting pauses

were not the result of DNA sequence. The nature of the heterogeneity and its biological relevance in the cell is under debate.

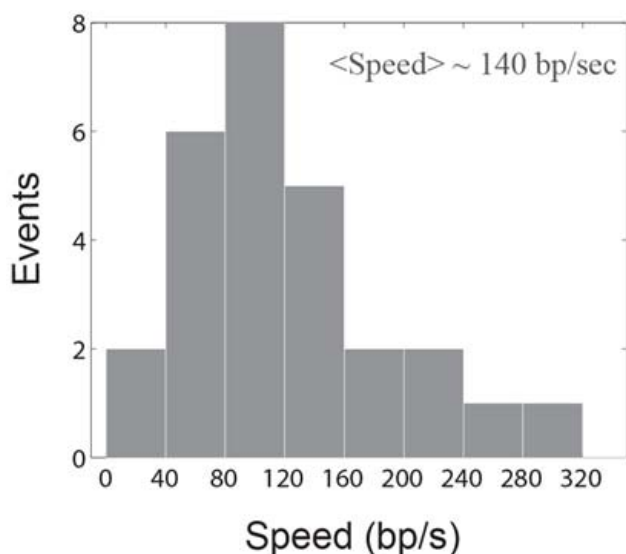


Figure 6-10. Rep-X unwinding speed distribution

6.3.4 Mutation in 1B-2B domain interaction surface enhance unwinding activity

Instead of cross linking 1B and 2B domains we wanted to test the helicase activity of Rep by changing the nature of the interaction between these two domains. UvrD helicase, which shares 40% of its sequence with Rep, has a mutant *uvrD303* that exhibits a higher specific activity for DNA-dependent ATP hydrolysis and unwinds partial dsDNA up to 10 times more efficiently than the wild type UvrD [54]. The enhanced unwinding activity was observed even with 448-bp long dsDNA [54]. *UvrD303* is a mutant variant with two aspartic acids substituted to alanines at the 1B-2B domain interface (D403A/D404A) [54]. The same mutant variant of Rep helicase, RepDD, has been purified by Sua Myong¹. We have tested this mutant in the optical trap for processivity and helicase unwinding activity (**Figure 6-11**).

We used the same dsDNA substrate that we used for Rep-X and wild-type Rep experiments. As soon as we formed tethers we started force feedback at 10 pN. There was an apparent difference from wild type Rep and Rep-X measurements; this time we saw partial unwinding in 20% of formed tethers with subsequent dissociation (**Figure 6-11** green and blue

¹ Sua Myong Assistant Professor, Bioengineering department
University of Illinois, Urbana Champaign

traces). It is worthwhile to mention that we still saw full unwinding in 3% of the traces, consistent with observations in wild type. Interestingly we observed slipping events, in which the protein dissociated from the DNA and then reengaged with it (**Figure 6-11** green trace). These are observed also in Rep-X but at much larger forces (see subsection below).

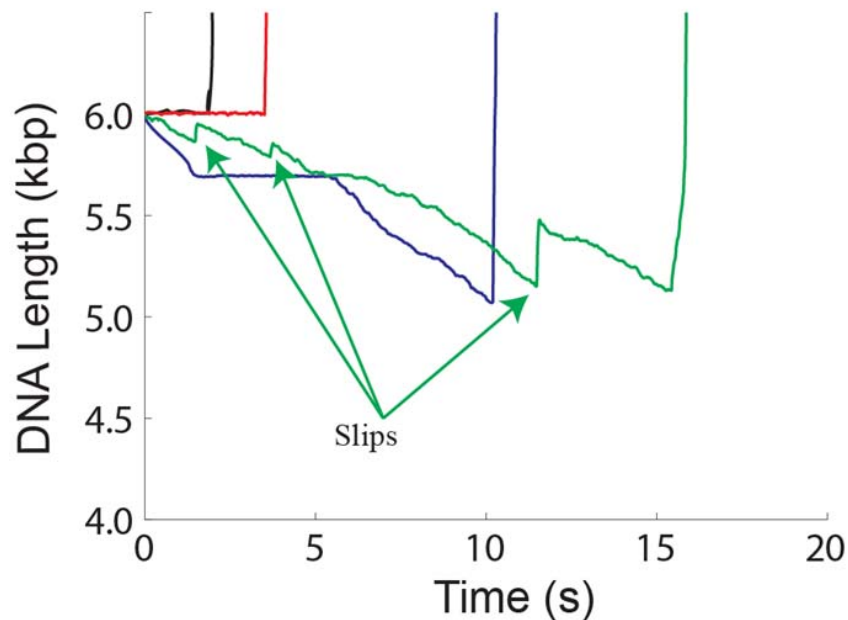


Figure 6-11. Example traces with no helicase activity (red and black) and unwinding activity (blue and green).

These results suggest that above mutation in Rep at the interaction surface between 1B and 2B domains stabilize the “closed” conformation, which leads to improved processivity.

6.3.5 A powerful super helicase

Since Rep-X can unwind long ssDNA with high processivity, it is reasonable to ask what happens at higher forces. Can we see the protein stall or disruption in the protein-DNA interactions?

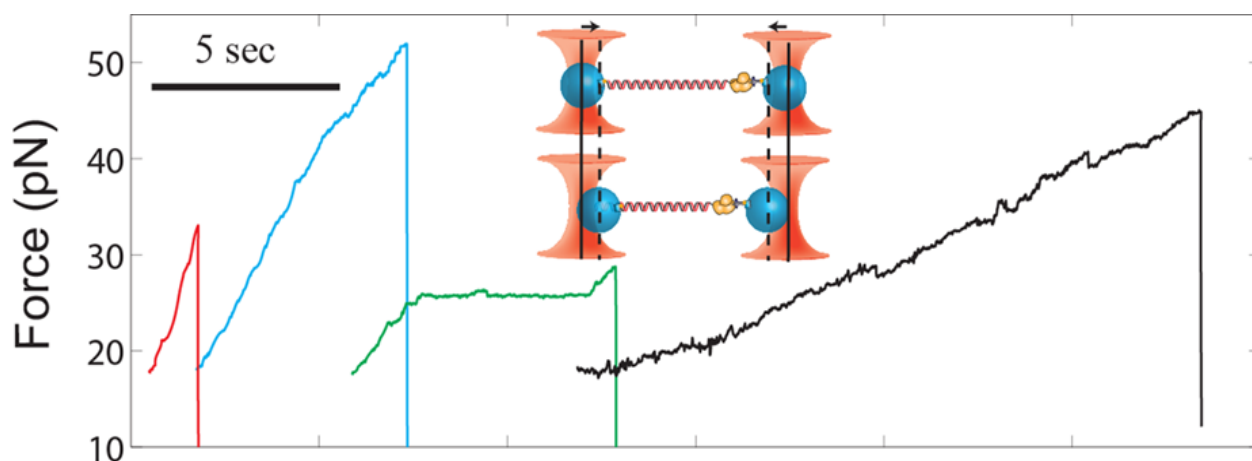


Figure 6-12. Dissociation and slip force measurement experiment traces. Various behaviors are presented in various rates (traces shifted). Trap schematics of dissociation force measurement

The translocation mechanism of motor proteins can be studied by measuring how load forces affect unwinding rates [55-58]. To measure stall and dissociation forces we used our 15-nt 3' ssDNA construct to form tethers in the presence of saturating levels of ATP. As soon as a tether was formed and some helicase activity was observed, we stopped the force feedback. As the helicase unwound DNA, the force load applied on Rep-X helicase increased (**Figure 6-12**). Unlike in the study of RNA polymerase molecules where consistent changes in rates were exhibited with increasing applied force [58], the responses of Rep-X proteins were highly variable (**Figure 6-12**). Even at high applied force we see heterogeneity in the unwinding rates (**Figure 6-12**). Observation of individual traces suggests that we rarely reached stalled conditions and speeds were unaffected by moderate increases in force (**Figure 6-13**). The independence of velocity with respect to the applied load implies that the rate-limiting step in the enzymatic cycle does not involve motion along the substrate DNA. Furthermore, the unwinding motion was occasionally interrupted by episodes of qualitatively different behavior, where the protein abruptly slipped over variable distances from 30 to 300 bp and resumed its helicase activity afterwards (**Figure 6-12** black trace). Observed slips were unexpected and have not been reported in previous studies of Rep. This force-induced slipping may come from transient loss of Rep-X interaction with ssDNA. Moreover in most cases dissociation occurred possibly due to breakage of the linkages in the protein-anti penta histag or ssDNA-Rep-X interaction site. The

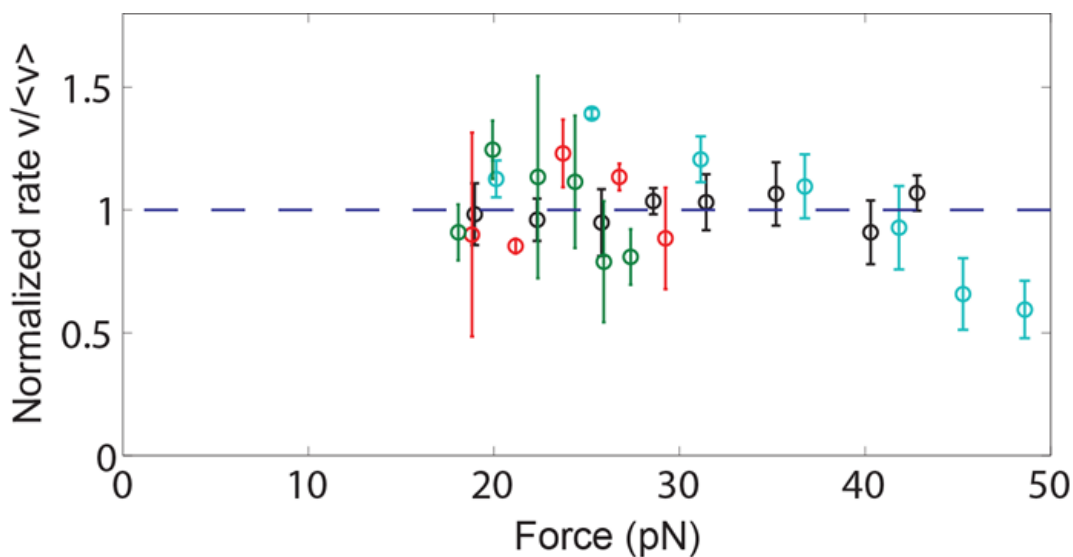


Figure 6-13. Normalized rates versus force plots from individual traces of dissociation force measurement from **Figure 6-12** with the same color coding.

distribution of all observed slip and dissociation forces are shown in **Figure 6-14**. The mean forces for both types of events are similar, 35 pN for slips and 40 pN for dissociation, suggesting that the nature of both processes might be the same.

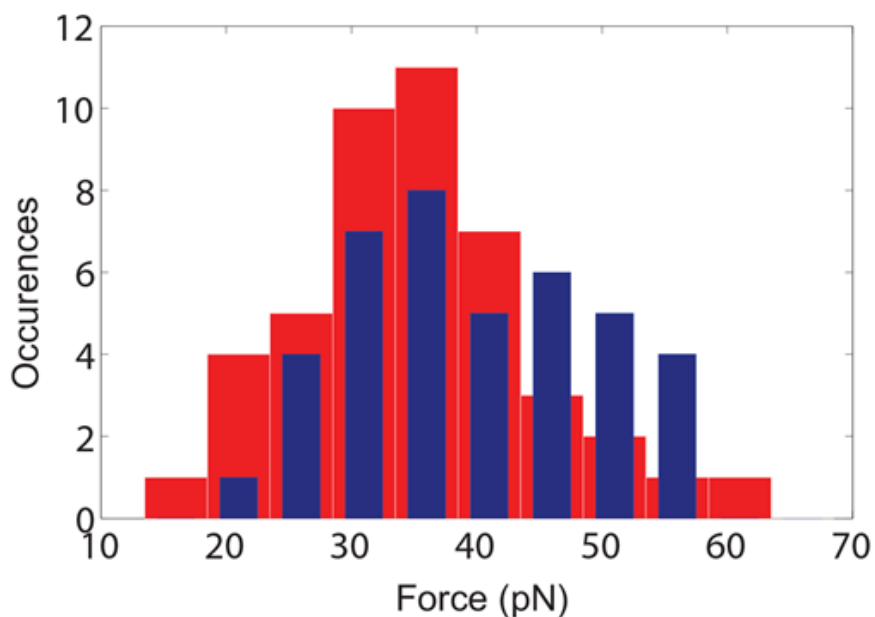


Figure 6-14. Dissociation (blue) and slips (red) force histograms.

With some certainty and confidence we can report now that this is the strongest and most processive helicase observed thus far [52, 59, 60]: Rep-X shows high processivity and fast unwinding rates against loads up to 50 pN. So far the most processive helicase known is RecBCD, which can unwind tens of thousands of basepairs at rates of 500 bp/sec and under load forces of up to 8 pN [52, 59, 60]. The existence of different unwinding states shows that the Rep-X-DNA complex exhibits remarkable functional polymorphism, whose biological functionality and significance has yet to be explored.

6.4 Extending conformational control to another SF1 helicase, PcrA

Enhancement in the helicase activity of Rep monomers by trapping its conformation in its “closed” form suggests that homologs of Rep may also exhibit the same kind of activity enhancement. *Bacillus stearothermophilus* PcrA is an SF1 helicase with a monomeric structure [14] that is very similar to the monomer structure of *E. coli* Rep. It has been reported that PcrA has an accessory protein RepD [61, 62]. RepD stimulates PcrA in the same way that CisA protein stimulates Rep during circular replication. Our collaborators in the Ha lab have engineered PcrA in its “closed” form, though with much lower yield of cross-linked 1B and 2B domains. In order to engineer PcrA-X, all cysteine residues had to be deleted, and two new cysteines were introduced in the same way that it was done for Rep-X. Using smFRET, our collaborators showed that PcrA-X can unwind short dsDNA as a monomer in the same way Rep-X does. Furthermore, wild type PcrA fails to unwind under the same conditions, similar to wild-type Rep.

We measured the processivity of PcrA-X using dual optical traps on the same 6 kbp DNA substrate as used for Rep-X (**Figure 6-15**). We could form short-lived tethers with wild type PcrA and observe unwinding activity with PcrA-X. PcrA unwinding speed is slower than that of Rep [63] and observed unwinding rates are ~10 bp/sec. The percentage of unwinding events was much lower compared to Rep-X due to inefficient internal cross-linking of PcrA (<40% data not shown). However our results agree well with smFRET measurement. This observation suggests that all SF-1 helicases should exhibit processive unwinding activity in “closed” form. Different conformations inside cell could be controlled by processivity factors locking helicases in the “closed” form.

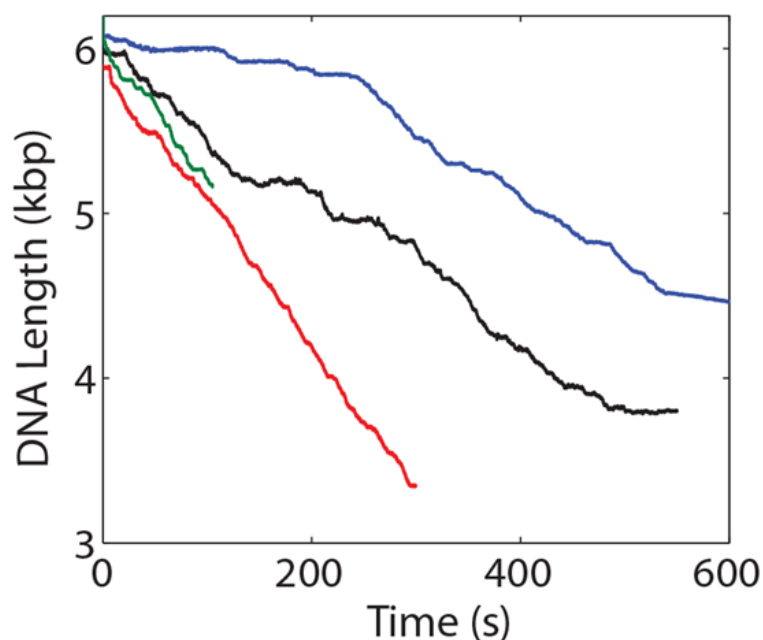


Figure 6-15. Duplex DNA unwinding traces by PcrA-X at force feedback of 10pN

6.5 Summary

Using force spectroscopy methods we have shown that two of the SF1 family helicases, Rep and PcrA, can exhibit processive helicase activity as monomers in their closed forms. The engineered Rep helicase, in particular, is very processive and perhaps the strongest helicase known to date. Rep in complex with the accessory CisA protein is highly processive [47, 48], being able to unwind an entire ~6 kbp genome. Similarly, plasmid replication protein RepD enhances DNA unwinding processivity of PcrA [61, 62]. And finally, MutL can facilitate UvrD helicase activity, which must be able to unwind at least 1 kbp processively during methyl-directed mismatch repair [64-68]. Therefore the processivity of each of these helicases can be increased through interaction with accessory proteins. We propose that most likely these accessory proteins trap helicases in their “closed” 2B conformations.

6.6 References

1. Lohman, T.M., *DNA Helicases: Dimeric Enzyme Action*. Encyclopedia of Biological Chemistry, 2004. 1: p. 618-623.

2. T. M. Lohman, J.H., N. K. Maluf, W. Cheng, A. L. Lucius, C. J. Fischer, K. M. Brendza, S. Korolev, G. Waksman, *DNA Helicases, Motors that Move Along Nucleic Acids: Lessons from the SF1 Helicase Superfamily*. The Enzymes, 2003. XXIII: p. 303-369.
3. Korolev, S., et al., *Major domain swiveling revealed by the crystal structures of complexes of E. coli Rep helicase bound to single-stranded DNA and ADP*. Cell, 1997. 90(4): p. 635-47.
4. Geider, K. and H. Hoffmann-Berling, *Proteins controlling the helical structure of DNA*. Annu Rev Biochem, 1981. 50: p. 233-60.
5. Hill, T.L. and T. Tsuchiya, *Theoretical aspects of translocation on DNA: adenosine triphosphatases and treadmilling binding proteins*. Proc Natl Acad Sci U S A, 1981. 78(8): p. 4796-800.
6. Lohman, T.M., *Escherichia coli DNA helicases: mechanisms of DNA unwinding*. Mol Microbiol, 1992. 6(1): p. 5-14.
7. Lohman, T.M., *Helicase-catalyzed DNA unwinding*. J Biol Chem, 1993. 268(4): p. 2269-72.
8. Lohman, T.M. and K.P. Bjornson, *Mechanisms of helicase-catalyzed DNA unwinding*. Annu Rev Biochem, 1996. 65: p. 169-214.
9. Wong, I. and T.M. Lohman, *A double-filter method for nitrocellulose-filter binding: application to protein-nucleic acid interactions*. Proc Natl Acad Sci U S A, 1993. 90(12): p. 5428-32.
10. Ellis, N.A., *DNA helicases in inherited human disorders*. Curr Opin Genet Dev, 1997. 7(3): p. 354-63.
11. Ellis, N.A., et al., *The Bloom's syndrome gene product is homologous to RecQ helicases*. Cell, 1995. 83(4): p. 655-66.
12. Yu, C.E., et al., *Positional cloning of the Werner's syndrome gene*. Science, 1996. 272(5259): p. 258-62.
13. Goralenya, A.E. and E.V. Koonin, *Helicases - Amino-Acid-Sequence Comparisons and Structure-Function-Relationships*. Current Opinion in Structural Biology, 1993. 3(3): p. 419-429.
14. Subramanya, H.S., et al., *Crystal structure of a DExx box DNA helicase*. Nature, 1996. 384(6607): p. 379-83.
15. Velankar, S.S., et al., *Crystal structures of complexes of PcrA DNA helicase with a DNA substrate indicate an inchworm mechanism*. Cell, 1999. 97(1): p. 75-84.
16. Lee, J.Y. and W. Yang, *UvrD helicase unwinds DNA one base pair at a time by a two-part power stroke*. Cell, 2006. 127(7): p. 1349-1360.
17. Jia, H.F., et al., *Rotations of the 2B Sub-domain of E-coli UvrD Helicase/Translocase Coupled to Nucleotide and DNA Binding*. Journal of Molecular Biology, 2011. 411(3): p. 633-648.
18. Ha, T., et al., *Initiation and re-initiation of DNA unwinding by the Escherichia coli Rep helicase*. Nature, 2002. 419(6907): p. 638-41.
19. Maluf, N.K. and T.M. Lohman, *Self-association equilibria of Escherichia coli UvrD helicase studied by analytical ultracentrifugation*. J Mol Biol, 2003. 325(5): p. 889-912.
20. Patel, S.S. and K.M. Picha, *Structure and function of hexameric helicases*. Annual Review of Biochemistry, 2000. 69: p. 651-697.

21. Chao, K.L. and T.M. Lohman, *DNA and Nucleotide-Induced Conformational-Changes in the Escherichia-Coli Rep and Helicase-Ii (UvrD) Proteins*. Journal of Biological Chemistry, 1990. 265(2): p. 1067-1076.
22. Wong, I., et al., *DNA-Induced Dimerization of the Escherichia-Coli Rep Helicase - Allosteric Effects of Single-Stranded and Duplex DNA*. Journal of Biological Chemistry, 1992. 267(11): p. 7596-7610.
23. Cheng, W., et al., *E. coli Rep oligomers are required to initiate DNA unwinding in vitro*. J Mol Biol, 2001. 310(2): p. 327-50.
24. Brendza, K.M., et al., *Autoinhibition of Escherichia coli Rep monomer helicase activity by its 2B subdomain*. Proceedings of the National Academy of Sciences of the United States of America, 2005. 102(29): p. 10076-10081.
25. Fischer, C.J., N.K. Maluf, and T.M. Lohman, *Mechanism of ATP-dependent translocation of E.coli UvrD monomers along single-stranded DNA*. J Mol Biol, 2004. 344(5): p. 1287-309.
26. Tomko, E.J., et al., *A nonuniform stepping mechanism for E. coli UvrD monomer translocation along single-stranded DNA*. Mol Cell, 2007. 26(3): p. 335-47.
27. Bird, L.E., H.S. Subramanya, and D.B. Wigley, *Helicases: a unifying structural theme?* Current Opinion in Structural Biology, 1998. 8(1): p. 14-18.
28. Soultanas, P., et al., *Uncoupling DNA translocation and helicase activity in PcrA: direct evidence for an active mechanism*. Embo Journal, 2000. 19(14): p. 3799-3810.
29. Mechanic, L.E., M.C. Hall, and S.W. Matson, *Escherichia coli DNA helicase II is active as a monomer*. Journal of Biological Chemistry, 1999. 274(18): p. 12488-12498.
30. Brendza, K.M., et al., *The 2B domain of E-coli rep protein is not required for helicase activity*. Biophysical Journal, 2003. 84(2): p. 365a-365a.
31. Bialkowskahobrzanska, H. and D.T. Denhardt, *The Rep Mutation .7. Cloning and Analysis of the Functional Rep Gene of Escherichia-Coli-K-12*. Gene, 1984. 28(1): p. 93-102.
32. Bialkowskahobrzanska, H., C.A. Gilchrist, and D.T. Denhardt, *Rep Mutation .8. Escherichia-Coli-Rep Gene - Identification of the Promoter and N-Terminus of the Rep Protein*. Journal of Bacteriology, 1985. 164(3): p. 1004-1010.
33. Colasanti, J. and D.T. Denhardt, *The Escherichia-Coli Rep Mutation .10. Consequences of Increased and Decreased Rep Protein-Levels*. Molecular & General Genetics, 1987. 209(2): p. 382-390.
34. Kornberg, A., J.F. Scott, and L.L. Bertsch, *Atp Utilization by Rep Protein in Catalytic Separation of DNA Strands at a Replicating Fork*. Journal of Biological Chemistry, 1978. 253(9): p. 3298-3304.
35. Takahashi, S., et al., *Rep Mutation .6. Purification and Properties of the Escherichia-Coli Rep Protein, DNA Helicase-Iii*. Canadian Journal of Biochemistry, 1979. 57(6): p. 855-866.
36. Lane, H.E.D. and D.T. Denhardt, *Rep Mutation .4. Slower Movement of Replication Forks in Escherichia-Coli Rep Strains*. Journal of Molecular Biology, 1975. 97(1): p. 99-&.
37. Lane, H.E.D. and D.T. Denhardt, *Rep Mutation .3. Altered Structure of Replicating Escherichia-Coli Chromosome*. Journal of Bacteriology, 1974. 120(2): p. 805-814.

38. Yancey-wrona, J.E. and S.W. Matson, *Bound Lac Repressor Protein Differentially Inhibits the Unwinding Reactions Catalyzed by DNA Helicases*. Nucleic Acids Research, 1992. 20(24): p. 6713-6721.
39. Matson, S.W., D.W. Bean, and J.W. George, *DNA Helicases - Enzymes with Essential Roles in All Aspects of DNA Metabolism*. Bioessays, 1994. 16(1): p. 13-22.
40. Michel, B. and M. Uzest, *Lethality of Double Mutations Rep-RecB and Rep-Recc in Escherichia-Coli*. Journal of Cellular Biochemistry, 1995: p. 114-114.
41. Zieg, J., V.F. Maples, and S.R. Kushner, *Recombination Levels of Escherichia-Coli K-12 Mutants Deficient in Various Replication, Recombination, or Repair Genes*. Journal of Bacteriology, 1978. 134(3): p. 958-966.
42. Bridges, B.A. and A. Vonwright, *Influence of Mutations at the Rep Gene on Survival of Escherichia-Coli Following Ultraviolet-Light Irradiation or 8-Methoxypsoralen Photosensitization - Evidence for a RecA+Rep+-Dependent Pathway for Repair of DNA Crosslinks*. Mutation Research, 1981. 82(2): p. 229-238.
43. Fassler, J.S., I. Tessman, and E.S. Tessman, *Lethality of the Double Mutations Rho Rep and Rho Ssb in Escherichia-Coli*. Journal of Bacteriology, 1985. 161(2): p. 609-614.
44. Washburn, B.K. and S.R. Kushner, *Construction and Analysis of Deletions in the Structural Gene (UvrD) for DNA Helicase-Ii of Escherichia-Coli*. Journal of Bacteriology, 1991. 173(8): p. 2569-2575.
45. Denhardt, D.T., D.H. Dressler, and A. Hathaway, *Abortive Replication of Phix174 DNA in a Recombination-Deficient Mutant of Escherichia Coli*. Proceedings of the National Academy of Sciences of the United States of America, 1967. 57(3): p. 813-&.
46. Eisenberg, S., J.F. Scott, and A. Kornberg, *Enzymatic Replication of Viral and Complementary Strands of Duplex DNA of Phage Phix174 Proceeds by Separate Mechanisms*. Proceedings of the National Academy of Sciences of the United States of America, 1976. 73(9): p. 3151-3155.
47. Eisenberg, S., J. Griffith, and A. Kornberg, *Phix174 Cistron-a Protein Is a Multifunctional Enzyme in DNA-Replication*. Proceedings of the National Academy of Sciences of the United States of America, 1977. 74(8): p. 3198-3202.
48. Scott, J.F., et al., *Enzyme-System for Replication of Duplex Circular DNA - Replicative Form of Phage Phix174 .3. Mechanism of Duplex DNA-Replication Revealed by Enzymatic Studies of Phage Phix174 - Catalytic Strand Separation in Advance of Replication*. Proceedings of the National Academy of Sciences of the United States of America, 1977. 74(1): p. 193-197.
49. Cheng, W., et al., *The 2B domain of the Escherichia coli Rep protein is not required for DNA helicase activity*. Proc Natl Acad Sci U S A, 2002. 99(25): p. 16006-11.
50. Chao, K. and T.M. Lohman, *DNA and nucleotide-induced conformational changes in the Escherichia coli Rep and helicase II (UvrD) proteins*. J Biol Chem, 1990. 265(2): p. 1067-76.
51. Myong, S., et al., *Repetitive shuttling of a motor protein on DNA*. Nature, 2005. 437(7063): p. 1321-1325.
52. Perkins, T.T., et al., *Forward and reverse motion of single RecBCD molecules on DNA*. Biophys J, 2004. 86(3): p. 1640-8.
53. Svoboda, K., P.P. Mitra, and S.M. Block, *Fluctuation analysis of motor protein movement and single enzyme kinetics*. Proc Natl Acad Sci U S A, 1994. 91(25): p. 11782-6.

54. Zhang, G., et al., *Identification and characterization of Escherichia coli DNA helicase II mutants that exhibit increased unwinding efficiency*. Journal of Bacteriology, 1998. 180(2): p. 377-87.
55. Finer, J.T., R.M. Simmons, and J.A. Spudich, *Single myosin molecule mechanics: piconewton forces and nanometre steps*. Nature, 1994. 368(6467): p. 113-9.
56. Leibler, S. and D.A. Huse, *Porters versus rowers: a unified stochastic model of motor proteins*. J Cell Biol, 1993. 121(6): p. 1357-68.
57. Svoboda, K. and S.M. Block, *Force and velocity measured for single kinesin molecules*. Cell, 1994. 77(5): p. 773-84.
58. Wang, M.D., et al., *Force and velocity measured for single molecules of RNA polymerase*. Science, 1998. 282(5390): p. 902-7.
59. Bianco, P.R., et al., *Processive translocation and DNA unwinding by individual RecBCD enzyme molecules*. Nature, 2001. 409(6818): p. 374-8.
60. Roman, L.J. and S.C. Kowalczykowski, *Characterization of the helicase activity of the Escherichia coli RecBCD enzyme using a novel helicase assay*. Biochemistry, 1989. 28(7): p. 2863-73.
61. Soultanas, P., et al., *Plasmid replication initiator protein RepD increases the processivity of PcrA DNA helicase*. Nucleic Acids Res, 1999. 27(6): p. 1421-8.
62. Zhang, W., et al., *Directional loading and stimulation of PcrA helicase by the replication initiator protein RepD*. J Mol Biol, 2007. 371(2): p. 336-48.
63. Niedziela-Majka, A., et al., *Bacillus stearothermophilus PcrA monomer is a single-stranded DNA translocase but not a processive helicase in vitro*. Journal of Biological Chemistry, 2007. 282(37): p. 27076-27085.
64. Yamaguchi, M., V. Dao, and P. Modrich, *MutS and MutL activate DNA helicase II in a mismatch-dependent manner*. J Biol Chem, 1998. 273(15): p. 9197-201.
65. Mechanic, L.E., B.A. Frankel, and S.W. Matson, *Escherichia coli MutL loads DNA helicase II onto DNA*. J Biol Chem, 2000. 275(49): p. 38337-46.
66. Matson, S.W. and A.B. Robertson, *The UvrD helicase and its modulation by the mismatch repair protein MutL*. Nucleic Acids Res, 2006. 34(15): p. 4089-97.
67. Robertson, A.B., et al., *MutL-catalyzed ATP hydrolysis is required at a post-UvrD loading step in methyl-directed mismatch repair*. J Biol Chem, 2006. 281(29): p. 19949-59.
68. Modrich, P., *DNA mismatch correction*. Annu Rev Biochem, 1987. 56: p. 435-66.

Appendix A

Measurement of binding free energy

The effect of force on a molecular reaction is well described in the context of RNA and DNA conformational dynamics [1, 2]. The same formalism can be used to describe the force-induced transition between SSB-wrapped and unwrapped states of the DNA molecule. It is useful to define a force-dependent wrapping equilibrium constant $K_{wrap}(F)$ for this reaction. This constant can be written in terms of the difference in standard free energy (*at zero force*) between the wrapped and unwrapped states ΔG^0 [3]:

$$K_{wrap}(F) = \exp(-\Delta G^0 + \Delta G'_{stretch}(F))/k_B T),$$

where the thermodynamic quantity $\Delta G'_{stretch}(F)$ accounts for the free energy in stretching the molecule,

$$\Delta G'_{stretch}(F) = \int_0^F x_w(F')dF' - \int_0^F x_u(F')dF'.$$

By geometry, this is simply equal to the area between the protein-*wrapped* force extension curve, $x_w(F)$, and the *unwrapped* curve, $x_u(F)$, integrated from 0 to force F . Note that this quantity also can be expressed in terms of the extension change upon SSB binding $\Delta x(F) = x_w(F) - x_u(F)$ in

Fig. 3-5, i.e. $\Delta G'_{stretch}(F) = \int_0^F \Delta x(F')dF'$. Since $\Delta G'_{stretch}(0) = 0$, the equilibrium constant at zero force is given by $K_{wrap}^0 = \exp(-\Delta G^0/k_B T)$, and these expressions combine to give

$$K_{wrap}(F) = K_{wrap}^0 \exp(-\int_0^F dF' \Delta x(F')/k_B T)$$

which is used to obtain Eq. (4-5) in Chapter 4.

1. Liphardt, J., et al., *Reversible unfolding of single RNA molecules by mechanical force*. Science, 2001. **292**(5517): p. 733-7.
2. Woodside, M.T., et al., *Nanomechanical measurements of the sequence-dependent folding landscapes of single nucleic acid hairpins*. Proc Natl Acad Sci U S A, 2006. **103**(16): p. 6190-5.
3. Tinoco, I., Jr. and C. Bustamante, *The effect of force on thermodynamics and kinetics of single molecule reactions*. Biophys Chem, 2002. **101-102**: p. 513-33.

Appendix B

Average angle between applied force and SSB orientation

The SSB orientation is agitated by thermal rotation motion and opposed by force applied through DNA handles [1]. We consider the effect of thermal motion on SSB which is free to rotate. The potential energy U of a molecule under torque is.

$$U = -F\Delta s = -Fs \cos(\theta),$$

where θ is the angle between the SSB orientation and the applied force.

According to the Boltzmann distribution law the relative probability of finding a protein in an element of solid angle $d\Omega$ is proportional to $\exp(-U/k_B T)$, and

$$\langle \cos \theta \rangle = \frac{\int e^{-\beta U} \cos \theta d\Omega}{\int e^{-\beta U} d\Omega},$$

where $\beta = 1/k_B T$,

$$\langle \cos \theta \rangle = \frac{\int_0^{2\pi} \int_0^{2\pi} 2\pi \sin \theta \cos \theta e^{\beta F s \cos \theta} d\theta}{\int_0^{2\pi} \int_0^{2\pi} 2\pi \sin \theta e^{\beta F s \cos \theta} d\theta}.$$

Let change $s = \cos \theta$ and $x = Fs/k_B T$, so

$$\langle \cos \theta \rangle = \int_{-1}^1 e^{sx} s ds \bigg/ \int_{-1}^1 e^{sx} ds = \frac{d}{dx} \log \int_{-1}^1 e^{sx} ds = \frac{d}{dx} \log(e^x - e^{-x}) - \frac{d}{dx} \log x = \coth x - \frac{1}{x} = L(x)$$

which is used to obtain Eq. (3-2) in Chapter 3.

1. Kittel, C., *Introduction to solid state physics*. 3rd ed. 1966, New York,: Wiley. 387-389.

Protocols

DNA constructs

3.2 kbp dsDNA + short ssDNA construct

Materials:

- Forward Primer RH: 5'-/5DigN/GGG CAA ACC AAG ACA GCT AA -3'
- Reverse Primer RH: 5' - CCC GTC ATA CAC TTG CTC CT -3'
- Forward Primer LH: 5'-/5Biosg/ TGA AGT GGT GGC CTA ACT ACG -3'
- Reverse Primer LH: 5' - TTG CAT GAT AAA GAA GAC AGT CAT -3'
- 70nt polyT Insert: 5'-/5Phos/CCT GGT TTT TTT TTT TTT TTT TTT TTT TTT
TTT TTT TTT TTT TTT TTT TTT TTT TTT TTT TTT TTT TTT CCC ACT GGC
-3'
- 175 polyT Insert: 5'-/5Phos/CCT GGT TTT TTT TTT TTT TTT TTT TTT TTT
TTT TTT TTT TTT TTT TTT TTT TTT TTT TTT TTT TTT TTT TTT TTT TTT
TTT TTT TTT TTT TTT TTT TTT TTT TTT TTT TTT TTT TTT TTT TTT TTT
TTT TTT TTT TTT TTT TTT TTT TTT TTT TTT TCC CAC TGG C -3'
- 2x Phusion Master Mix from Finnzymes
- PCR purification and Gel extraction kit from Quiagen
- PspGI, TspRI and ligase from NEB
- pBR322 from Fermentas
- λ DNA from Promega

1. PCR the two handles

- Make two sets of the following (50 μ l volume each tube)

	Left Handle (μl)	Right Handle (μl)
2x Phusion Mix	25	25
FWD (primer)	2.5	2.5
REV (primer)	2.5	2.5
DNA	2 (10 ng) pBR322	1 (11 ng) λ

DMSO	1.5	1.5
H ₂ O (dnase free)	16.5	17.5

- PCR mix is 2x Phusion Master Mix with 100% DMSO.
- Primers should be 10 μ M each (diluted in IDTE).
- PCR program protocol: follow Phusion Master Mix booklet.

2. PCR purify

- Combine two Left handle product in one: final volume 100ul. The same thing should be done with Right handle.

3. Digestion to cut the handles

Need to do each handle separately in PCR machine. Use PCR tubes.

- Left handle

Add to DNA: 3.5 μ l NEB2 10x, 2 μ l PspGI(20U total). 1 hour at 75 C.

- Right handle

Add to DNA: 3.5 μ l NEB4 10x, 2 μ l TspRI (20U total). 1 hour at 65 C.

4. Gel purify

- Make gel. 60 ml 0.5x TBE buffer, 0.6 g agarose (1%) LMP (low melting point).
Microwave. Then add to cool mix 1 μ l ethidium bromide. Pour into gel box. Use second comb spot. Wait 1-2 hours at RT. Don't keep overnight.
- To load gel: 3 μ l 100% glycerol (amount needed to keep in well, ~10% total), 2 μ l dye, DNA (~35 μ l). Preheat right handle to 65 C for 1 min first.
- Run gel 75 V for 1 hour.
- Bands will be a bit messy. Cut out handles with razor blade. Weigh it on tray (~100 mg).
Put into 1.5 ml tubes. Do QIAquick gel extraction kit protocol (p 25). Final amount 30ul.

5. Ligate handles to ssDNA

- a. Can first run test ligations to try to optimize ratio of handles to ssDNA.

Left Handle	Insert	Right Handle	H ₂ O
1	0.25	1	5.75
1	0.5	1	5.5
1	1	1	5

1	3	1	3
---	---	---	---

* Oligo concentration is 40 nM(diluted in IDTE).

- Then for each add: 1 µl 10x T4 DNA ligase buffer, 1 µl 100x T4 DNA ligase (20 units, dilutes to 10x).
- Run at room temperature for 30 min.
- Previously the 1:3:1 ratio looked best.

6. Final ligation

15 µl	Right Handle
15 µl	Left Handle
4 µl 10x	T4 DNA ligase buffer
4 µl 25x	T4 DNA ligase
2 µl	800 nM ssDNA

* (dilute 2 µl of ssDNA @ 40 µM into 98 µl H₂O)

- 40 µl total. This gives 5% glycerol (from 50% glycerol in ligase, should be OK).
- Run at room temperature for 30 min.

7. Purify

- Make gel (as above).
- Run gel (as above).
- The bands I should get are: construct, uncut right handle (faint), mix of right – left – right+oligo – left+oligo, oligo self-ligation, oligo.
- Purify gel (as above).
- Keep everything in the fridge.

3.4 kbp dsDNA

Materials

1. Forward Primer: 5' - /5Bio/ACA GCA TCG CCA GTC ACT ATG -3'
2. Reverse Primer: 5' - /5DigN/CAA CAA CGT TGC GCA AAC T -3'
3. 2x Phusion Master Mix from Finnzymes
4. PCR purification kit from Qiagen
5. pBR322 from Fermentas

1. PCR DNA

- 25 µl 2x Phusion master mix
- 2.5 µl FWD primer (10µM)
- 2.5 µl REV primer (10µM)
- 1 µl pBR322 DNA (10 ng/ µl)
- 1.5 µl DMSO
- 17.5 µl H₂O

2. PCR purify in final volume of 50 µl

dsDNA (~3kbp) + long ssDNA (~1700nt)

Materials:

1. Forward Primer RH:5'- AGA TTC CTG GGA TAA GCC AAG -3'
2. Reverse Primer RH:5'- TAA ACT GTC GCT TGG TCA GAT C -3'
3. oligo LH:5'-/5Bio/ACA GCA TCG CCA GTC ACT ATG -3'
4. complementary oligo LH:5'- /5Phos/AGC TCA TAG TGA CTG GCG ATG CTG T -3'
5. PCR DIG probe synthesis kit from Roche
6. PCR purification kit from Quiagen
7. HindIII, EcorI, MfeI, Nb.BsmI, Exo III and ligase from NEB
8. pBR322 from Fermentas
9. λ DNA from Promega

1. PCR Right Handle (DIG labeled 1kbp dsDNA)

	Right Handle (µl)
PCR buffer(3°)	5
dNTP's (2°)	5
FWD (primer)	2.5
REV (primer)	2.5
DNA	1 (11 ng) λ
Enzyme(1°)	0.75
H ₂ O	33.25

- Primers should be 10 µM each (diluted in IDTE).

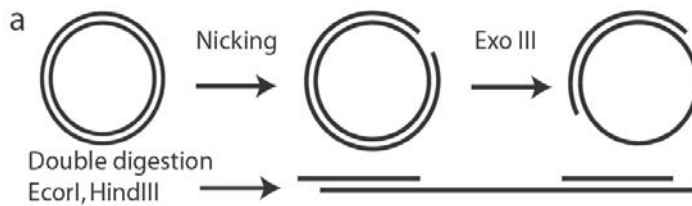
- PCR program protocol: follow PCR booklet from Roche.
- PCR purify
- **Digestion into 500bp**

Add to DNA: 6 μ L NEB4 10x, 1.5 μ L MfeI (15U total). 1 hour at 37 °C, then deactivate for 20 minutes at 65 °C.

2. Left handle (Biotin labeled 20bp+binding site)

Anneal FWD LH and REV LH to a final of 1 μ M concentration each.

3. Ds-ss DNA hybrid



- Nick pBR322 plasmid with Nb.BsmI.

- 12.5 μ L of PBR322(500ng/ μ L)
- 3 μ L NEB2 buffer
- 5,5 μ L Nb,BsmI(10U/ μ L)
- 9 μ L H₂O

Incubate for 1 hour at 65 °C, then deactivate for 20 minutes at 80 °C.

- Exo III treatment.

Temperate 30 μ L for 2 minutes at 37 °C, add 1 μ L of Exo III (100U).

Incubate for 3 minutes at 37 °C, then add 1 μ L of 0.5M EDTA, deactivate for 10 minutes at 75 °C.

- PCR purify into 30 μ L. Leave 1 μ L to Mung bean treatment.

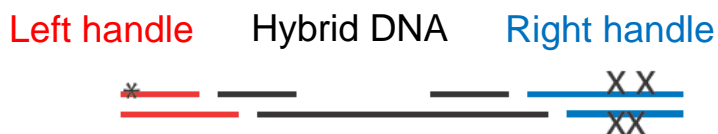
- Double digestion of plasmid with Hind III, Ecor I.

- 29 μ L ss-dsDNA plasmid
- 3 μ L EcorI buffer
- 1 μ L Hind III(100U/ μ L)
- 1 μ L EcorI(100U/ μ L).

Incubate for 2 hours at 37 °C, then deactivate for 20 minutes at 65 °C.

- PCR purify into 30 μ L. Leave 2 μ L to Mung bean treatment.

- Mung bean treatment (To find the length of ssDNA).
To 1 μL and 2 μL add 0.8 μL Mung bean buffer, 0,3 μL Mung bean, ?? μL H_2O to have 8 μL at the end.
- Run the gel to see the length.



Ligation of three parts.

Component	Volume /
Right handle	1 μL
ss-dsDNA	1 μL
Left handle	.25 μL
Ecor I(10U/ μL).	0.5 μL
Hind III(10U/ μL).	0.5 μL
Mfe I(10U/ μL).	0.5 μL
Ligase Buffer	1.5 μL
BSA(10x)	1.5 μL
ligase(20U/ μL).	1 μL
H_2O	7.25 μL

Overnight ligation

Cycle step	Temp	Time	Number of cycles
Ligation	16 $^{\circ}\text{C}$	20 min	18
Digestion	37 $^{\circ}\text{C}$	20 min	
Final Digestion	37 $^{\circ}\text{C}$	40 min	1
	4 $^{\circ}\text{C}$	hold	

Run the gel after ligation to see product.

Bead preparation

Anti Digoxigenin coated beads

Material

- 1.0% w/v 0.86 μm Protein G beads (Spherotech Inc.) – polystyrene particles
- Anti-Digoxigenin (polyclonal antibody, immunoglobulin)
- Phosphate buffered saline with 0.1 Tween 20, pH 7.0 (1 \times PBS)

Procedure

- Wash 40 μL of 1.0% w/v beads (protein G, 0.86 μm) in 160 μL 1X PBS twice:
- Spin @ 7.5 krpm for 1 minute
- Remove supernatant
- Add 200 μL 1X PBS
- Resuspend pellet by vortexing 10 – 30 s on high
- Repeat
- Add 10 μL anti-DIG antibody reconstituted to PBS after final wash
- Shake for 30 min on vortexer (high)
- Wash with 1X PBS three times
- Spin @ 7.5 krpm for 1 min
- Remove supernatant
- Add 200 μL 1X PBS (storage solution)
- Resuspend pellet by vortexing 1 min
- Repeat
- Store in final wash

Streptavidin beads

Material

- 1.0% w/v 0.79 μm streptavidin polystyrene particles (Spherotech Inc.)
- TMS with 0.1% tween 20, pH 7.0

Procedure

- Wash 20 μL of 1.0% w/v beads (Streptavidin beads, 0.79 μm) in 160 μL 1 X TMS three times:

- Spin @ 7.5 krpm for 1 minute
- Remove supernatant
- Add 200 μ L 1X TMS
- Resuspend pellet by vortexing 10 – 30 s on high
- Repeat